Закрученные частицы: генерация и потенциальные приложения в квантовой физике

Дмитрий Карловец

Университет ИТМО

23.05.2024

d.karlovets@gmail.com

ПИЯФ

Outline

1. Intro
2. Quantum tomography of the evolved states in QFT:
   a. With the plane-wave electrons/protons/ions…
   b. With the generalized measurements

2. Vortex electrons, ions, nuclei,… - generation strategies at accelerators
   a. Magnetized cathode technique
   b. Magnetized stripping foil technique

3. Acceleration of charged particles with vortices and photon emission

Classical light:

- Plane waves
- Spherical waves
- Cylindrical waves

Each wave can be represented as a superposition
of the waves from the other set

Quantum light:

- Plane-wave photons
- Spherical (waves of) photons
- Cylindrical (waves of) photons

  or the twisted photons

Each wave function (eigenvector) in a set
can be represented
as a superposition of the wave functions (eigenvectors)
from the other set

Plane vs. spherical:

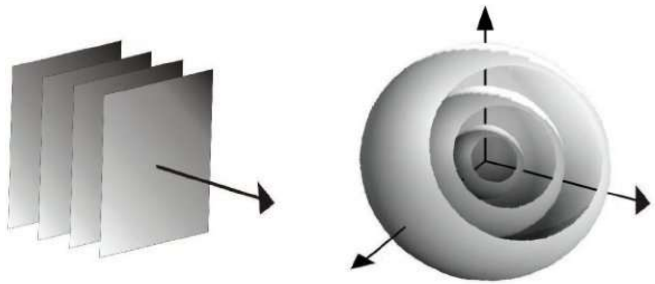

https://www.researchgate.net/profile/Miikka-Tikander-2/publication/242641740/figure/fig1/AS:298423984115712@1448161230440/Propagation-of-a-plane-waves-and-b-spherical-waves_W640.jpg

Quantum light

- Plane-wave photons: k_x, k_y, k_z + polarization
- Spherical (waves of) photons: $|\boldsymbol{k}|$, l, m (= L_z) + polarization
- The cylindrical (twisted) photons: $k_\perp$, k_z, m (= L_z or J_z) + polarization

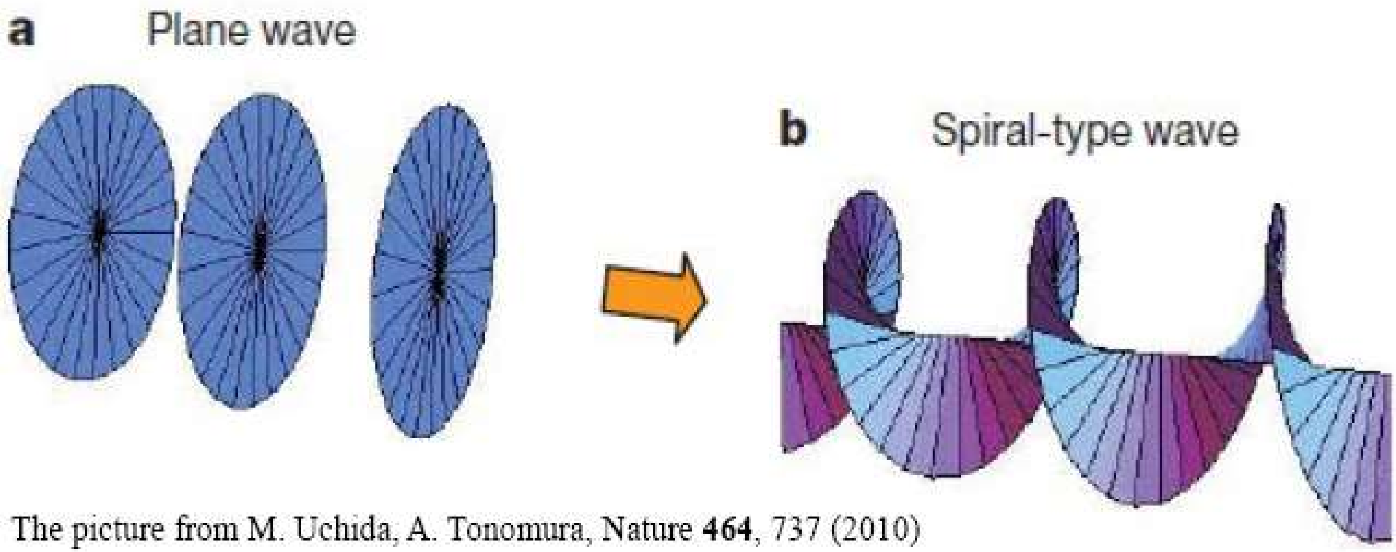

The picture from M. Uchida, A. Tonomura, Nature **464**, 737 (2010)

Радиально поляризованный свет

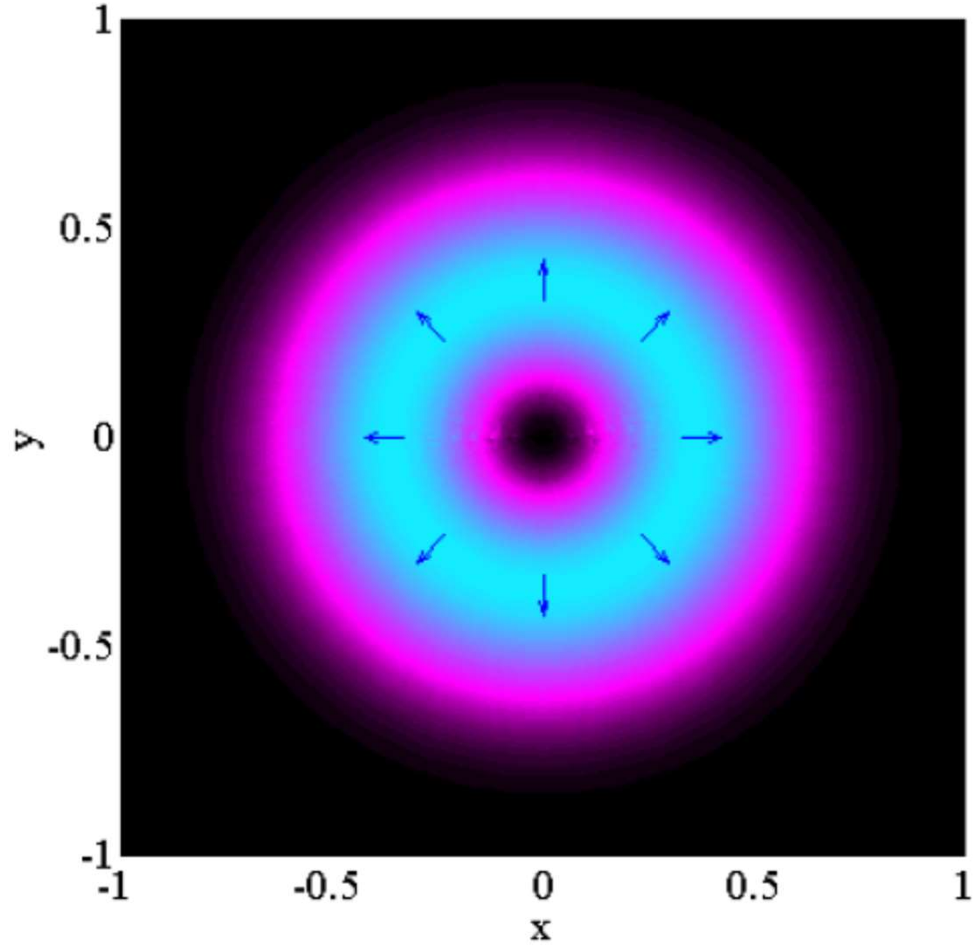

Youngworth, Brown, Optics express 7, 77-87 (2000)

Beams with quantized angular momentum

Basic exact solutions to the wave equations

$$\boxed{\psi_{\mathbf{k}}(\mathbf{r}) = \exp\left(\mathrm{i}\mathbf{k}\mathbf{r}\right),}$$ – plane waves

$$\boxed{\psi_{klm}(\mathbf{r}) = \sqrt{\frac{2\pi}{kr}}\, J_{l+1/2}(kr)\, Y_{lm}(\theta_r, \varphi_r),}$$ – spherical waves

$$\boxed{\psi_{\varkappa m k_z}(\mathbf{r}) = J_m(\varkappa\rho)\exp\left[\mathrm{i}(m\varphi_r + k_z z)\right]}$$ – cylindrical waves (Bessel beams)

$$\hat{l}_z = [\hat{\boldsymbol{r}} \times \hat{\boldsymbol{p}}]_z = -i\frac{\partial}{\partial \phi_r}$$

K.Y. Bliokh, et al.,
PRL 99 (2007) 190404

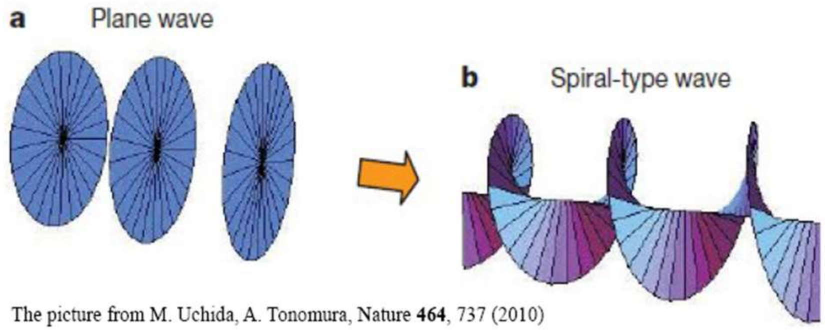

The picture from M. Uchida, A. Tonomura, Nature **464**, 737 (2010)

Generalizations for relativistic bosons and fermions
are straightforward!

The uncertainty relation:
the definite L_z implies indefinite azimuthal angle!

$$\langle(\Delta L_z)^2\rangle\langle(\Delta \sin\phi_r)^2\rangle \geq \frac{1}{4}\langle\cos\phi_r\rangle^2$$

P. Carruthers, M.M. Nieto,
Rev. Mod. Phys. **40**, 411 (1968)

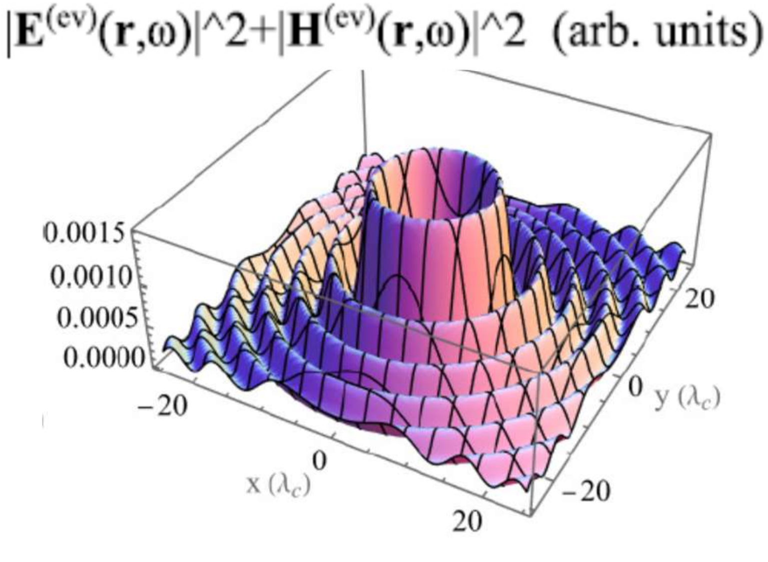

Doughnut- (or bagel-, Brezel-) shaped
spatial distribution


Цилиндрическая волна
с угловым моментом = 0

First Observation of Photons Carrying Orbital Angular Momentum in Undulator Radiation

J. Bahrdt, K. Holldack, P. Kuske, R. Müller, M. Scheer, and P. Schmid
Helmholtz-Zentrum Berlin, Albert-Einstein-Straße 15, 12489 Berlin, Germany
(Received 26 February 2013; published 15 July 2013)

Photon beams of 99 eV energy carrying orbital angular momentum (OAM) have been observed in the 2nd harmonic off-axis radiation of a helical undulator at the 3rd generation synchrotron radiation light source BESSY II. For detection, the OAM carrying photon beam was superimposed with a reference beam without OAM. The interference pattern, a spiral intensity distribution, was recorded in a plane perpendicular to the propagation direction. The orientation of the observed spiral structure is related to the helicity of the undulator radiation. Excellent agreement between measurements and simulations has been found.

DOI: 10.1103/PhysRevLett.111.034801

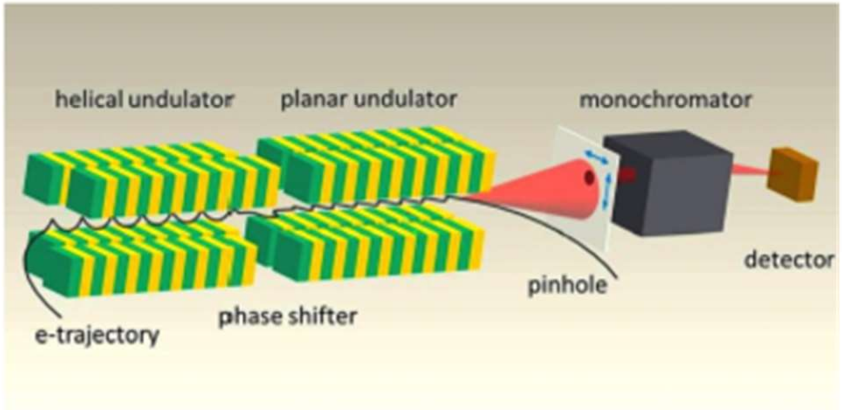

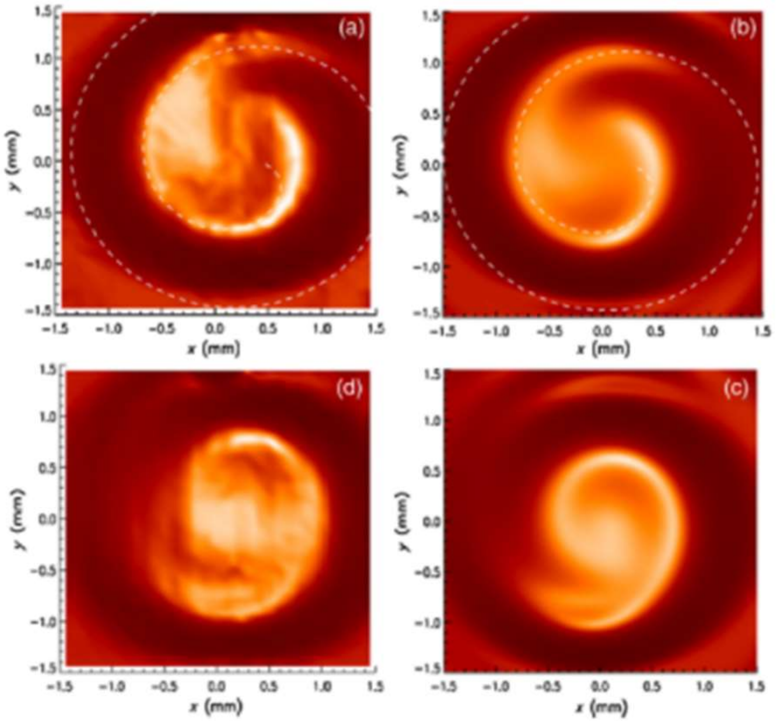

Classically: the radiation is twisted always when the electron trajectory is helical!

PRL **118,** 094801 (2017) PHYSICAL REVIEW LETTERS week ending 3 MARCH 2017

Angular Momentum of Twisted Radiation from an Electron in Spiral Motion

M. Katoh,[1,2,*] M. Fujimoto,[1,2] H. Kawaguchi,[3] K. Tsuchiya,[4] K. Ohmi,[4] T. Kaneyasu,[5] Y. Taira,[6] M. Hosaka,[7] A. Mochihashi,[7] and Y. Takashima[7]

[1]*Institute for Molecular Science, National Institutes of Natural Sciences, Okazaki 444-8585, Japan*
[2]*Sokendai (the Graduated University for Advanced Studies), Okazaki 444-8585, Japan*
[3]*Muroran Institute of Technology, Muroran 050-0071, Japan*
[4]*High Energy Accelerator Research Organization (KEK), Tsukuba 305-0801, Japan*
[5]*Saga Light Source, Tosu 841-0005 Japan*
[6]*National Institute of Advanced Industrial Science and Technology (AIST), Tsukuba 305-8568, Japan*
[7]*Nagoya University, Nagoya 464-0814, Japan*

(Received 10 October 2016; published 27 February 2017)

We theoretically demonstrate for the first time that a single free electron in circular or spiral motion emits twisted photons carrying well-defined orbital angular momentum along the axis of the electron circulation, in adding to spin angular momentum. We show that, when the electron velocity is relativistic, the radiation field contains harmonic components and the photons of lth harmonic carry $l\hbar$ total angular momentum for each. This work indicates that twisted photons are naturally emitted by free electrons and are more ubiquitous in laboratories and in nature than ever thought.

DOI: 10.1103/PhysRevLett.118.094801

PHYSICAL REVIEW LETTERS **124,** 192001 (2020)

Featured in Physics

Doing Spin Physics with Unpolarized Particles

Igor P. Ivanov *
CFTP, Instituto Superior Tecnico, Universidade de Lisboa, Lisbon 1049-001, Portugal

Nikolai Korchagin †
Institute of Modern Physics, Chinese Academy of Sciences, Lanzhou 730000, China

Alexandr Pimikov ‡
Institute of Modern Physics, Chinese Academy of Sciences, Lanzhou 730000, China
and Research Institute of Physics, Southern Federal University, Rostov-na-Donu 344090, Russia

Pengming Zhang §
School of Physics and Astronomy, Sun Yat-sen University, Zhuhai 519082, China

(Received 4 December 2019; accepted 8 April 2020; published 13 May 2020)

Twisted, or vortex, particles refer to freely propagating non-plane-wave states with helicoidal wave fronts. In this state, the particle possesses a nonzero orbital angular momentum with respect to its average propagation direction. Twisted photons and electrons have been experimentally demonstrated, and creation of other particles in twisted states can be anticipated. If brought in collisions, twisted states offer a new degree of freedom to particle physics, and it is timely to analyze what new insights may follow. Here, we theoretically investigate resonance production in twisted photon collisions and twisted e^+e^- annihilation and show that these processes emerge as a completely novel probe of spin and parity-sensitive observables in fully inclusive cross sections with unpolarized initial particles. This is possible because the initial state with a nonzero angular momentum explicitly breaks the left-right symmetry even when averaging over helicities. In particular, we show how one can produce almost 100% polarized vector mesons in unpolarized twisted e^+e^- annihilation and how to control its polarization state.

DOI: 10.1103/PhysRevLett.124.192001

Beams with quantized angular momentum

The first generation of vortex electrons

- M. Uchida and A. Tonomura, Nature 464, 737 (2010),
- J. Verbeeck, et al., Nature 467 (2010) 301–304,
- B. J. McMorran, et al., Science 331, 192 (2011)

- The highest electron energy is 300 keV
- The highest angular momentum so far is ~ 1000!
- The smallest spot size is 0.1 nm!

Atomic scale!

Two main methods:

Spiral phase plates | Gratings with a fork dislocation

Spiral phase plate

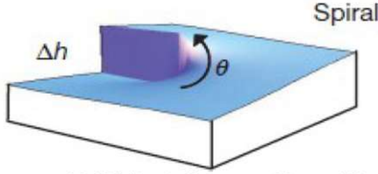

M. Uchida, A. Tonomura, Nature **464**, 737 (2010)

Diffraction grating with an edge dislocation made of Pt foil

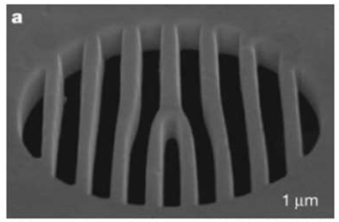

J. Verbeeck, et al., Nature **467**, 301 (2010)

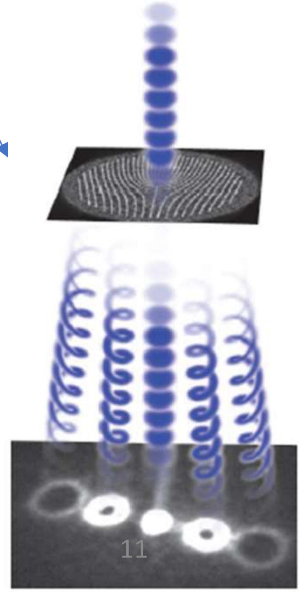

Beams with quantized angular momentum

Vortex electrons: the probability current has an azimuthal component
(recall the Bohmian interpretation of QM)

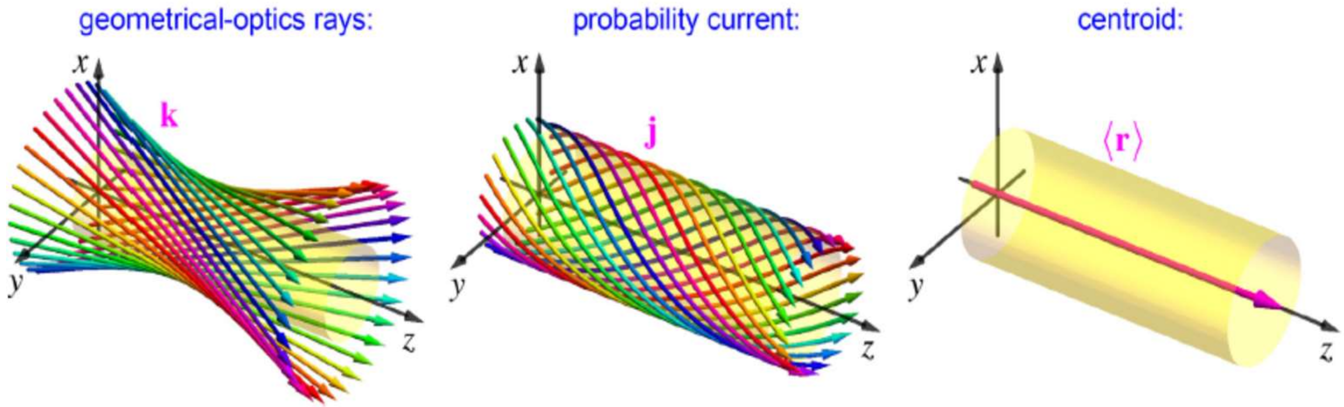

K.Y. Bliokh et al. / Physics Reports 690 (2017) 1–70

The electron magnetic moment can be huge!

$$\mathbf{M} = \frac{1}{2c}\frac{\int \mathbf{r}\times\mathbf{j}_e\, d^3\mathbf{r}}{\int \rho\, d^3\mathbf{r}} = \frac{e}{2m_e c}\langle\mathbf{L}\rangle$$

$$\mu \propto \mu_B(\mathbf{l}+2\mathbf{s})$$

If the OAM is large, $l_z \equiv m \gg \hbar$, then $\mu \gg \mu_B$!

Twisted photons generated in neutron stars

Relativistic Landau states in a magnetic field

$$\boldsymbol{H} = \{0, 0, H\} \qquad H_c = 4.4 \times 10^9 \text{ T}$$

$$\Psi_i(x) = N_i^{\uparrow} \begin{pmatrix} (m+\varepsilon)\Phi_{s,\ell-1/2}(\rho)e^{-i\varphi/2} \\ 0 \\ p_z \Phi_{s,\ell-1/2}(\rho)e^{-i\varphi/2} \\ -ieH\Phi_{s,\ell+1/2}(\rho)e^{i\varphi/2} \end{pmatrix} e^{-it\varepsilon + i\ell\varphi + ip_z z}$$

The evolved photon state:

$$|\gamma\rangle_{ev} = \sum_{\lambda=\pm 1} \int \frac{d^3k}{(2\pi)^3} |\boldsymbol{k}, \lambda\rangle S_{fi}^{(1)} = (\varepsilon - \varepsilon') \sum_{\lambda=\pm 1} \mathcal{F} \int_0^{2\pi} d\varphi_k |\boldsymbol{k}, \lambda\rangle e^{i(\ell-\ell')\varphi_k}.$$

DK, Di Piazza, PRD 108, 063007 (2023); Pavlov, DK, PRD 109, 036017 (2024)

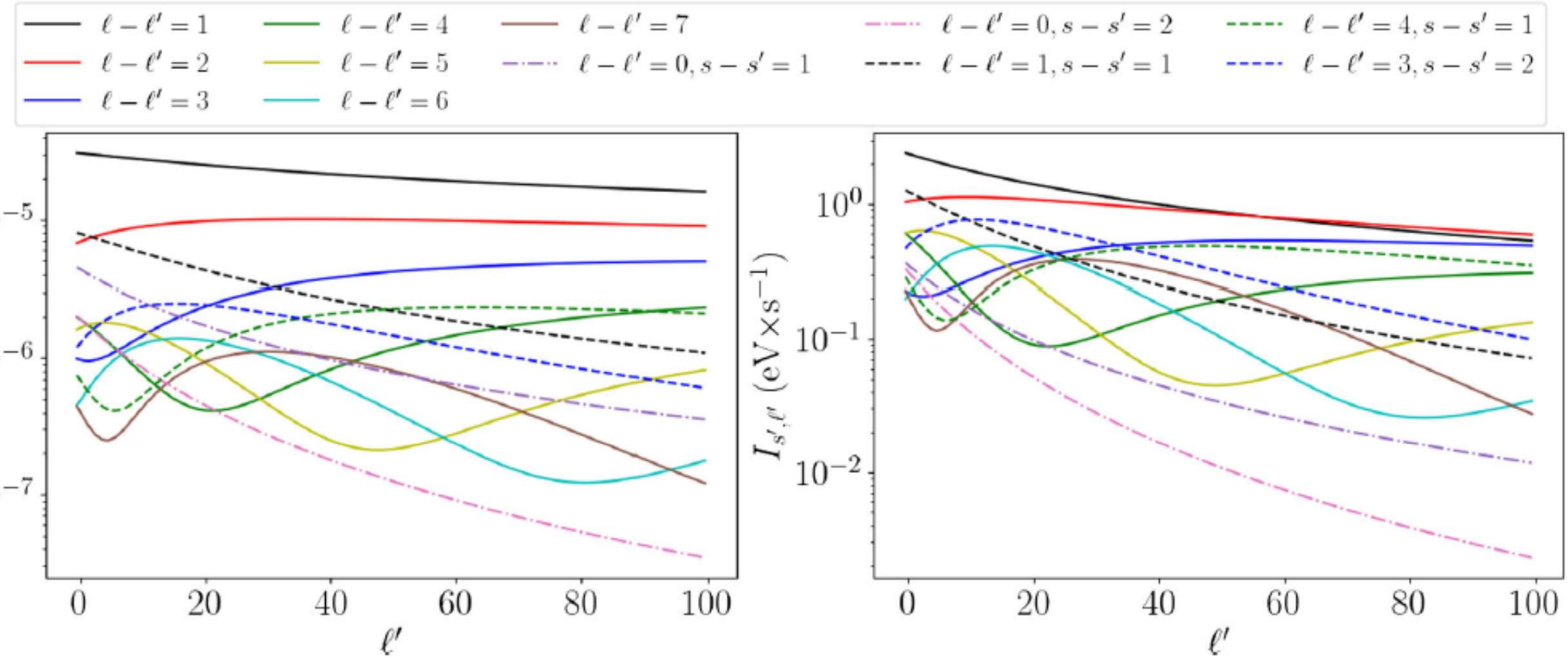

FIG. 1. The emission probability (31) (left) and the corresponding intensity (32) (right) for $H = H_c$, $p_z = 10^{-3}mc$, and no spin flip. For the solid lines, $s = s' = 20$; the dashed lines correspond to the twisted photons with a simultaneous change of the radial quantum number, $s \to s' \neq s$; and the dash-dotted lines correspond to the untwisted photons with the TAM $j_z = \ell - \ell' = 0$.

DK, Di Piazza, PRD 108, 063007 (2023); Pavlov, DK, PRD 109, 036017 (2024)

Vortex/twisted neutrons

LETTER

doi:10.1038/nature15265

Controlling neutron orbital angular momentum

Charles W. Clark[1], Roman Barankov[2], Michael G. Huber[3], Muhammad Arif[3], David G. Cory[4,5,6,7] & Dmitry A. Pushin[6,8]

Rule of twos:

- Energy of 20 meV
- Wavelength of 2 Å
- Speed of 2000 m/s

At the National Institute of Standards and Technology (NIST), USA: Created in a 20 MW reactor, cooled in a cryogenic moderator to 20K, and transported through 30 m of neutron guides.

E = 11 meV, wavelength = 0.27 nm ,
Transverse coherence length: 60 nm – 1 μm
Beam diameter: 15 mm
Fluence ~ 10^5 – 10^7 neutrons/cm^2*sec.

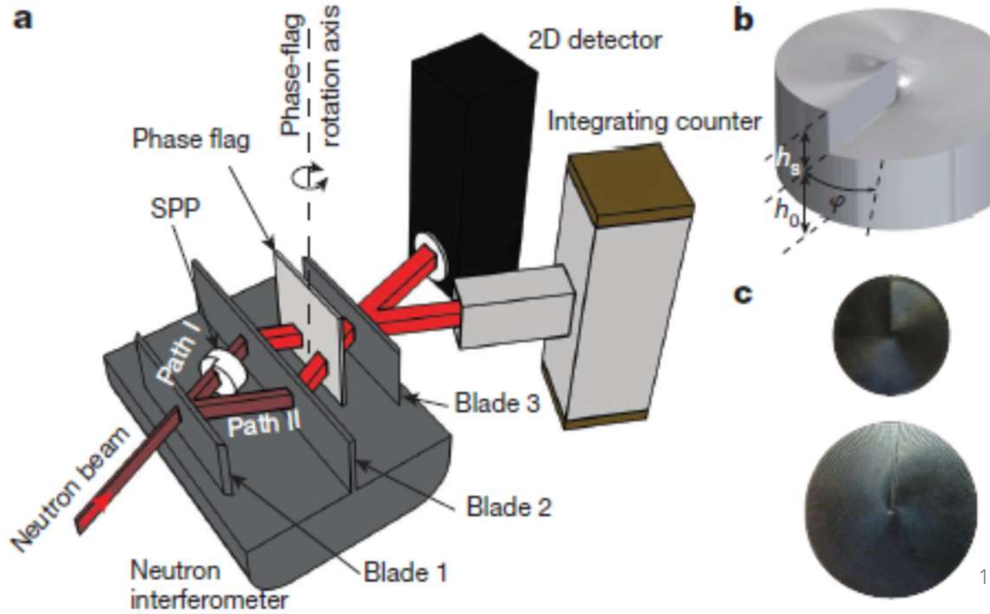

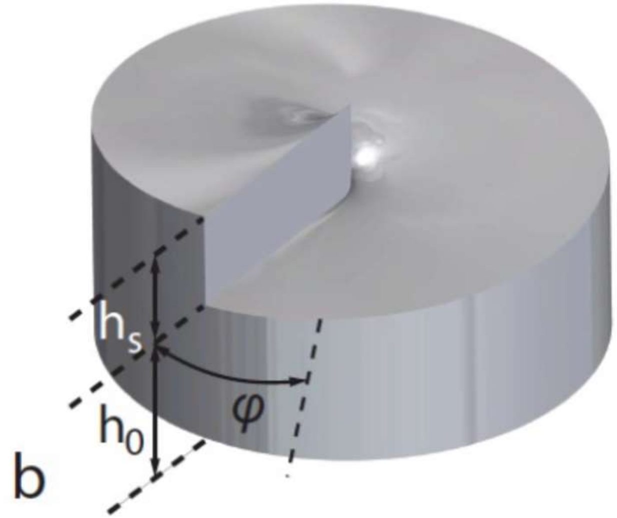

Aluminum spiral phase plates for neutrons

$$h = h_0 + \frac{h_s \varphi}{2\pi}$$

Phase of wavefunction increases linearly with azimuthal angle φ.

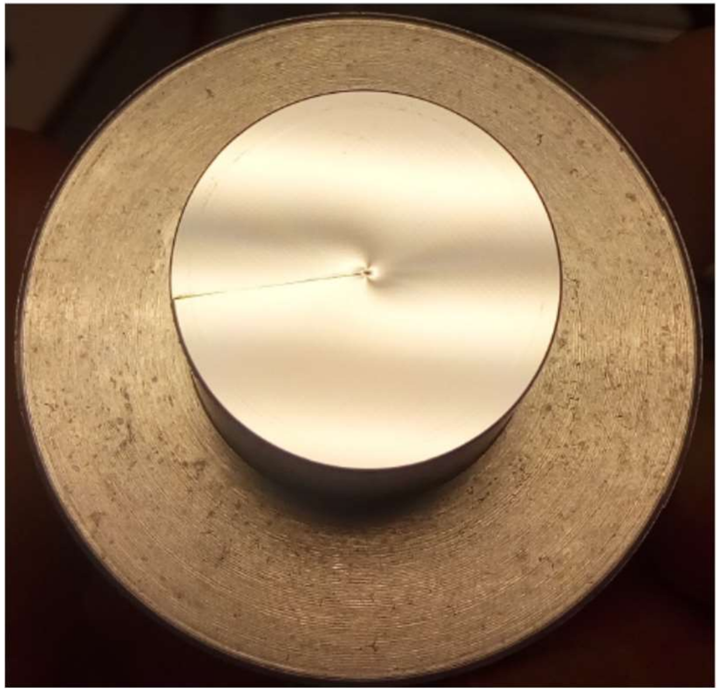

SPPs as seen from above, 25 mm diameter respectively. Milled from Al 6061 dowel by diamond turning.

h_s = 112 μ per 2π phase step.

Index of refraction $n = 1 - 2.43 \times 10^{-6}$

Control phase of λ =0.271 nm wave motion with 0.1 mm dimensional figure!

Visualization of the neutron transverse coherence length

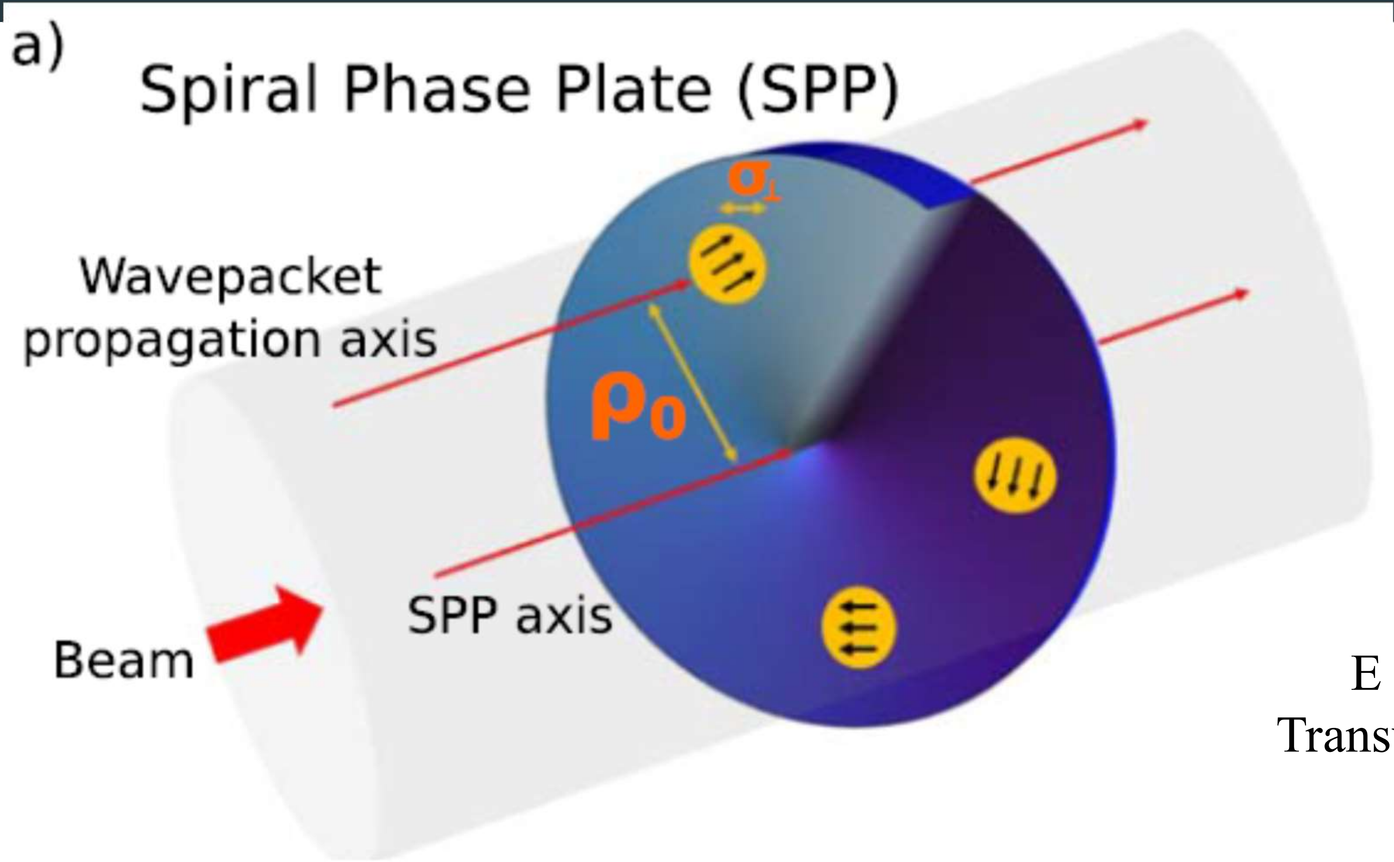

Recall Bohmian interpretation of QM!

E = 11 meV, wavelength = 0.27 nm ,
Transverse coherence length: 60 nm – 1 µm
Beam diameter: 15 mm

Vortex/twisted neutrons

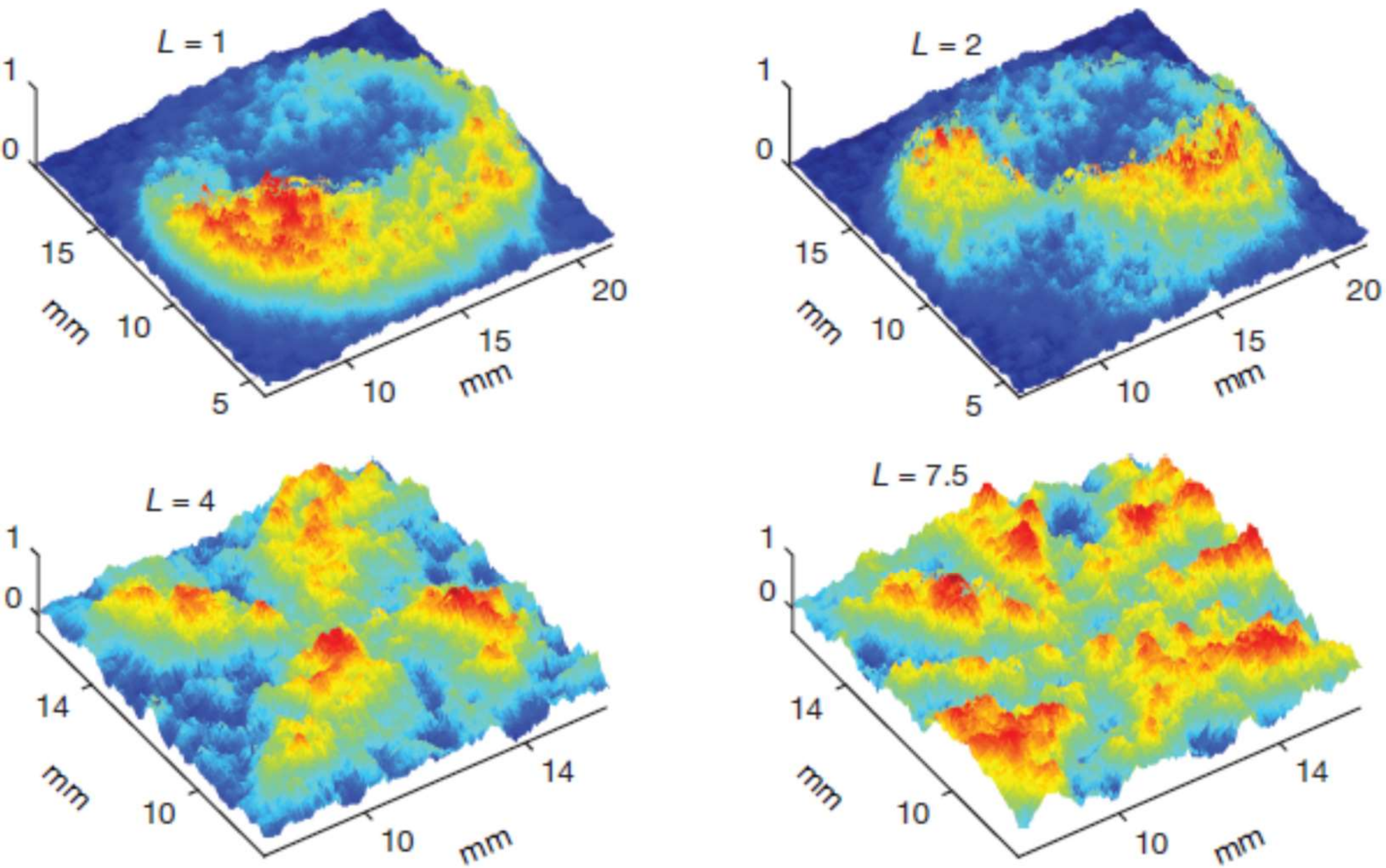

Figure 2 | OAM interferograms. Spatial distribution of the neutron counts in the 2D detector[30] of the neutron interferometer for four SPPs, with values of $L = 1, 2, 4$ and 7.5, as labelled. The horizontal and vertical positions on the 2D neutron detector are shown in millimetres. For the integer values of L these distributions display the simple OAM interference pattern expressed in equation (2); for $L = 7.5$ we have the superposition of OAM modes given by equation (4) in Methods. The 2D detector is a centroid-type event-counting detector with a spatial resolution of 100 µm and an 18% quantum efficiency (that is, counts registered per neutron incident on the detector). Its operation is shot-noise (Poisson-noise) limited in this regime. The neutron counts were collected over 3.5 days and normalized by the maximal pixel count, which is about 45.

Research Article Vol. 24, No. 20 | 3 Oct 2016 | OPTICS EXPRESS 22528
Optics EXPRESS

Holography with a neutron interferometer

Dusan Sarenac,[1,2,*] Michael G. Huber,[3] Benjamin Heacock,[4,5] Muhammad Arif,[3] Charles W. Clark,[3,6] David G. Cory,[2,7,8,9] Chandra B. Shahi,[6,10] and Dmitry A. Pushin[1,2]

[1] Department of Physics, University of Waterloo, Waterloo, ON, N2L3G1, Canada
[2] Institute for Quantum Computing, University of Waterloo, Waterloo, ON, N2L3G1, Canada
[3] National Institute of Standards and Technology, Gaithersburg, MD 20899, USA
[4] North Carolina State University, Raleigh, North Carolina 27695, USA
[5] Triangle Universities Nuclear Laboratory, Durham, North Carolina 27708, USA
[6] Joint Quantum Institute, College Park, MD 20742, USA
[7] Department of Chemistry, University of Waterloo, Waterloo, ON, N2L3G1, Canada
[8] Perimeter Institute for Theoretical Physics, Waterloo, ON, N2L2Y5, Canada
[9] Canadian Institute for Advanced Research, Toronto, Ontario, M5G 1Z8, Canada
[10] Physics and Engineering Physics Department, Tulane University, New Orleans, LA 70188, USA
* dsarenac@uwaterloo.ca

Abstract: We use a Mach-Zehnder interferometer to perform neutron holography of a spiral phase plate. The object beam passes through a spiral phase plate, acquiring the phase twist characteristic of orbital angular momentum states. The reference beam passes through a fused silica prism, acquiring a linear phase gradient. The resulting hologram is a fork dislocation image, which could be used to reconstruct neutron beams with various orbital angular momenta. This work paves the way for novel applications of neutron holography, diffraction and imaging.

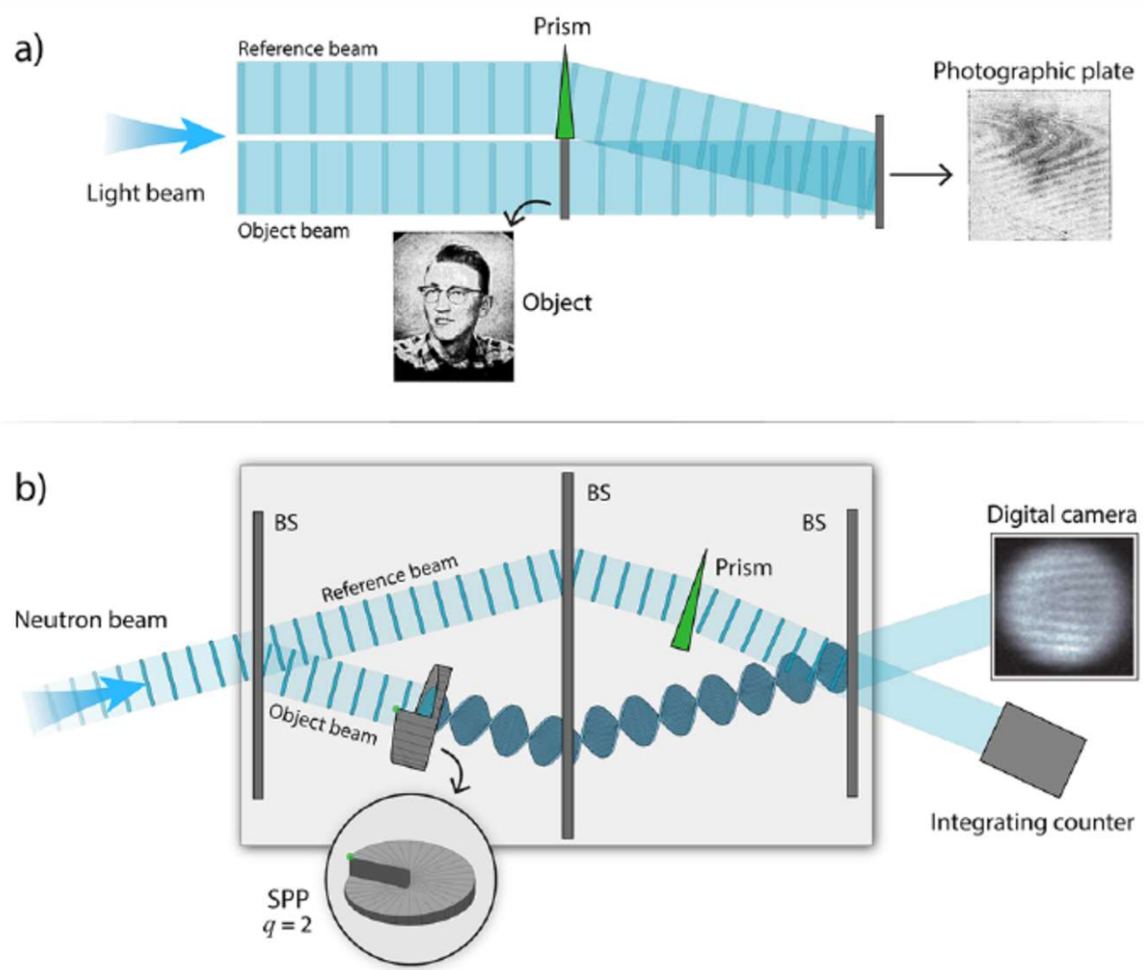

«Note that the experiment is an expectation valued measurement over many events, each of which involves only a single neutron. That is, there is one neutron at a time in the interferometer and the hologram is build up from an incoherent superposition of many events»

Twisted atoms and ions

RESEARCH

RESEARCH ARTICLE

QUANTUM PHYSICS

Vortex beams of atoms and molecules

Alon Luski[1]†, Yair Segev[1]†‡, Rea David[1], Ora Bitton[1], Hila Nadler[1], A. Ronny Barnea[2], Alexey Gorlach[3], Ori Cheshnovsky[2], Ido Kaminer[3], Edvardas Narevicius[1]*

Angular momentum plays a central role in quantum mechanics, recurring in
microscopic interactions of light and matter to the macroscopic behavior of su
intrinsic orbital angular momentum (OAM), are now regularly generated with
photons and electrons. Thus far, the creation of a vortex beam of a noneleme
demonstrated experimentally. We present vortex beams of atoms and molec
supersonic beams of helium atoms and dimers off transmission gratings. Thi
be applied to most atomic and molecular gases. Our results may open new fron
additional degree of freedom of OAM to probe collisions and alter fundament

August 2021!

Wavelength = 90 pm,
Transverse coherence length ~ 840 nm

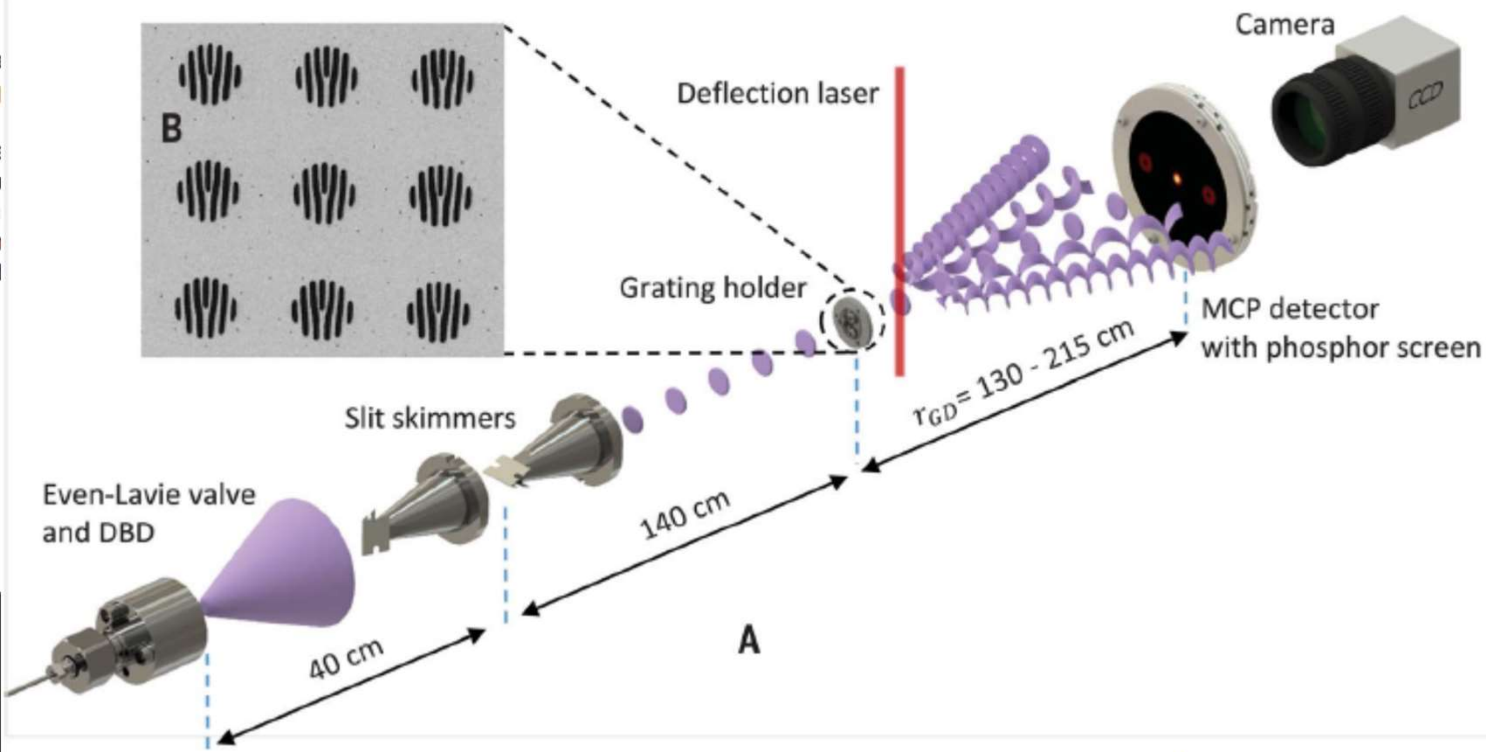

Luski et al., Science 373, 1105 (2021)

Twisted atoms and ions

Helium and neon atoms and dimers

Wavelength = 90 pm,

Transverse coherence length ~ 840 nm

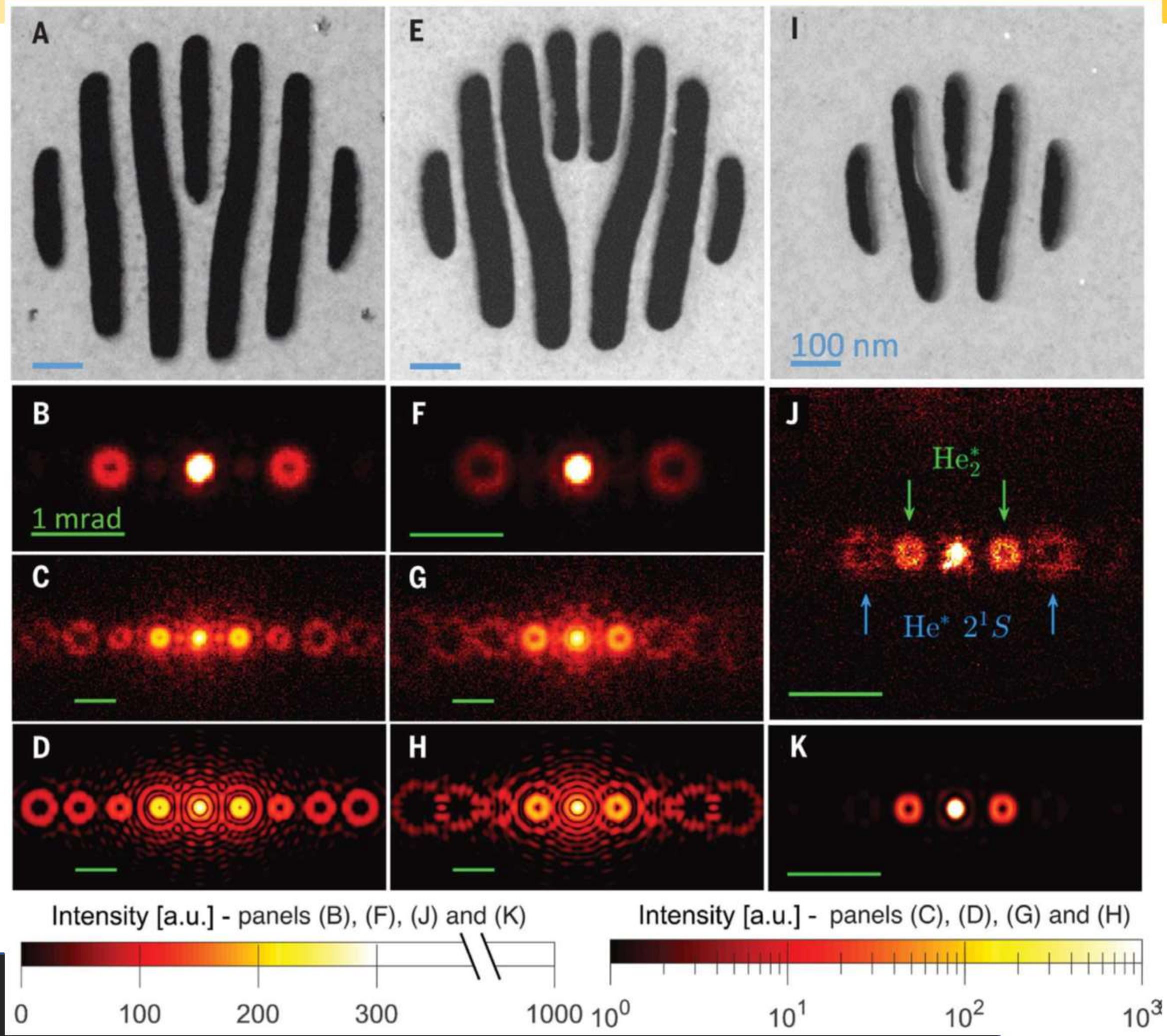

Luski et al., Science 373, 1105 (2021)

The statement
(rather optimistic)

it is possible to obtain twisted photons, electrons, protons, ions, …

in pretty much all QED/QCD/weak processes:

non-linear Thomson/Compton scattering, e-e+ annihilation, Cherenkov emission, etc.

We choose the final states as twisted ones

and calculate the probability

(which can be lower or higher)!

On a deeper level
(moderately optimistic)

1. The choice of the final states implies existence of such a detector

For instance, one can calculate the probability for the generation of gamma-ray vortices via non-linear Compton sc., but how do we make such a detector?

2. Without specifying the detector, one can judge if the state is twisted

via the formalism of evolved states:

$$|e', \gamma\rangle = \left(\hat{1} + \hat{S}^{(1)}\right)|\text{in}\rangle \qquad \hat{S} = \hat{1} + \hat{S}^{(1)} = \hat{1} - ie\int d^4x\, \hat{j}^{\mu}(x)\hat{A}_{\mu}(x)$$

3. Once we know that a twisted state is generated,

we can detect it with whichever detector we have!

The probability to detect a twisted state →

→ the probability <u>amplitude</u> to generate the twisted state

Differences from the standard approach:

1. No dependence on the detector choice: we derive the state as it is
2. The dependence on a phase of an S-matrix element is kept

QFT approach for photon emission

$$e \to e' + \gamma \qquad |e', \gamma\rangle^{(\mathrm{ev})} = \hat{S}^{(1)} |\mathrm{in}\rangle$$

The field operators:

$$\hat{\boldsymbol{A}}(\boldsymbol{r}, t) = \sum_{\lambda_\gamma = \pm 1} \int \frac{d^3k}{(2\pi)^3} \left(\boldsymbol{A}_{\boldsymbol{k}\lambda_\gamma}(\boldsymbol{r}, t)\, \hat{c}_{\boldsymbol{k}\lambda_\gamma} + \mathrm{h.c.} \right),$$

$$\hat{\boldsymbol{E}}(\boldsymbol{r}, t) = -\frac{\partial \hat{\boldsymbol{A}}(\boldsymbol{r}, t)}{\partial t} = \sum_{\lambda_\gamma = \pm 1} \int \frac{d^3k}{(2\pi)^3}\, i\omega \left(\boldsymbol{A}_{\boldsymbol{k}\lambda_\gamma}(\boldsymbol{r}, t)\, \hat{c}_{\boldsymbol{k}\lambda_\gamma} - \mathrm{h.c.} \right),$$

$$\hat{\boldsymbol{H}}(\boldsymbol{r}, t) = \nabla \times \hat{\boldsymbol{A}}(\boldsymbol{r}, t) = \sum_{\lambda_\gamma = \pm 1} \int \frac{d^3k}{(2\pi)^3}\, i\mathrm{k} \times \left(\boldsymbol{A}_{\boldsymbol{k}\lambda_\gamma}(\boldsymbol{r}, t)\, \hat{c}_{\boldsymbol{k}\lambda_\gamma} - \mathrm{h.c.} \right)$$

$$\boldsymbol{A}_{\boldsymbol{k}\lambda_\gamma}(\boldsymbol{r}, t) = \frac{\sqrt{4\pi}}{\sqrt{2\omega}}\, \boldsymbol{e}_{\boldsymbol{k}\lambda_\gamma}\, e^{-i\omega t + i\boldsymbol{k}\cdot\boldsymbol{r}},$$

QFT approach for photon emission

1. The probability amplitude in momentum space:

$$S_{fi}^{(1)} = \langle f_e, f_\gamma | \hat{S}^{(1)} | \text{in} \rangle = \langle \mathbf{p}, \lambda; \mathbf{k}, \lambda_\gamma | \hat{S}^{(1)} | \text{in} \rangle$$

2. The probability amplitude in space-time:

$$\langle 0 | \hat{\psi}(\boldsymbol{r}_e, t_e) \hat{\mathbf{A}}(\boldsymbol{r}_\gamma, t_\gamma) | e', \gamma \rangle^{(\text{ev})}$$

$$|e', \gamma\rangle = \left(\hat{1} + \hat{S}^{(1)}\right) |\text{in}\rangle$$

$$= \int \frac{d^3 p}{(2\pi)^3} \frac{d^3 k}{(2\pi)^3} \sum_{\lambda_\gamma = \pm 1} \sum_{\lambda = \pm 1/2} \frac{\sqrt{4\pi}}{\sqrt{2\omega}} \frac{1}{\sqrt{2\varepsilon}} u_{p\lambda} \, \boldsymbol{e}_{k\lambda_\gamma} \, S_{fi}^{(1)} \, e^{-i\varepsilon t_e + i \boldsymbol{p} \cdot \boldsymbol{r}_e - i\omega t_\gamma + i \boldsymbol{k} \cdot \boldsymbol{r}_\gamma}$$

The 2-particle entangled state:

$$|e', \gamma\rangle = |\text{in}\rangle + \sum_{\lambda'=\pm 1/2, \lambda_\gamma = \pm 1} \int \frac{d^3k}{(2\pi)^3} \frac{d^3p'}{(2\pi)^3} |\mathbf{p}', \lambda'\rangle \otimes |\mathbf{k}, \lambda_\gamma\rangle \, S_{fi}^{(1)}$$

If the electron is detected in a state $\langle f_e^{(\text{det})}|$ the photon evolved state becomes

$$|\gamma\rangle = \langle f_e^{(\text{det})}|e_{\text{in}}\rangle|0_\gamma\rangle + \sum_{\lambda', \lambda_\gamma} \int \frac{d^3k}{(2\pi)^3} \frac{d^3p'}{(2\pi)^3} |\mathbf{k}, \lambda_\gamma\rangle \, (f_e^{(\text{det})}(\mathbf{p}', \lambda'))^* \, S_{fi}^{(1)},$$

The electron detector function

If the electron is a plane wave:

$$\delta(\mathbf{p}'_\perp + \mathbf{k}_\perp) = \delta(p'_x + k_x)\delta(p'_y + k_y) = \frac{1}{p'_\perp}\,\delta(p'_\perp - k_\perp)\left(\delta(\phi' - (\phi_k - \pi))\Big|_{\phi_k \in [\pi, 2\pi]} + \delta(\phi' - (\phi_k + \pi))\Big|_{\phi_k \in [0, \pi]}\right)$$

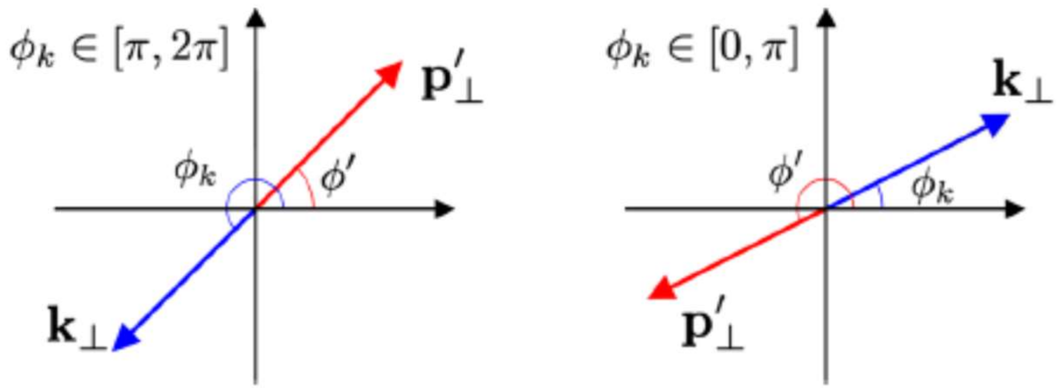

$$|\gamma\rangle = \langle f_e^{(\mathrm{det})}|e_{\mathrm{in}}\rangle|0_\gamma\rangle + \sum_{\lambda', \lambda_\gamma} \int \frac{d^3k}{(2\pi)^3}\frac{d^3p'}{(2\pi)^3}\,|\mathbf{k}, \lambda_\gamma\rangle\,(f_e^{(\mathrm{det})}(\mathbf{p}', \lambda'))^*\,S_{fi}^{(1)},$$

3 delta-functions   4 delta-functions

The photon evolved state is a plane wave!

Quantum tomography naturally arises in photon emission

(even if the detected electron is a plane wave)

$$\mathcal{W}(\mathbf{r},t) = \frac{1}{8\pi}\langle\gamma|\hat{\boldsymbol{E}}^2(\boldsymbol{r},t) + \hat{\boldsymbol{H}}^2(\boldsymbol{r},t)|\gamma\rangle - \frac{\varepsilon_0}{4\pi} = \frac{1}{4\pi}\left(\left|\langle 0|\hat{\boldsymbol{E}}(\boldsymbol{r},t)|\gamma\rangle\right|^2 + \left|\langle 0|\hat{\boldsymbol{H}}(\boldsymbol{r},t)|\gamma\rangle\right|^2\right),$$

The vacuum contribution

$$\langle 0|\hat{\boldsymbol{E}}(\boldsymbol{r},t)|\gamma\rangle = \sum_{\lambda_\gamma}\int \frac{d^3k}{(2\pi)^3} i\omega \boldsymbol{A}_{\boldsymbol{k}\lambda_\gamma}(\boldsymbol{r},t)\, S_{fi}^{(\mathrm{GM})}(\mathbf{k},\lambda_\gamma),$$

$$\boldsymbol{A}_{\boldsymbol{k}\lambda_\gamma}(\boldsymbol{r},t) = \frac{\sqrt{4\pi}}{\sqrt{2\omega}}\boldsymbol{e}_{\boldsymbol{k}\lambda_\gamma}\, e^{-i\omega t + i\boldsymbol{k}\cdot\boldsymbol{r}},$$

$$S_{fi}^{(\mathrm{GM})}(\mathbf{k},\lambda_\gamma) = \sum_{\lambda'}\int \frac{d^3p'}{(2\pi)^3}\,(f_e^{(\mathrm{det})}(\mathbf{p}',\lambda'))^*\, S_{fi}^{(1)}(\mathbf{p}',\lambda',\mathbf{k},\lambda_\gamma)$$

Quantum tomography naturally arises in photon emission

(even if the detected electron is a plane wave)

$$\frac{1}{4\pi}\left|\langle 0|\hat{\boldsymbol{E}}(\boldsymbol{r},t)|\gamma\rangle\right|^2 = \frac{1}{4\pi}\sum_{\lambda_\gamma,\tilde{\lambda}_\gamma}\int\frac{d^3K}{(2\pi)^3}\frac{d^3k}{(2\pi)^3}\,\boldsymbol{E}^*_{\tilde{\lambda}_\gamma}(\mathbf{K}-\mathbf{k}/2)\cdot\boldsymbol{E}_{\lambda_\gamma}(\mathbf{K}+\mathbf{k}/2)\,e^{-it(\omega(\mathbf{K}+\mathbf{k}/2)-\omega(\mathbf{K}-\mathbf{k}/2))+i\mathbf{r}\cdot\mathbf{k}} =$$

$$= \int\frac{d^3K}{(2\pi)^3}\,\mathcal{W}(\mathbf{r},\mathbf{K},t),$$

The photon Wigner function:

$$\mathcal{W}(\mathbf{r},\mathbf{K},t) = \frac{1}{4\pi}\sum_{\lambda_\gamma,\tilde{\lambda}_\gamma}\int\frac{d^3k}{(2\pi)^3}\,\boldsymbol{E}^*_{\tilde{\lambda}_\gamma}(\mathbf{K}-\mathbf{k}/2)\cdot\boldsymbol{E}_{\lambda_\gamma}(\mathbf{K}+\mathbf{k}/2)\,e^{-it(\omega(\mathbf{K}+\mathbf{k}/2)-\omega(\mathbf{K}-\mathbf{k}/2))+i\mathbf{r}\cdot\mathbf{k}},$$

$$\boldsymbol{E}_{\lambda_\gamma}(\mathbf{k}) = \frac{i\omega\sqrt{4\pi}}{\sqrt{2\omega n^2}}\,e_{\mathbf{k}\lambda_\gamma}\sum_{\lambda}\int\frac{d^3p}{(2\pi)^3}\,f_e^{(\mathrm{in})}(\mathbf{p},\lambda)S^{(1)}_{fi}(\mathbf{p},\lambda,\mathbf{k},\lambda_\gamma)$$

The first marginal distribution:

$$\int d^3x\, \mathcal{W}(\mathbf{r},\mathbf{K},t) = \frac{\omega}{2n^2}\left|\sum_\lambda \int \frac{d^3p}{(2\pi)^3}\, f_e^{(\mathrm{in})}(\mathbf{p},\lambda) S_{fi}^{(1)}(\mathbf{p},\lambda,\mathbf{k},\lambda_\gamma)\right|^2 =$$

$$= \frac{\omega}{2n^2}(2\pi)^2 \frac{T}{2\pi}\delta(\varepsilon(\mathbf{p}) - \varepsilon' - \omega)\, \frac{4\pi}{2\omega(\mathbf{k})n^2(\omega(\mathbf{k}))2\varepsilon(\mathbf{p})2\varepsilon'(\mathbf{p}')} \left|\sum_\lambda f_e^{(\mathrm{in})}(\mathbf{p},\lambda)\, M_{fi}(\mathbf{p},\mathbf{k},\lambda,\lambda_\gamma)\right|^2_{\mathbf{p}=\mathbf{p}'+\mathbf{k}}$$

The customary probability in momentum space!

The second marginal distribution:

$$\int \frac{d^3K}{(2\pi)^3}\, \mathcal{W}(\mathbf{r},\mathbf{K},t) = \frac{1}{4\pi}\left|\langle 0|\hat{\boldsymbol{E}}(\boldsymbol{r},t)|\gamma\rangle\right|^2$$

The probability in space-time!

Quantum tomography naturally arises in photon emission

(even if the detected electron is a plane wave)

1. The energy density of the photon evolved state in space-time depends on the shape of the incoming electron packet:

a snapshot of the electron wave function!

$$\frac{1}{4\pi}\left|\langle 0|\hat{\boldsymbol{E}}(\boldsymbol{r},t)|\gamma\rangle\right|^2 \propto \left|\psi_e^{(\mathrm{in})}(\boldsymbol{r},t)\right|^2$$

2. Complementary measurements – the phase space and the Wigner functions come into play!

PHYSICAL REVIEW A **90**, 012118 (2014)

Structured x-ray beams from twisted electrons by inverse Compton scattering of laser light

D. Seipt,[1,*] A. Surzhykov,[1] and S. Fritzsche[1,2]
[1]Helmholtz-Institut Jena, Fröbelstieg 3, 07743 Jena, Germany
[2]Universität Jena, Institut für Theoretische Physik, 07743 Jena, Germany

(Received 23 April 2014; revised manuscript received 27 June 2014; published 31 July 2014)

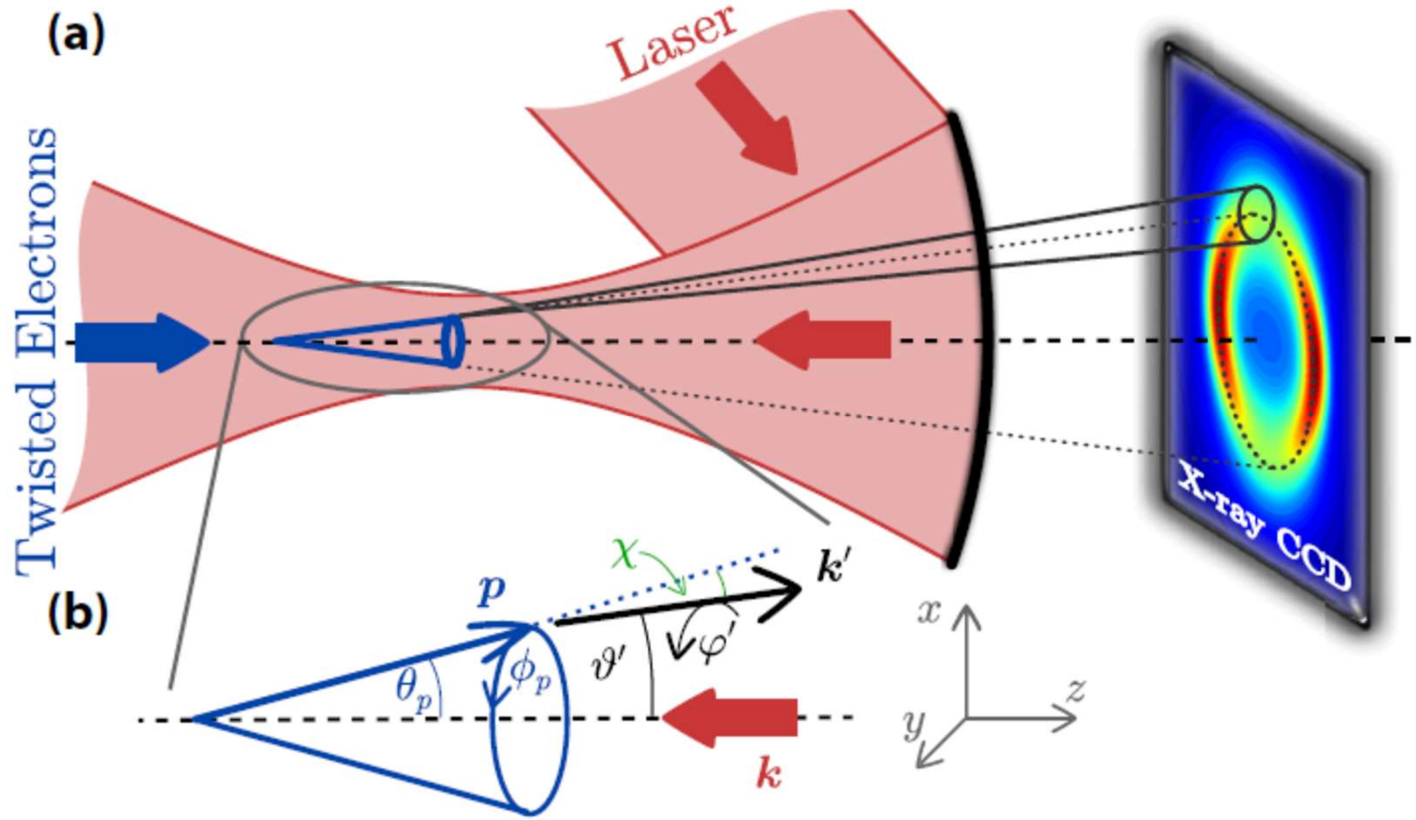

Now let's detect the electron in the generalized measurement scheme

1. Projective (von Neumann) measurements: the errors are vanishing
2. Generalized (realistic) measurements: some errors can be finite:
   a. Without the loss of information
   b. With the loss of information

The electron is detected in a state

$$|e'\rangle = \int \frac{d^3p'}{(2\pi)^3} f_P(\mathbf{p}')|\mathbf{p}', \lambda'\rangle$$

The detector function can be of the Gaussian form:

$$f_P(\mathbf{p}') \propto \prod_i \exp\left\{-(p'_i - \langle p_i \rangle)^2/(2\sigma_i)^2\right\}$$

Generation of vortex particles via generalized measurements

ITMO

Consider 2 → 2 scattering/annihilation:
en → en, np → np, ep → ep, e+mu → e+mu, etc.

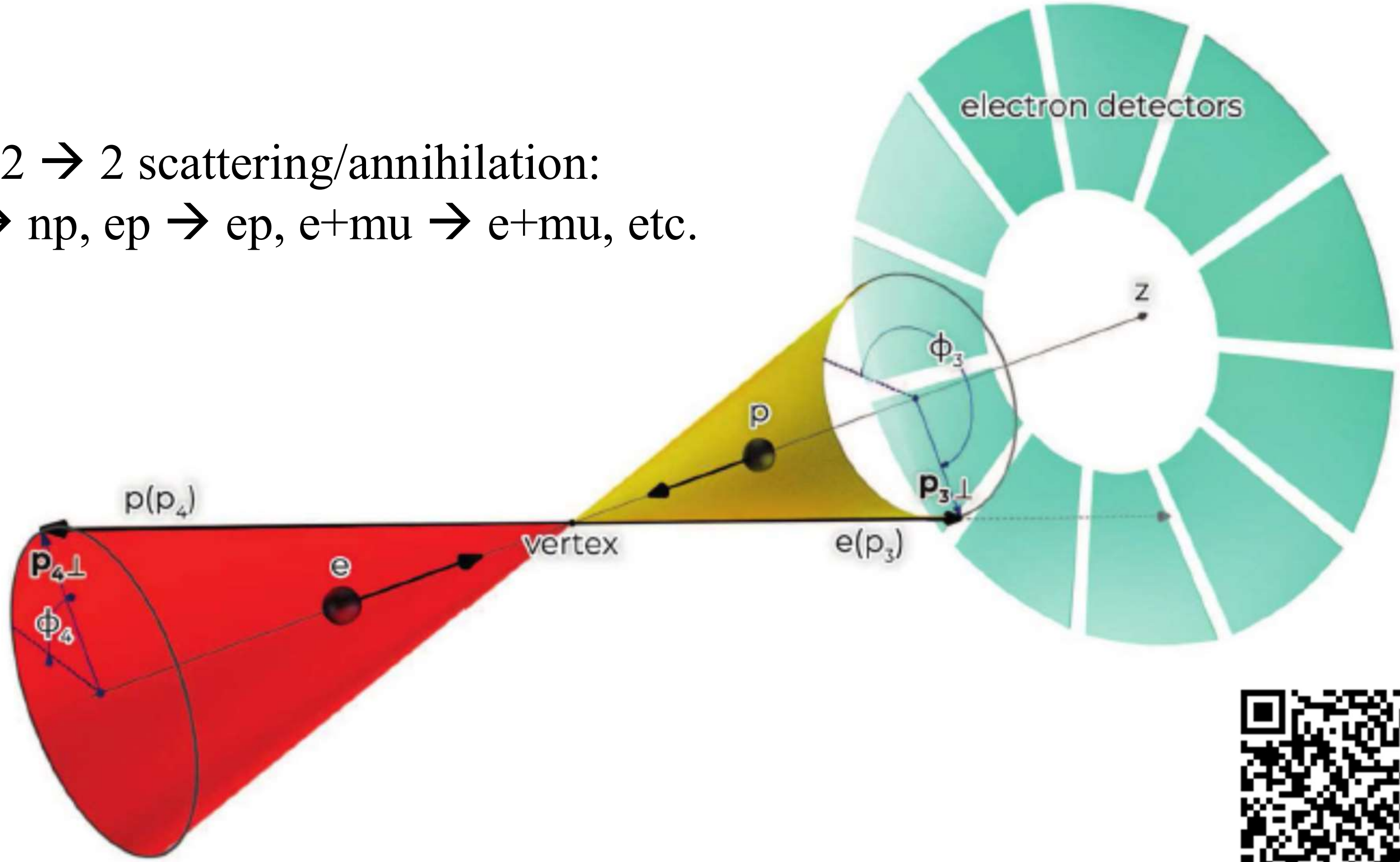

Generation of vortex particles via generalized measurements

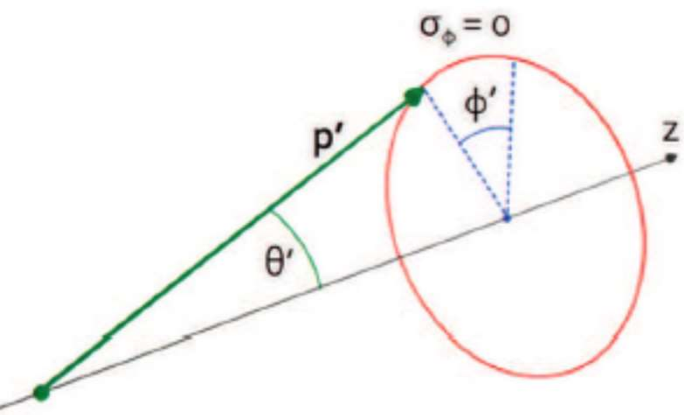

Projective: a plane-wave state

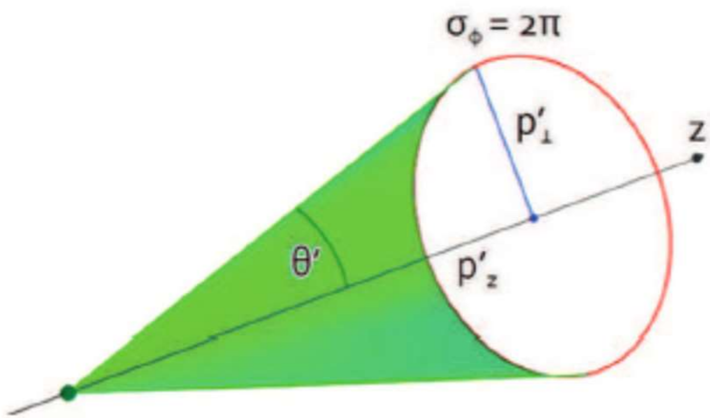

Projective: a Bessel beam

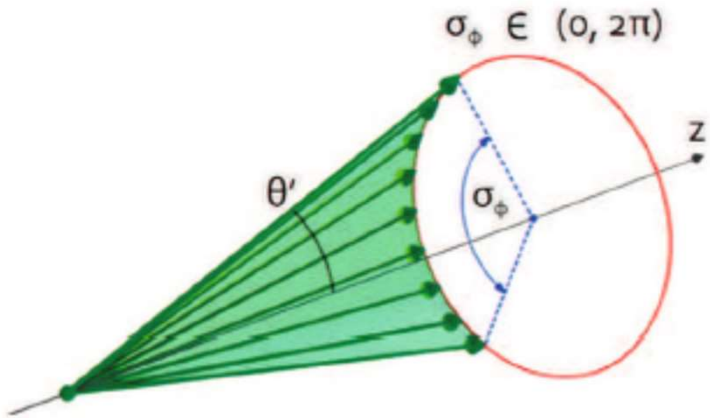

Generalized: a Bessel-like wave packet

D.K., et al., Eur. Phys. J. C 83, 372 (2023)

Generation of vortex particles via generalized measurements

When the uncertainty approaches 2 pi:

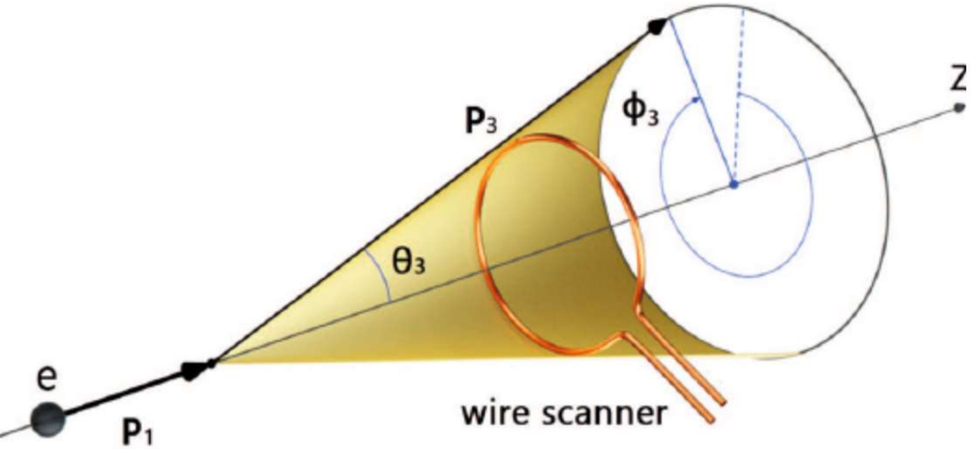

Cherenkov radiation:
the electron scattering angle
is ~ 10^-6 – 10^-5 rad!

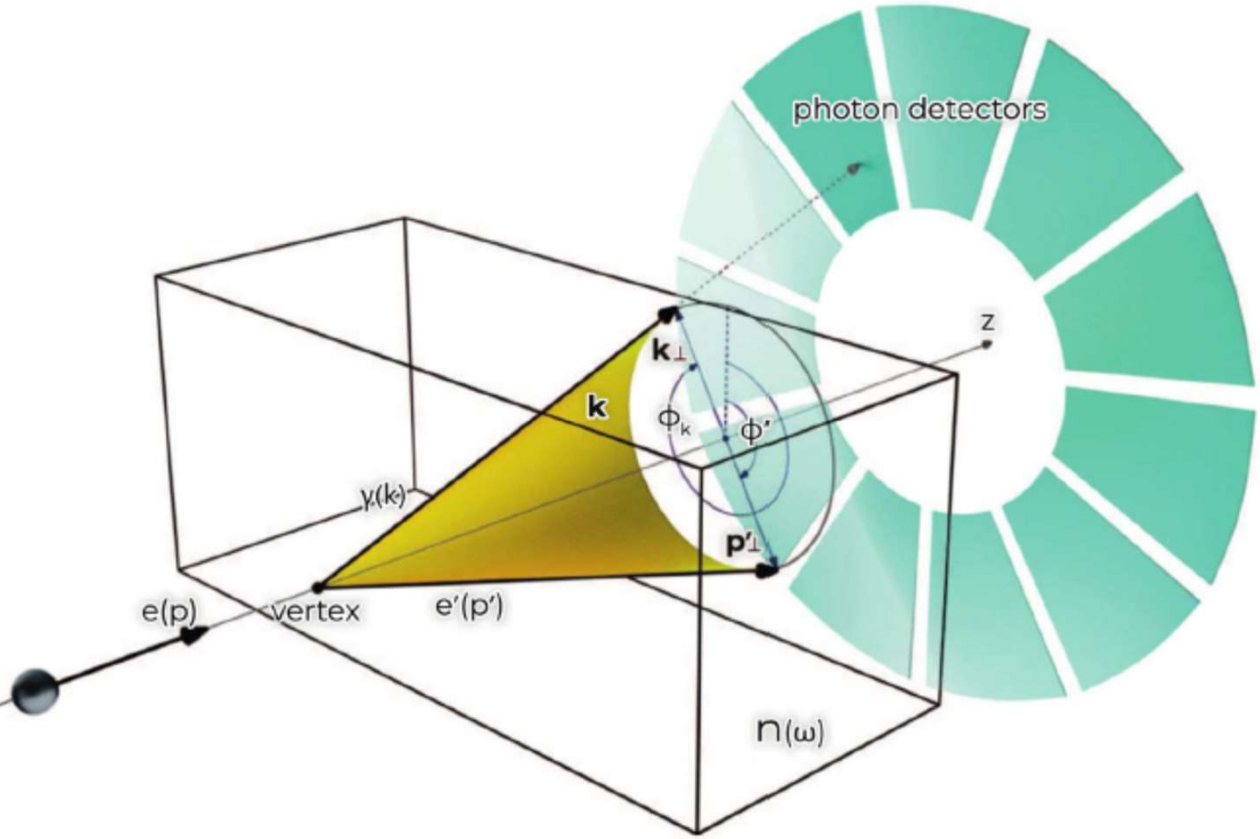

D.K., et al., Eur. Phys. J. C 83, 372 (2023)

First Observation of Photons Carrying Orbital Angular Momentum in Undulator Radiation

J. Bahrdt, K. Holldack, P. Kuske, R. Müller, M. Scheer, and P. Schmid
Helmholtz-Zentrum Berlin, Albert-Einstein-Straße 15, 12489 Berlin, Germany
(Received 26 February 2013; published 15 July 2013)

Photon beams of 99 eV energy carrying orbital angular momentum (OAM) have been observed in the 2nd harmonic off-axis radiation of a helical undulator at the 3rd generation synchrotron radiation light source BESSY II. For detection, the OAM carrying photon beam was superimposed with a reference beam without OAM. The interference pattern, a spiral intensity distribution, was recorded in a plane perpendicular to the propagation direction. The orientation of the observed spiral structure is related to the helicity of the undulator radiation. Excellent agreement between measurements and simulations has been found.

DOI: 10.1103/PhysRevLett.111.034801

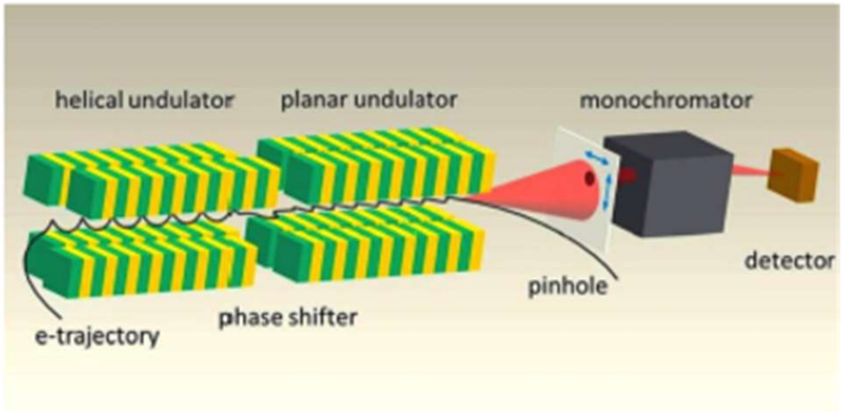

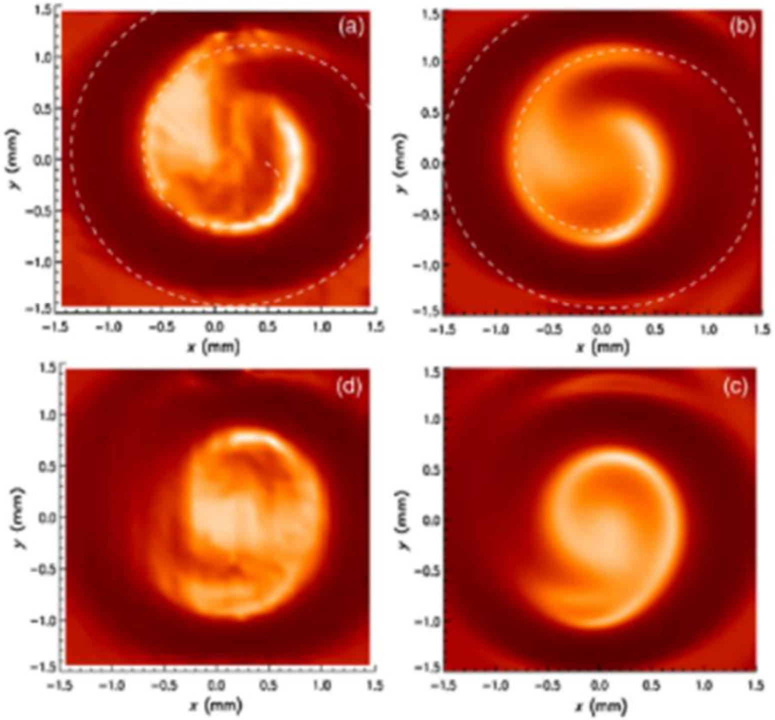

Here we have an effective projection to the state with the OAM=0,

detected at the vanishing scattering angle

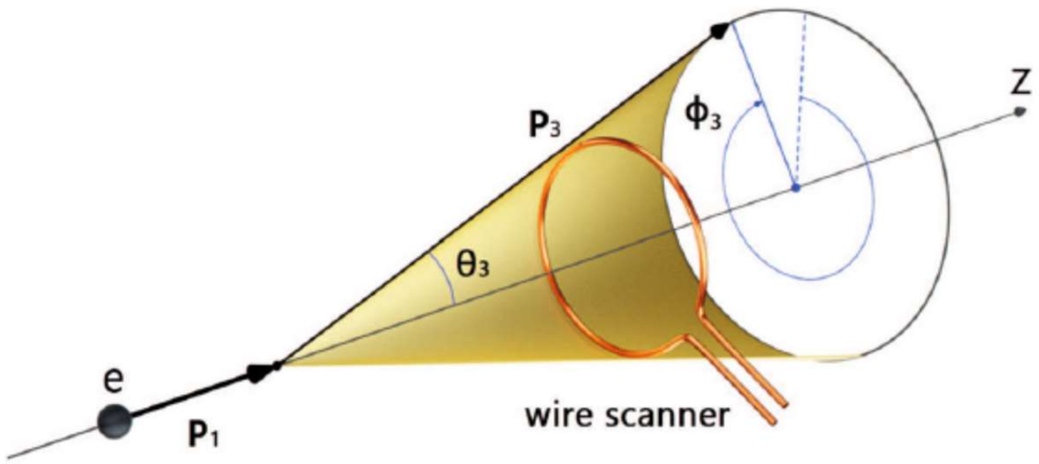

Undulator radiation at XFEL:

the electron scattering angles are ~ 10^-6 – 10^-3 rad!

D.K., et al., Eur. Phys. J. C 83, 372 (2023)

Generation of vortex particles via generalized measurements

When the uncertainty approaches 2 pi:

$$\mathbf{A}^{(\mathrm{ev})}(\mathbf{k},\omega) = \int_0^{2\pi} \frac{d\phi'}{2\pi} \sum_{\lambda_\gamma=\pm 1} e\, S_{fi}^{(\mathrm{pw})}$$

The vector potential of the evolved state

Example 1: Cherenkov radiation

$$\hat{j}_z^{(\gamma)} \mathbf{A}^{(\mathrm{ev})} = (\lambda - \lambda') \mathbf{A}^{(\mathrm{ev})},$$

Example 2: Non-linear Compton scattering at the s-th harmonic/helical undulator

$$\hat{j}_z^{(\gamma)} \mathbf{A}_{(\mathrm{g})}^{(\mathrm{ev},s)} = (s + \lambda - \lambda') \mathbf{A}_{(\mathrm{g})}^{(\mathrm{ev},s)},$$ - with a Volkov electron

$$\hat{j}_z^{(\gamma)} \mathbf{A}_{(\mathrm{g})}^{(f,s)} = (s + m - \lambda') \mathbf{A}_{(\mathrm{g})}^{(f,s)},$$ - with a Bessel-Volkov electron

D.K., et al., Eur. Phys. J. C 83, 372 (2023)

A POVM scheme: does the loss of information destroy the photon vorticity?

$$\hat{\rho}_\gamma^{(\mathrm{POVM})} = \mathrm{Tr}\{\hat{F}_e^{(\mathrm{det})}\,\hat{\rho}_{e\gamma}\}$$

If the plane-wave detector is used:

$$\hat{F}_e^{(\mathrm{det})} = \sum_{\lambda'} \int \frac{d^3p'}{(2\pi)^3}\, F_e^{(\mathrm{det})}(\mathbf{p}', \lambda')\, |\mathbf{p}', \lambda'\rangle\langle \mathbf{p}', \lambda'|,$$

$$\hat{\rho}_\gamma = T \sum_{\lambda', \lambda_\gamma, \lambda'_\gamma} \int d\Gamma\, F_e^{(\mathrm{det})}(\mathbf{p}', \lambda')\, T_{fi}^{(\lambda'\lambda_\gamma)} \left(T_{fi}^{(\lambda'\lambda'_\gamma)}\right)^* |\mathbf{k}, \lambda_\gamma\rangle\langle \mathbf{k}, \lambda'_\gamma|, \Rightarrow \langle \hat{J}_z \rangle = 0$$

For a cylindrical-basis detector:

$$\hat{F}_{tw-e}^{(\mathrm{det})} = \sum_{m'=-\infty}^{\infty} \sum_{\lambda'} \int \frac{dp'_z}{2\pi} \frac{p'_\perp\, dp'_\perp}{2\pi}\, F_{tw-e}^{(\mathrm{det})}(p'_z, p'_\perp, m', \lambda')\, |p'_z, p'_\perp, m', \lambda'\rangle\langle p'_z, p'_\perp, m', \lambda'| \Rightarrow \langle \hat{J}_z \rangle \neq 0$$

Even with the loss of information,
the twisted photons are still generated!

On the way to experiments at accelerators….

The project of the relativistic vortex electron source at Joint Institute for Nuclear research (Dubna):

- First at a 6-MeV electron photo-gun,
- Then at the 200-MeV linac

https://rscf.ru/en/project/23-62-10026/

Vortex electrons, ions, nuclei,… - generation strategies at accelerators

Planar-to-circular beam adapters:
analogous to Hermite-Gaussian → Laguerre-Gaussian conversion of light

- Round beams for circular colliders:

elimination of betatron resonances, increase of the beam lifetime.

- Flat beams for linear colliders:

to increase the luminosity and to suppress the beamstrahlung, and to enhance the efficiency of generation of em radiation from X-rays to THz (say, for Smith-Purcell radiation).

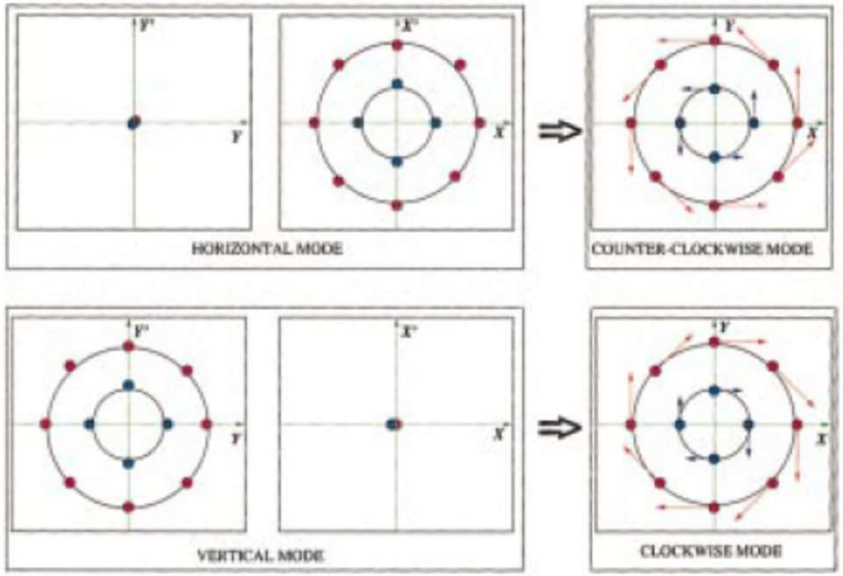

Burov A, Nagaitsev S and Derbenev Y, *Phys. Rev.* E **66** 016503, 2002

6. ***Berechnung der Bahn von Kathodenstrahlen im axialsymmetrischen elektromagnetischen Felde;***
von H. Busch

Vor einiger Zeit habe ich eine Methode der e/m-Bestimmung angegeben[1]), die — ursprünglich nur zu Unterrichtszwecken ausgearbeitet — sich im Laufe der Versuche als sehr geeignet zu Präzisionsmessungen erwies.[2]) Im folgenden sollen die theoretischen Grundlagen der Methode mitgeteilt werden.

Das Meßverfahren beruht auf der bekannten Erscheinung, daß ein von einem Punkte P ausgehendes divergentes Kathodenstrahlbündel durch ein longitudinales, d. h. parallel zur Bündelachse gerichtetes Magnetfeld wieder in einem Punkte P' vereinigt, „fokussiert" wird. Aus der Entfernung l zwischen Brennpunkt P' und Ausgangspunkt P in Verbindung mit der Stärke $\mathfrak{H}$ des Magnetfeldes erhält man eine Beziehung zwischen der Elektronengeschwindigkeit v und ihrer spezifischen Ladung $\eta = \frac{e}{m}$, die, in üblicher Weise mit einer zweiten, etwa aus dem von den Elektronen durchfallenen Entladungspotential V zu gewinnenden Gleichung kombiniert, η und v einzeln zu berechnen gestattet.

Im Falle eines homogenen Magnetfeldes ist jene Beziehung sehr einfach; hier bilden die Elektronenbahnen die bekannten regelmäßigen Schraubenlinien und die besagte Beziehung lautet:

$$l = \frac{2\pi v}{\eta \mathfrak{H}} \cos\alpha, \tag{1}$$

worin α den Winkel bedeutet, den die Anfangsrichtung der Elektronenbahn mit $\mathfrak{H}$ bildet.[3])

1) H. Busch, Physik. Ztschr. 23. S. 438. 1922.

2) Eine solche Präzisionsbestimmung ist im hiesigen Physikalischen Institut im Gange und steht kurz vor dem Abschluß.

3) Zu beachten ist, daß wegen des Faktors $\cos\alpha$ die Abbildung des Punktes P in P' — in der Sprache der geometrischen Optik — nicht

Busch H 1926 Berechnung der Bahn von Kathodenstrahlen im axialsymmetrischen elektromagnetischen Felde *Ann. Phys.* **386** 974

The Busch theorem:
a charged beam/particle in magnetic field gets vorticity

$$\hat{H} = \frac{(\hat{\boldsymbol{p}}^{\rm kin})^2}{2m} = \frac{(\hat{\boldsymbol{p}}^{\rm can})^2}{2m} - \omega_{\rm L}\hat{L}_z^{\rm can} + \frac{m}{2}\omega_{\rm L}^2\,\rho^2$$

$$\hat{\boldsymbol{p}}^{\rm can} = \hat{\boldsymbol{p}}^{\rm kin} + e\boldsymbol{A} = -{\rm i}\nabla$$

$$\hat{\boldsymbol{L}}^{\rm can} = \boldsymbol{r}\times\hat{\boldsymbol{p}}^{\rm can} \quad \text{and} \quad \hat{\boldsymbol{L}}^{\rm kin} = \boldsymbol{r}\times\hat{\boldsymbol{p}}^{\rm kin}$$

$$\langle \hat{L}_z^{\rm kin}\rangle = \ell - m\omega_{\rm L}\langle\rho^2\rangle = \ell - 2\,{\rm sgn}(e)\,\frac{\langle\rho^2\rangle}{\rho_{\rm H}^2} \qquad \rho_{\rm H} = \sqrt{\frac{4}{|e|H}} = 2\lambda_{\rm c}\sqrt{\frac{H_{\rm c}}{H}}$$

In quantum mechanics, the canonic OAM is an integer:

$$\langle \hat{L}_z^{\rm can}\rangle = \ell, \quad \ell = 0, \pm 1, \pm 2, \ldots \qquad (\hbar=1)$$

The Busch theorem:
a charged beam/particle in magnetic field gets vorticity

$$\langle \hat{L}_z^{\mathrm{kin}} \rangle = 0 \quad \Rightarrow \quad \ell = \frac{eH}{2}\langle \rho^2 \rangle = 2\,\mathrm{sgn}(e)\,\frac{\langle \rho^2 \rangle}{\rho_{\mathrm{H}}^2} = \frac{1}{2}\,\mathrm{sgn}(e)\,\frac{\langle \rho^2 \rangle}{\lambda_{\mathrm{c}}^2}\,\frac{H}{H_{\mathrm{c}}},$$

The flux of the field through the area of the beam (classical) or of the wave packet (quantum):

$$\langle \Phi \rangle = H\pi \langle \rho^2 \rangle$$

Akin to the Aharonov-Bohm effect:

$$\Psi \to \Psi\ \exp\left\{ i\theta \frac{q}{2\pi\hbar} \left\langle \oint A dl \right\rangle \right\} = \Psi\, e^{i\ell\theta}$$

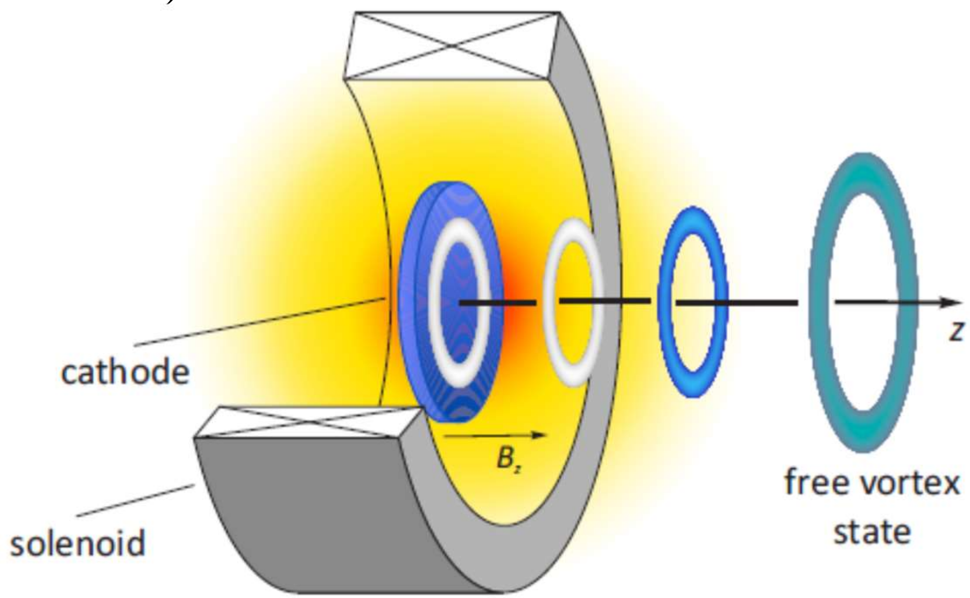

PHYSICAL REVIEW SPECIAL TOPICS - ACCELERATORS AND BEAMS 7, 123501 (2004)

Generation of angular-momentum-dominated electron beams from a photoinjector

Y.-E Sun,[1,*] P. Piot,[2,†] K.-J. Kim,[1,3] N. Barov,[4,‡] S. Lidia,[5] J. Santucci,[2] R. Tikhoplav,[6] and J. Wennerberg[2,§]
[1]*University of Chicago, Chicago, Illinois 60637, USA*
[2]*Fermi National Accelerator Laboratory, Batavia, Illinois 60510, USA*
[3]*Argonne National Laboratory, Argonne, Illinois 60439, USA*
[4]*Northern Illinois University, DeKalb, Illinois 60115, USA*
[5]*Lawrence Berkeley National Laboratory, Berkeley, California 94720, USA*
[6]*University of Rochester, Rochester, New York 14627, USA*
(Received 2 November 2004; published 22 December 2004)

Various projects under study require an angular-momentum-dominated electron beam generated by a photoinjector. Some of the proposals directly use the angular-momentum-dominated beams (e.g., electron cooling of heavy ions), while others require the beam to be transformed into a flat beam (e.g., possible electron injectors for light sources and linear colliders). In th
an angular-momentum-dominated beam produced in a ph
angular momentum on initial conditions. We also briefly dis
results of the experiment, carried out at the Fermilab/NICAI
in good agreement with theoretical and numerical models.

DOI: 10.1103/PhysRevSTAB.7.123501

Up to <L> ~ 10^8*ħ!

- UV laser, cesium telluride photocathode
- e: **4 MeV/c → 16 MeV/c** after the booster cavity

<L> is conserved during the acceleration!

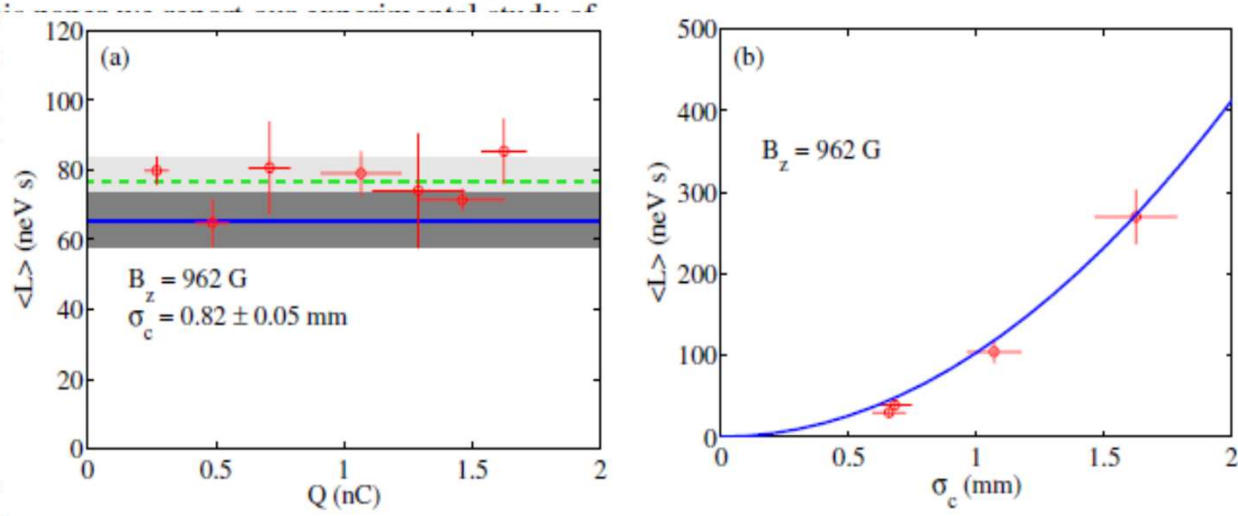

Canonical angular momentum versus charge (a) and photocathode drive-laser beam spot size (b)

Electron wave packets: reference numbers

The rms-radii in SEMs, TEMs, electron accelerators, photo-electrons, etc.:

$$\sqrt{\langle\rho^2\rangle} \sim \mathbf{1\text{-}100\ nm}$$

Example 1: a radius of the ground Landau state in the field H ~ 0.1-10 T is

$$\rho_{\rm H} = \sqrt{\frac{4}{|e|H}} \sim \mathbf{10\text{-}100\ nm}$$

Example 2: the transverse coherence length of an electron from a Tungsten photo-cathode or a field-emitter (at room temperature) is*

$$\sqrt{\langle\rho^2\rangle} \sim \mathbf{0.5\ \text{-}\ 1\ nm}$$

*Ehberger D, et al., Phys. Rev. Lett. **114,** 227601 (2015)

PRL 114, 227601 (2015) PHYSICAL REVIEW LETTERS week ending 5 JUNE 2015

Highly Coherent Electron Beam from a Laser-Triggered Tungsten Needle Tip

Dominik Ehberger,[1,2,*] Jakob Hammer,[1,2] Max Eisele,[2,†] Michael Krüger,[1,2,‡]
Jonathan Noe,[3] Alexander Högele,[3] and Peter Hommelhoff[1,2,4,§]
[1]Department of Physics, Friedrich Alexander University Erlangen-Nuremberg, Staudtstrasse 1, D-91058 Erlangen, Germany, EU
[2]Max Planck Institute of Quantum Optics, Hans-Kopfermann-Strasse 1, D-85748 Garching/Munich, Germany, EU
[3]Fakultät für Physik and Center for NanoScience (CeNS), Ludwig-Maximilians-Universität München, Geschwister-Scholl-Platz 1, 80539 München, Germany, EU
[4]Max Planck Institute for the Science of Light, Günther-Scharowsky-Strasse 1/ Building 24, D-91058 Erlangen, Germany, EU
(Received 10 December 2014; published 5 June 2015)

We report on a quantitative measurement of the spatial coherence of electrons emitted from a sharp metal needle tip. We investigate the coherence in photoemission triggered by a near-ultraviolet laser with a photon energy of 3.1 eV and compare it to dc-field emission. A carbon nanotube is brought into close proximity to the emitter tip to act as an electrostatic biprism. From the resulting electron matter wave interference fringes, we deduce an upper limit of the effective source radius both in laser-triggered and dc-field emission mode, which quantifies the spatial coherence of the emitted electron beam. We obtain (0.80 ± 0.05) nm in laser-triggered and (0.55 ± 0.02) nm in dc-field emission mode, revealing that the outstanding coherence properties of electron beams from needle tip field emitters are largely maintained in laser-induced emission. In addition, the relative coherence width of 0.36 of the photoemitted electron beam is the largest observed so far. The preservation of electronic coherence during emission as well as ramifications for time-resolved electron imaging techniques are discussed.

van Cittert–Zernicke theorem

$$r_{\mathrm{eff}} = \frac{\lambda_{\mathrm{dB}} \cdot l_{s\text{-}d}}{\pi \cdot \xi_{\perp}}$$

“We use a freestanding carbon nanotube (CNT) as an electron beam splitter, which acts as a biprism filament with nanometer radius”

At room temperature!

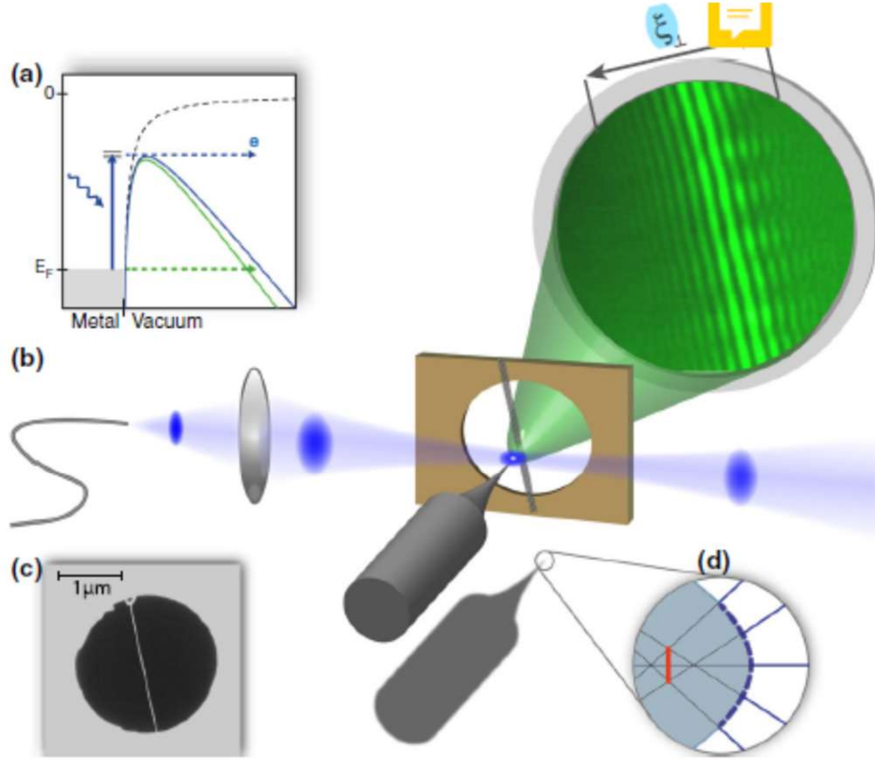

The Busch theorem: a charged beam/particle in magnetic field gets vorticity

The realistic estimate:

$$|q| = |eZ| \qquad |\ell| \approx 1.5 \times 10^{-3}\, |Z| \langle r^2 \rangle [\mathrm{nm}^2]\, |B_{z,0}| [\mathrm{T}],$$

For electrons

- H > 100 T for Tungsten at room temperature,
- Or to cool the emitter down to ~10 K: the electron inelastic mean free path in metals is ~ 10 nm - 1000 nm for of 3.5–178 K,
- Or to employ special cathodes: GaAs, ring-shaped, photo-cathode with a twisted laser, etc.

Floettmann, DK., PRA **102**, 043517 (2020); DK., New J. Phys. **23** (2021) 033048

The Busch theorem:
a charged beam/particle in magnetic field gets vorticity

1. The photon OAM can be transferred to photo-electrons

2. The electron transverse coherence length can correlate with that of the photon

3. The pulsed magnetic field higher than 1 T can be used; it is required only in the generation region!

4. Photocathodes with a ring-shaped emissive area on a non-emissive background (also, for field emission!) can be used

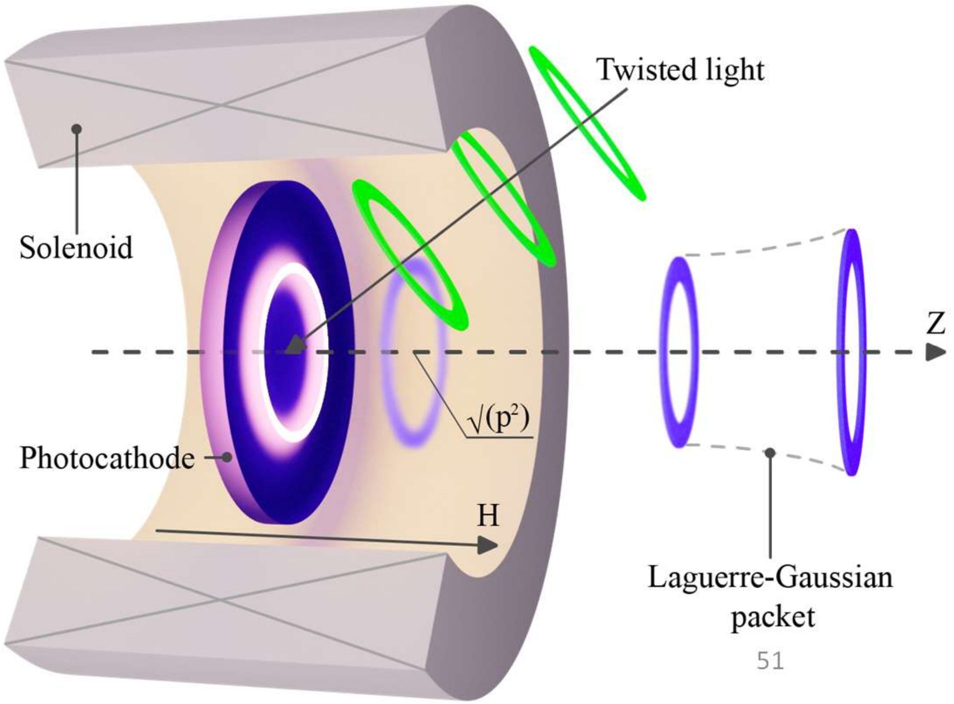

Magnetized stripping foil technique for ions

PRL **113,** 264802 (2014) PHYSICAL REVIEW LETTERS week ending 31 DECEMBER 2014

Experimental Proof of Adjustable Single-Knob Ion Beam Emittance Partitioning

L. Groening,* M. Maier, C. Xiao, L. Dahl, P. Gerhard, O. K. Kester, S. Mickat, H. Vormann, and M. Vossberg
GSI Helmholtzzentrum für Schwerionenforschung GmbH, Darmstadt D-64291, Germany

M. Chung
Ulsan National Institute of Science and Technology, Ulsan 698-798, Republic of Korea
(Received 26 September 2014; published 30 December 2014)

The performance of accelerators profits from phase-space tailoring by coupling of degrees of fre
Previously applied techniques swap the emittances among the three degrees but the set of ava
emittances is fixed. In contrast to these emittance exchange scenarios, the emittance transfer sc
presented here allows for arbitrarily changing the set of emittances as long as the product of the emit
is preserved. This Letter is the first experimental demonstration of transverse emittance transfer
an ion beam line. The amount of transfer is chosen by setting just one single magnetic field
The envelope functions (beta) and slopes (alpha) of the finally uncorrelated and repartitioned be
the exit of the transfer line do not depend on the amount of transfer.

Nitrogen: Z from +3 to +7

The foil (carbon, 200 $\mu g/cm^2$, 30 mm in diameter)

The energies: from 10s to 100s MeV/u

Nuclear Instruments and Methods in Physics Research A 767 (2014) 153–158

Contents lists available at ScienceDirect

Nuclear Instruments and Methods in Physics Research A

journal homepage: www.elsevier.com/locate/nima

ELSEVIER

Minimization of the emittance growth of multi-charge particle beams in the charge stripping section of RAON

CrossMark

Ji-Gwang Hwang[a], Eun-San Kim[a,*], Hye-Jin Kim[b,*], Dong-O Jeon[b]

[a] *Department of Physics, Kyungpook National University, Daegu 702-701, Korea*
[b] *Rare Isotope Science Project, Institute for Basic Science, Jeonmin-dong, Yuseong-gu, Daejeon, Korea*

ARTICLE INFO

Article history:
Received 20 April 2014
Received in revised form
26 July 2014
Accepted 13 August 2014
Available online 21 August 2014

Keywords:
Rare Isotope Science Project
Beam dynamics for multicharge particles
Emittance growth in dispersive section
Correction of high-order aberration

ABSTRACT

The charge stripping section of the Rare isotope Accelerator Of Newness (RAON), which is one of the critical components to achieve a high power of 400 kW with a short lianc, is a source of transverse emittance growth. The dominant effects are the angular straggling in the charge stripper required to increase the charge state of the beam and chromatic aberrations in the dispersive section required to separate the selected ion beam from the various ion beams produced in the stripper. Since the main source of transverse emittance growth in the stripper is the angular straggling, it can be compensated for by changing the angle of the phase ellipse. Therefore the emittance growth is minimized by optimizing the Twiss parameters at the stripper. The emittance growth in the charge selection section is also minimized by the correction of high-order aberrations using six sextupole magnets. In this paper, we present a method to minimize the transverse emittance growth in the stripper by changing the Twiss parameters and in the charge selection section by using sextupole magnets.

Uranium: Z from +33-34 to +77-81

Magnetized stripping foil technique for ions

The quantum Busch theorem for ions:

$$\ell = \frac{q_{\text{out}} - q_{\text{in}}}{2} H\langle\rho^2\rangle = (Z_{\text{out}} - Z_{\text{in}})\,\frac{eH}{2}\langle\rho^2\rangle$$

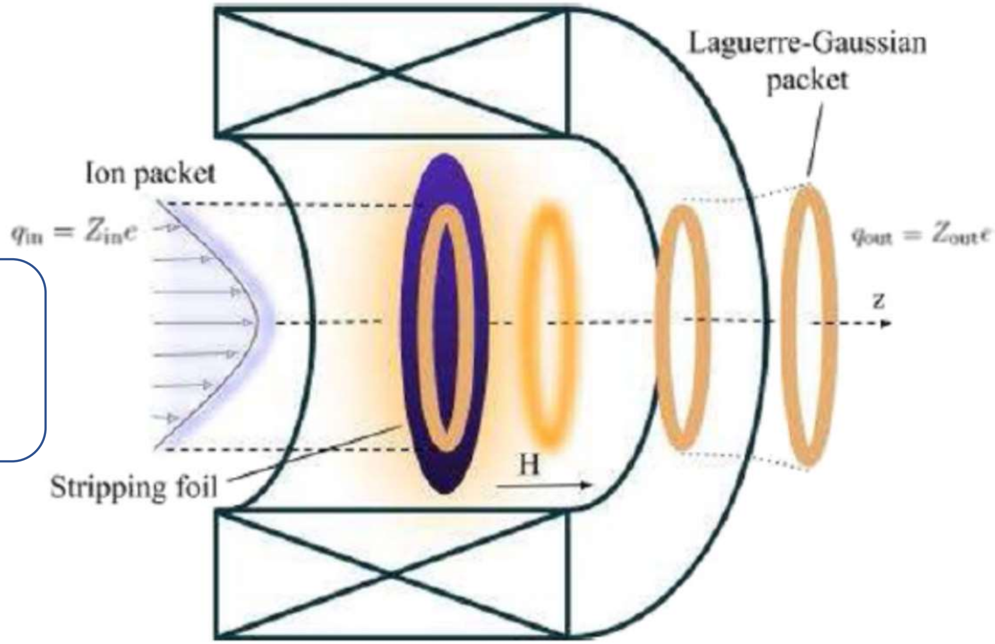

Requirements:

- Negligible space charge (no Coulomb repulsion)
- The transverse coherence larger than 100 nm at H ~ 1 T
- No emittance degradation: small scattering in the target

Magnetized stripping foil technique for ions

The general spreading law is

$$\langle \rho^2 \rangle(t) = \langle \rho^2 \rangle(0) + \frac{\partial \langle \rho^2 \rangle(0)}{\partial t}\, t + \langle u_\perp^2 \rangle\, t^2,$$

For the LG packet in the far-field (<z> >> z_R):

$$\boxed{\langle z \rangle = \frac{\langle p \rangle}{2n + |\ell| + 1}\sqrt{\langle \rho^2 \rangle(\langle z \rangle)}\sqrt{\langle \rho^2 \rangle(0)} \equiv \frac{\rho \rho_0}{\lambda}\frac{1}{2n + |\ell| + 1},}$$

For the ground mode, n= ell=0, this is the van Cittert–Zernike theorem!

Magnetized stripping foil technique for ions

Examples:

1. A 100 keV proton with $n = \ell = 0$ spreads from $\rho(0) \sim 1$ Angstrom to $1 - 100$ μm: the needed distance is $\langle z \rangle \sim 7$ mm $- 70$ cm, respectively.
2. For higher energies of $\varepsilon \sim 1$ MeV, the distance to spread from 1 nm to ~ 100 μm is $1 - 10$ meters.

Good news: $|\ell| \sim 10^2 - 10^4$

But can we really neglect scattering in the foil?
(for beams of many ions - yes)

Magnetized stripping foil technique for ions

If the final ion is an LG:

$$p_\perp \rho = 2n + |\ell| + 1,$$

$$\rho \equiv \sqrt{\langle \rho^2 \rangle}$$

$$p_\perp \equiv \sqrt{\langle p_\perp^2 \rangle}$$

Decreases as the LG packet spreads

From the Busch theorem

Assuming n << ell we get $p_\perp \approx \dfrac{|\ell|}{\rho} = \dfrac{|Z_{\text{in}} - Z_{\text{out}}|}{2\rho} \dfrac{\rho^2}{\lambda_c^2} \dfrac{H}{H_c},$

We require that the opening angle of the momentum cone

$$\tan\theta_0 = \tan \frac{p_\perp}{p_z} \approx \frac{p_\perp}{p_z} \ll 1,$$

be larger than the scattering angle in the foil

Magnetized stripping foil technique for ions

We take light ions or protons with the energy of a few 100 keV with

$$\rho \sim 1 - 10\,\mu\mathrm{m}$$

$$H \sim 0.5 - 1\ \mathrm{T},$$

$$|Z_{\rm in} - Z_{\rm out}| \sim 1,$$

and get:

$$p_\perp \sim 0.1 - 1\,\mathrm{keV} \qquad \theta_0 \sim 1 - 100\,\mu\mathrm{rad}$$

Whereas the typical scattering angles are

(https://web-docs.gsi.de/~weick/atima/atima14.html)

~ 1-100 mrad!

It this that pessimistic as it seems?

Magnetized stripping foil technique for ions

- An ion interacts with the solenoid magnetic field and a nucleus of the foil
- The scattered ions are projected on the plane waves - what defines their azimuthal angle for a thin target (carbon)?
- If the ion packet is very wide, there is no preferential angle, and the ion evolved state may not necessarily be the plane wave
- This can no longer be a pure state but a mixed one, “averaged” over impact-parameters

So, there is no solid reason to think that the ion evolved state is a plane wave

Magnetized stripping foil technique for ions

If the final ion is an LG (pure or mixed):

$$\rho \equiv \sqrt{\langle \rho^2 \rangle}$$

$$p_\perp \equiv \sqrt{\langle p_\perp^2 \rangle}$$

$$p_\perp \rho = 2n + |\ell| + 1,$$

Defined by the scattering

From the Busch theorem

Large scattering angles imply large transverse momenta, so

1. Either it is not an LG that is generated – it can well be!
2. Or it still is an LG but with n >> ell – it is also possible!

Acceleration of charged particles with vortices and photon emission

The fields may be inhomogeneous for a beam,
but still homogeneous for an ion/proton/electron packet!

The real **in**homogeneous fields can be approximated as:

$$H_z(\rho, z) = H_z(0, z) - \frac{\rho^2}{4} H_z''(0, z) + \mathcal{O}(\rho^4),$$

$$H_\rho(\rho, z) = -\frac{\rho}{2} H'(z) + \mathcal{O}(\rho^3),$$

$$\boldsymbol{E} = E_\rho(\rho)\, \boldsymbol{e}_\rho + E_z\, \boldsymbol{e}_z,$$

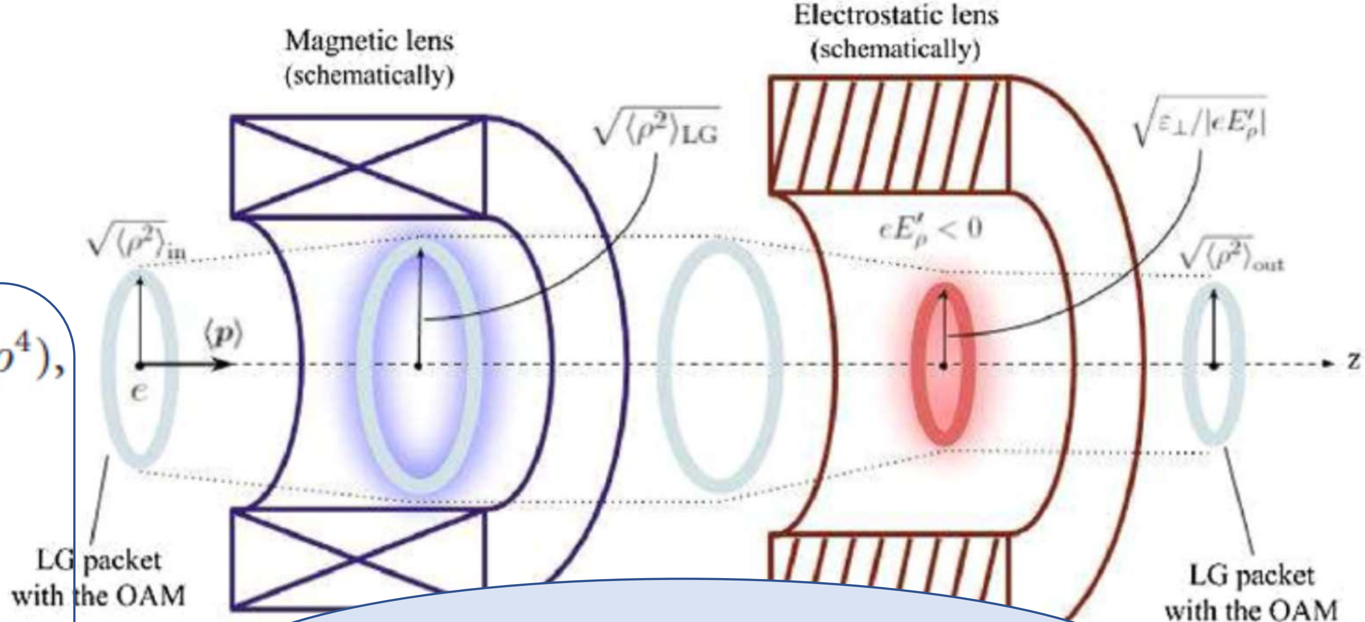

In linear fields, the OAM, the beam quality, and the emittance are conserved!

Inside a magnetic lens, the vortex electron is in the Landau state

Relativistic Landau states

$$\boldsymbol{H} = \{0, 0, H\}$$

$$H_c = 4.4 \times 10^9 \text{ T}$$

$$\Psi_i(x) = N_i^{\uparrow} \begin{pmatrix} (m+\varepsilon)\Phi_{s,\ell-1/2}(\rho)e^{-i\varphi/2} \\ 0 \\ p_z \Phi_{s,\ell-1/2}(\rho)e^{-i\varphi/2} \\ -ieH\Phi_{s,\ell+1/2}(\rho)e^{i\varphi/2} \end{pmatrix} e^{-it\varepsilon+i\ell\varphi+ip_z z}$$

The evolved photon state:

$$|\gamma\rangle_{ev} = \sum_{\lambda=\pm 1} \int \frac{d^3k}{(2\pi)^3} |\boldsymbol{k}, \lambda\rangle S_{fi}^{(1)} = (\varepsilon - \varepsilon') \sum_{\lambda=\pm 1} \mathcal{F} \int_0^{2\pi} d\varphi_k |\boldsymbol{k}, \lambda\rangle e^{i(\ell-\ell')\varphi_k}.$$

DK, Di Piazza, PRD 108, 063007 (2023); Pavlov, DK, PRD 109, 036017 (2024)

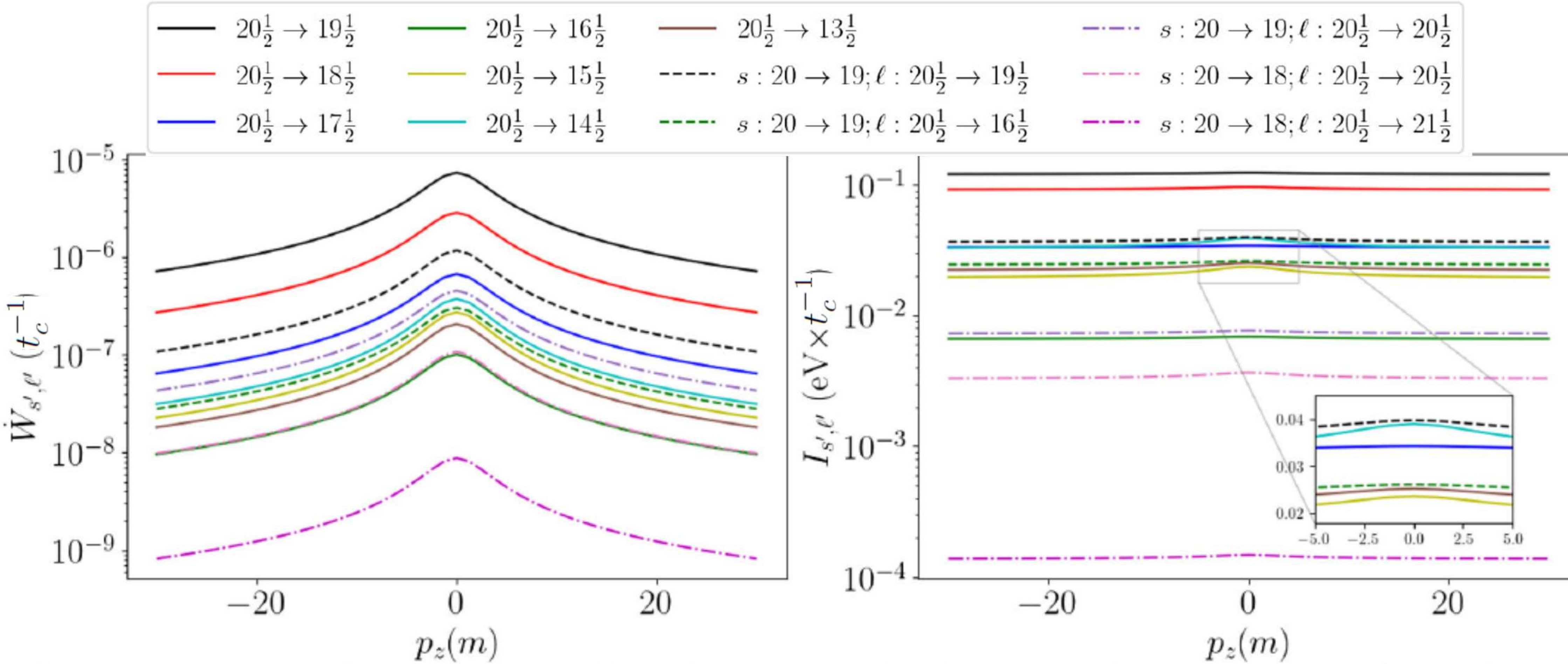

FIG. 5. The dependence of the emission probability (left) and the intensity (right) on the electron momentum p_z for $H = 0.1H_c$, $s = s' = 20$. The transition $20\frac{1}{2} \to 19\frac{1}{2}$ means $\ell = 20\frac{1}{2}$, $\ell' = 19\frac{1}{2}$, $s = s' = 20$; those with $\ell: 20\frac{1}{2} \to 20\frac{1}{2}$ correspond to the untwisted photons with $j_z = 0$. The green line overlaps with the pink dashed one on the left; the cyan line on the left overlaps with the blue one on the right. The magenta dash-dotted line corresponds to an increase of the electron OAM during the emission (so that the photon TAM is $\ell - \ell' = -1$).

DK, Di Piazza, PRD 108, 063007 (2023); Pavlov, DK, PRD 109, 036017 (2024)

An effective time period of loosing the vorticity: s=3, p_z << m

He2

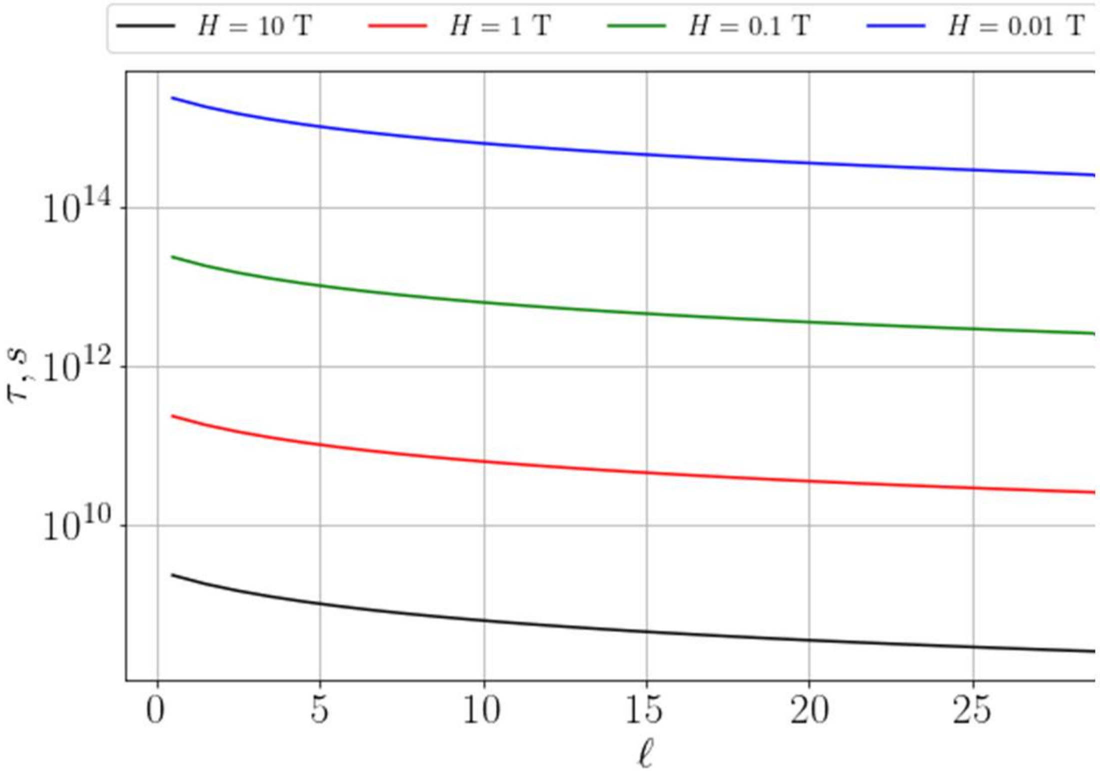

Li+

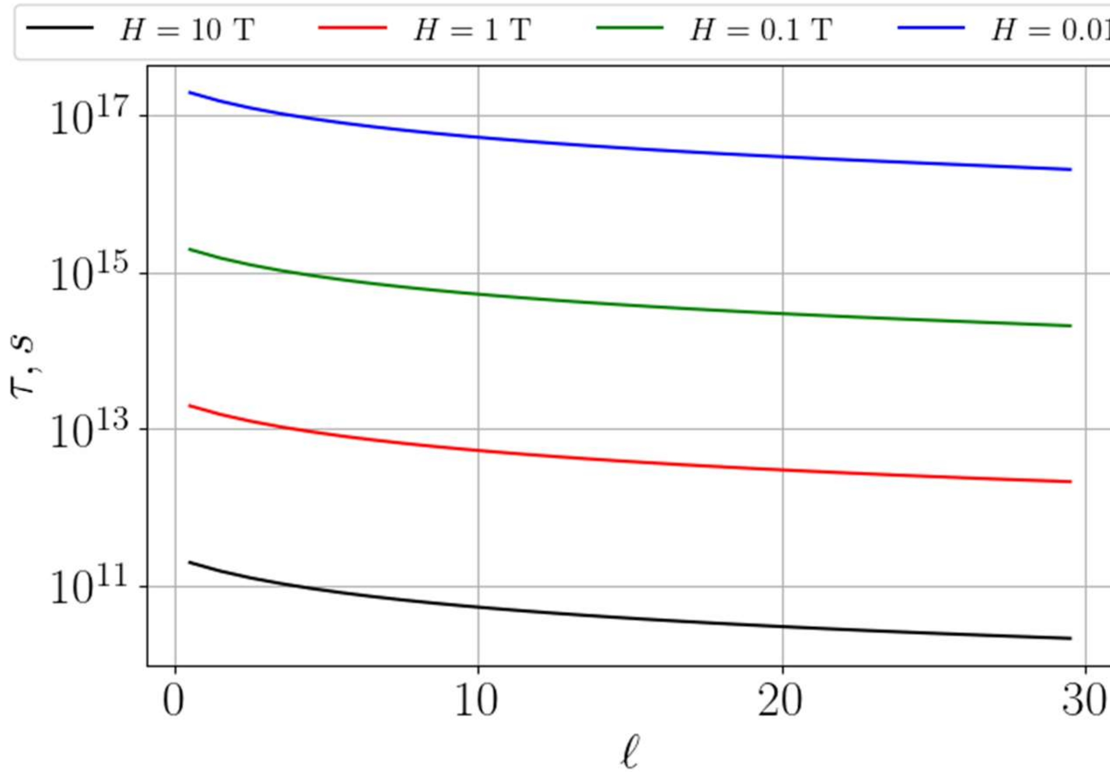

An effective time period of loosing the vorticity: s=3, p_z << m

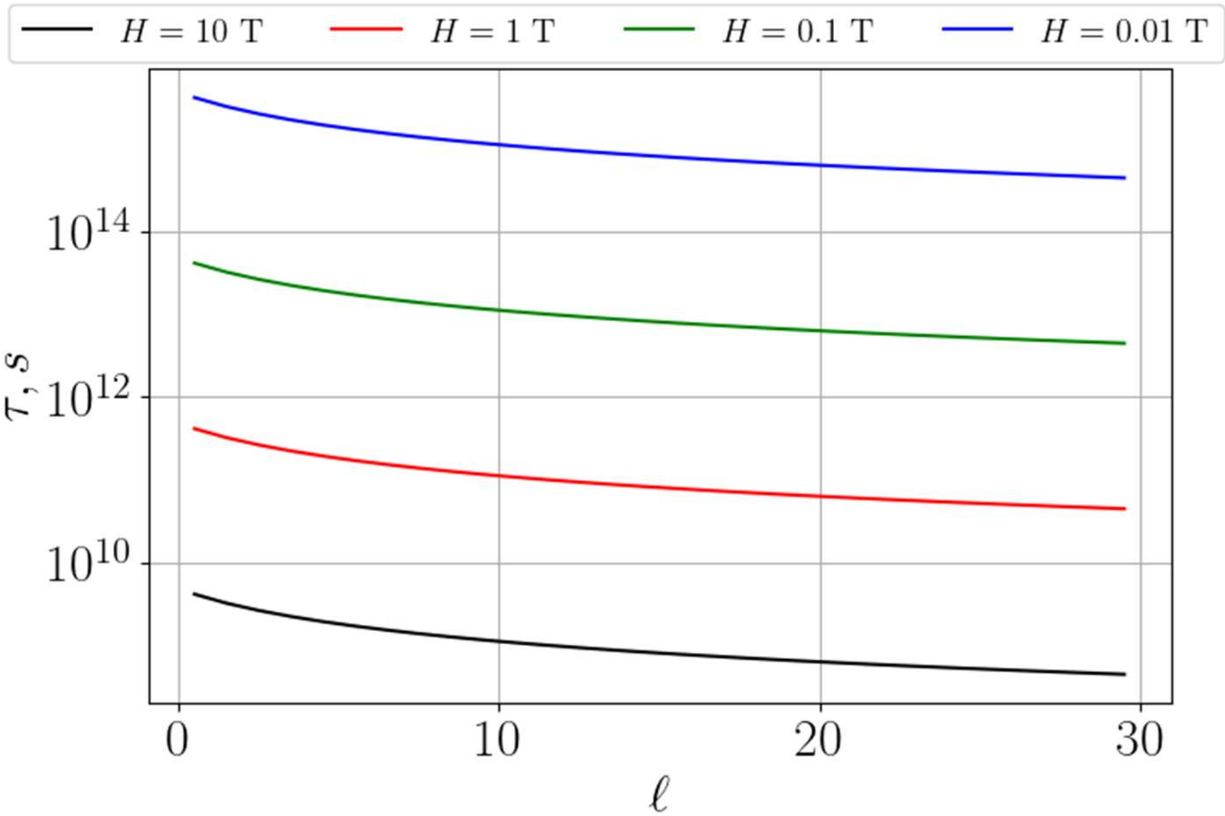

U238_37+

Summary

1. The evolved-state formalism says if the twisted states are really generated
2. With two final particles, one can make one of them twisted by projecting the other one onto the vortex – pure or mixed – state with the OAM =0
3. This generalized-measurement technique can be used to generate vortex states of highly energetic protons, nuclei, ions, atoms, and so forth
4. Even when projecting the electron to the plane-wave, the photon state depends on a phase and on a transverse coherence of the incoming electron (quantum tomography)
5. The magnetized cathode & stripping foil techniques for electrons and ions can be tested together with more conventional methods
6. Once twisted, charged particles can be accelerated in a linac without loss of the OAM

Potential applications

1. Twisted photons: optical manipulations, tweezers, non-dipole effects in atoms, nuclei, …
2. Vortex electrons: electron microscopy, magnetic materials, entanglement in QED, quantum measurements, etc.
3. Vortex protons: proton spin puzzle, deep inelastic ep, pp, … scattering, etc.
4. Vortex neutrons: low-energy nuclear physics, probing strong interactions beyond the perturbative QCD
5. Vortex atoms, ions, nuclei: the role of center-of-mass

Quantum optics with massive -- especially composite – particles is much fun!

department of PHYSICS

Thank you!

Special thanks to Andrei Surzhykov, Dima Glazov, Andrei Volotka, Valery Serbo, Igor Ivanov, Antonino Di Piazza as well to my group: George Sizykh, Alisa Chaikovskaia, Dima Grosman, Ilia Pavlov, and many others

d.karlovets@gmail.com
https://physics.itmo.ru/ru/research-group/5430

What's the use of twisted neutrons?

PHYSICAL REVIEW C **100**, 051601(R) (2019)

Rapid Communications

Schwinger scattering of twisted neutrons by nuclei

Andrei V. Afanasev[1] D. V. Karlovets,[2] and V. G. Serbo[3,4]

[1]*Department of Physics, The George Washington University, Washington, D.C. 20052, USA*
[2]*Tomsk State University, Lenina Avenue 36, 634050 Tomsk, Russia*
[3]*Novosibirsk State University, RUS-630090 Novosibirsk, Russia*
[4]*Sobolev Institute of Mathematics, RUS-630090 Novosibirsk, Russia*

(Received 28 March 2019; revised manuscript received 5 September 2019; published 25 November 2019)

Standard Schwinger cross section (plane waves):

$$\frac{d\sigma^{(st)}(\mathbf{e}_3, \mathbf{n}', \zeta)}{d\Omega'} = |a|^2 + \frac{1}{4}[\beta \cot(\theta'/2)]^2 - \beta\zeta_\perp(\mathrm{Im}\, a)\cot(\theta'/2)\sin(\varphi' - \varphi_\zeta).$$

$$\mathbf{n} = \mathbf{p}/p \text{ and } \mathbf{n}' = \mathbf{p}'/p \qquad \zeta_\perp = \zeta_\perp(\cos\varphi_\zeta, \sin\varphi_\zeta, 0)$$

J. Schwinger, Phys. Rev. **73**, 407 (1948)

Scattering amplitude:

$$f_{\lambda\lambda'}(\mathbf{n}, \mathbf{n}') = w_{\lambda'}^{\prime\dagger}(a + i\mathbf{B}\sigma)w_\lambda, \quad \mathbf{B} = \beta\frac{\mathbf{n}\times\mathbf{n}'}{(\mathbf{n}-\mathbf{n}')^2},$$

$$\beta = \frac{\mu_n Z e^2}{m_p c^2} = -Z \times 2.94 \times 10^{-16}\ \mathrm{cm},$$

a nucleus. For thermal neutrons with the energies near 25 meV and an $^{197}_{79}$Au nuclear target ($a = 7.63$ fm [19]), the relevant parameters are

$$\varepsilon \equiv |\beta/a| \approx 0.03, \quad |(\mathrm{Im}\, a)/a| \approx 2 \times 10^{-4}$$

No sensitivity to:

1. The neutron's helicity
2. Re a

What's the use of twisted neutrons?

$$\psi_{\varkappa m p_z \lambda}(\mathbf{r}) = \int \frac{d^2\mathbf{p}_\perp}{(2\pi)^2} a_{\varkappa m}(\mathbf{p}_\perp) i^\lambda w^{(\lambda)}(\mathbf{n}) e^{i\mathbf{pr}/\hbar} .$$

$$a_{\varkappa m}(\mathbf{p}_\perp) = i^{-m} e^{im\varphi} \frac{2\pi}{p_\perp} \delta(p_\perp - \hbar\varkappa). \qquad \mathbf{p} = (\mathbf{p}_\perp, p_z) = (\hbar\varkappa \cos\varphi, \hbar\varkappa \sin\varphi, p_z).$$

Macroscopic target (incoherent superposition of many nuclei):

$$\frac{d\bar{\sigma}(\theta, \theta', \varphi', \zeta)}{d\Omega'} = \frac{1}{\cos\theta} \int_0^{2\pi} \frac{d\sigma^{(\mathrm{st})}(\mathbf{n}, \mathbf{n}', \zeta)}{d\Omega'} \frac{d\varphi}{2\pi} = \frac{1}{\cos\theta} [|a|^2 + \beta^2 G(\theta, \theta') - \beta(\mathrm{Im}\, a)\zeta_\perp g(\theta, \theta') \sin(\varphi' - \varphi_\zeta)],$$

$$G(\theta, \theta') = \frac{1}{2|\cos\theta - \cos\theta'|} - \frac{1}{4},$$

$$g(\theta, \theta') = \begin{cases} \cot(\theta'/2), & \text{at } \theta' > \theta, \\ -\tan(\theta'/2) & \text{at } \theta' < \theta. \end{cases}$$

Angular singularity at $1/|\theta' - \theta|$ instead of 0!

What's the use of twisted neutrons?

PHYSICAL REVIEW C **103**, 054612 (2021)

Elastic scattering of twisted neutrons by nuclei

A. V. Afanasev,[1] D. V. Karlovets,[2,3] and V. G. Serbo[4,5]
[1]*Department of Physics, The George Washington University, Washington, DC 20052, USA*
[2]*Faculty of Physics, Tomsk State University, Lenina Avenue 36, 634050 Tomsk, Russia*
[3]*School of Physics and Engineering, ITMO University, Lomonosova 9, 191002 St. Petersburg, Russia*
[4]*Novosibirsk State University, 630090 Novosibirsk, Russia*
[5]*Sobolev Institute of Mathematics, 630090 Novosibirsk, Russia*

(Received 19 February 2021; accepted 10 May 2021; published 20 May 2021)

$$W_\lambda^{(m)}(\theta, \theta', \mathbf{b}) = \sum_{\lambda'} \left\langle \left| F_{\lambda\lambda'}^{(m)}(\theta, \theta', \varphi', \mathbf{b}) \right|^2 \right\rangle = \frac{1}{2}\Sigma^{(m)} + \lambda\Delta^{(m)},$$

Depends on Re a!

Neutron helicity!

Helicity asymmetry:

$$A_\lambda = \frac{W_{\lambda=1/2}^{(m)} - W_{\lambda=-1/2}^{(m)}}{W_{\lambda=1/2}^{(m)} + W_{\lambda=-1/2}^{(m)}} = \frac{\Delta^{(\mathrm{m})}}{\Sigma^{(\mathrm{m})}}.$$

For a target of a finite width, we average the probability with

$$n(\mathbf{b} - \mathbf{b}_t) = \frac{1}{2\pi\sigma_t^2} e^{-(\mathbf{b}-\mathbf{b}_t)^2/(2\sigma_t^2)}$$

What's the use of twisted neutrons?

Averaged over the azimuthal angle of the final neutron:

$$W_\lambda^{(m)}(\theta, \theta', \mathbf{b}) = \sum_{\lambda'} \langle |F_{\lambda\lambda'}^{(m)}(\theta, \theta', \varphi', \mathbf{b})|^2 \rangle \; = \frac{1}{2}\, \Sigma^{(m)} + \lambda\, \Delta^{(m)},$$

$$\Sigma^{(m)} = |a|^2 \big(J_{m-1/2}^2(\varkappa b) + J_{m+1/2}^2(\varkappa b)\big) + \sum_\sigma \langle (\mathbf{B}^{(\sigma)*}\mathbf{B}^{(\sigma)}) - 2\sigma\, \mathrm{Im}(\mathbf{B}^{(\sigma)*} \times \mathbf{B}^{(\sigma)})_z \rangle,$$

$$\Delta^{(m)} = [|a|^2 \cos\theta - (\mathrm{Re}\, a)\, \beta\, h(\theta, \theta')]\, \big(J_{m-1/2}^2(\varkappa b) - J_{m+1/2}^2(\varkappa b)\big) + \cos\theta \sum \langle 2\sigma\, (\mathbf{B}^{(\sigma)*}\mathbf{B}^{(\sigma)}) - \mathrm{Im}(\mathbf{B}^{(\sigma)*} \times \mathbf{B}^{(\sigma)})_z \rangle$$

$$- \sin\theta\, \langle \mathrm{Im}(\mathbf{B}^{(1/2)*} \times \mathbf{B}^{(-1/2)})_x - \mathrm{Re}(\mathbf{B}^{(1/2)*} \times \mathbf{B}^{(-1/2)})_y \rangle$$

What's the use of twisted neutrons?

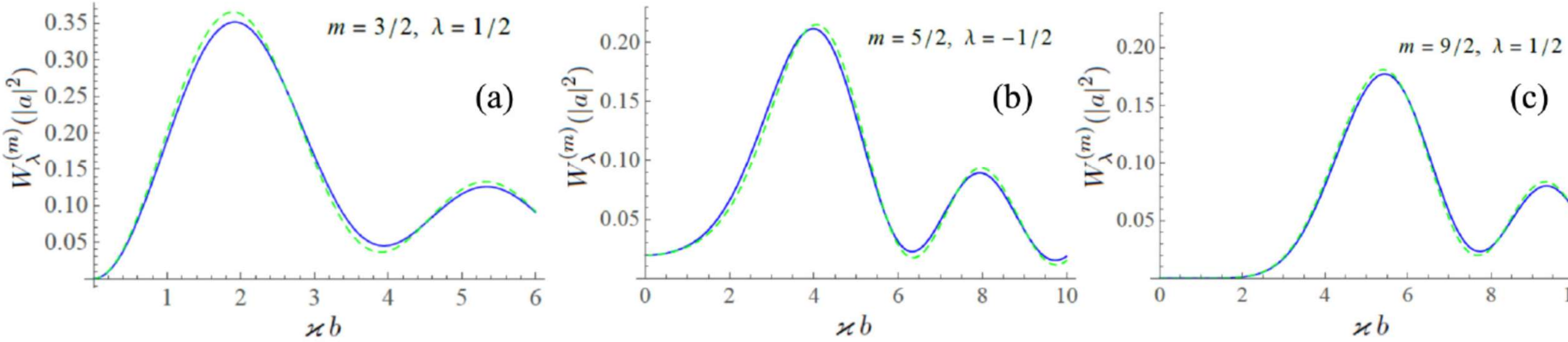

FIG. 7. The distribution (38) in units $|a|^2$ as a function of the $^{197}_{79}$Au nucleus position b for $\theta' = 0.04$ rad, $\theta = 0.07$ rad, and $\varepsilon = 0.03$. The case Im $a > 0$ is shown by blue solid lines, while the case Im $a < 0$ is shown by green dashed lines.

$$\theta' < \theta \approx 1^\circ\text{–}10^\circ$$

What's the use of twisted neutrons?

Within the momentum cone

$$\theta' < \theta \approx 1^\circ\text{–}10^\circ$$

the asymmetry reaches the values

$$\boxed{|A_\lambda| \approx 10^{-3}\text{–}10^{-1}}$$

$^{197}_{79}$Au nucleus $\quad a = 7.63$ fm

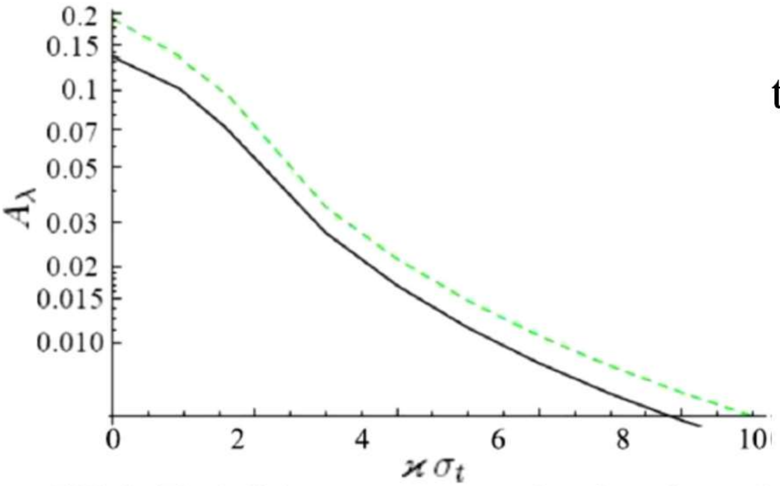

FIG. 9. The helicity asymmetry as a function of $\varkappa\sigma_t$ where σ_t is a width of the $^{197}_{79}$Au mesoscopic target for $m = 5/2$, $\theta' = 0.04$ rad, $\theta = 0.07$ rad, and $\varepsilon = 0.03$, $b_t = \varphi_t = 0$. The case Im $a > 0$ is shown by the black solid line, while the case Im $a < 0$ is shown by the green dashed line.

$\}/a| \approx 0.03$, $\quad |(\mathrm{Im}\, a)/a| \approx 2 \times 10^{-4}$

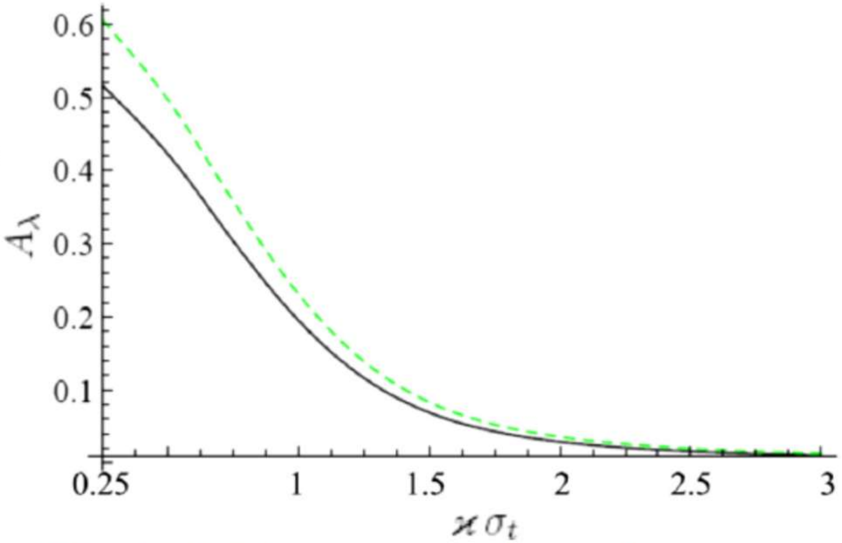

FIG. 8. The helicity asymmetry as a function of $\varkappa\sigma_t$ where σ_t is a width of the $^{197}_{79}$Au mesoscopic target for $m = 1/2$, $\theta' = 0.03$ rad, $\theta = 0.06$ rad, and $\varepsilon = 0.03$, $b_t = \varphi_t = 0$. The case Im $a > 0$ is shown by the black solid line, while the case Im $a < 0$ is shown by the green dashed line.

Generation and detection of spin-orbit coupled neutron beams

Dusan Sarenac[a,1], Connor Kapahi[a,b], Wangchun Chen[c,d], Charles W. Clark[e], David G. Cory[a,f,g,h], Michael G. Huber[i], Ivar Taminiau[a], Kirill Zhernenkov[a,j,k], and Dmitry A. Pushin[a,b]

20328–20332 | PNAS | October 8, 2019 | vol. 116 | no. 41

Spin-orbit coupling of light has come to the fore in nanooptics and plasmonics, and is a key ingredient of topological photonics and chiral quantum optics. We demonstrate a basic tool for incorporating analogous effects into neutron optics: the generation and detection of neutron beams with coupled spin and orbital angular momentum. The ^{3}He neutron spin filters are used in conjunction with specifically oriented triangular coils to prepare neutron beams with lattices of spin-orbit correlations, as demonstrated by their spin-dependent intensity profiles. These correlations can be tailored to particular applications, such as neutron studies of topological materials.

“The triangular coils induce perpendicular phase gradients along the directions that are also perpendicular to the direction of the incoming spin state. Pairs of triangular coils then effectively act as LOV prism pairs.”

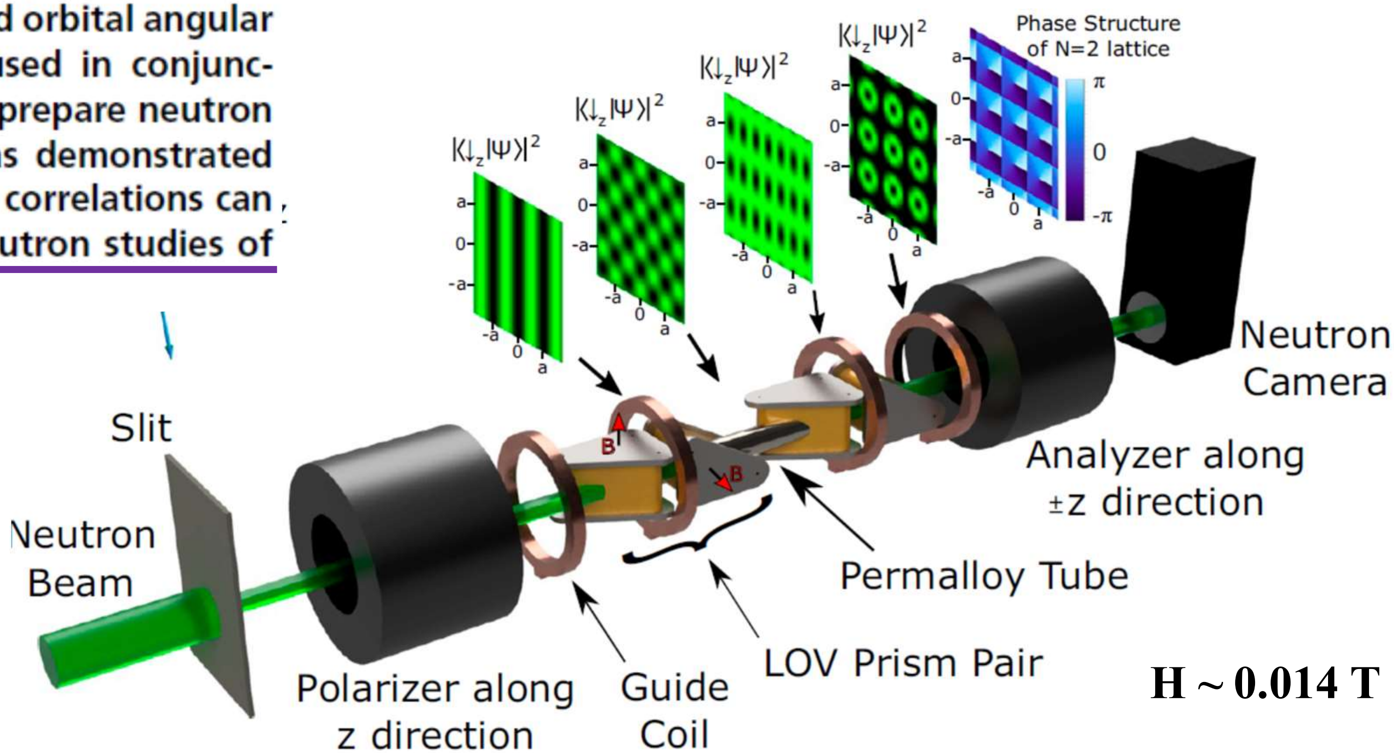

H ~ 0.014 T

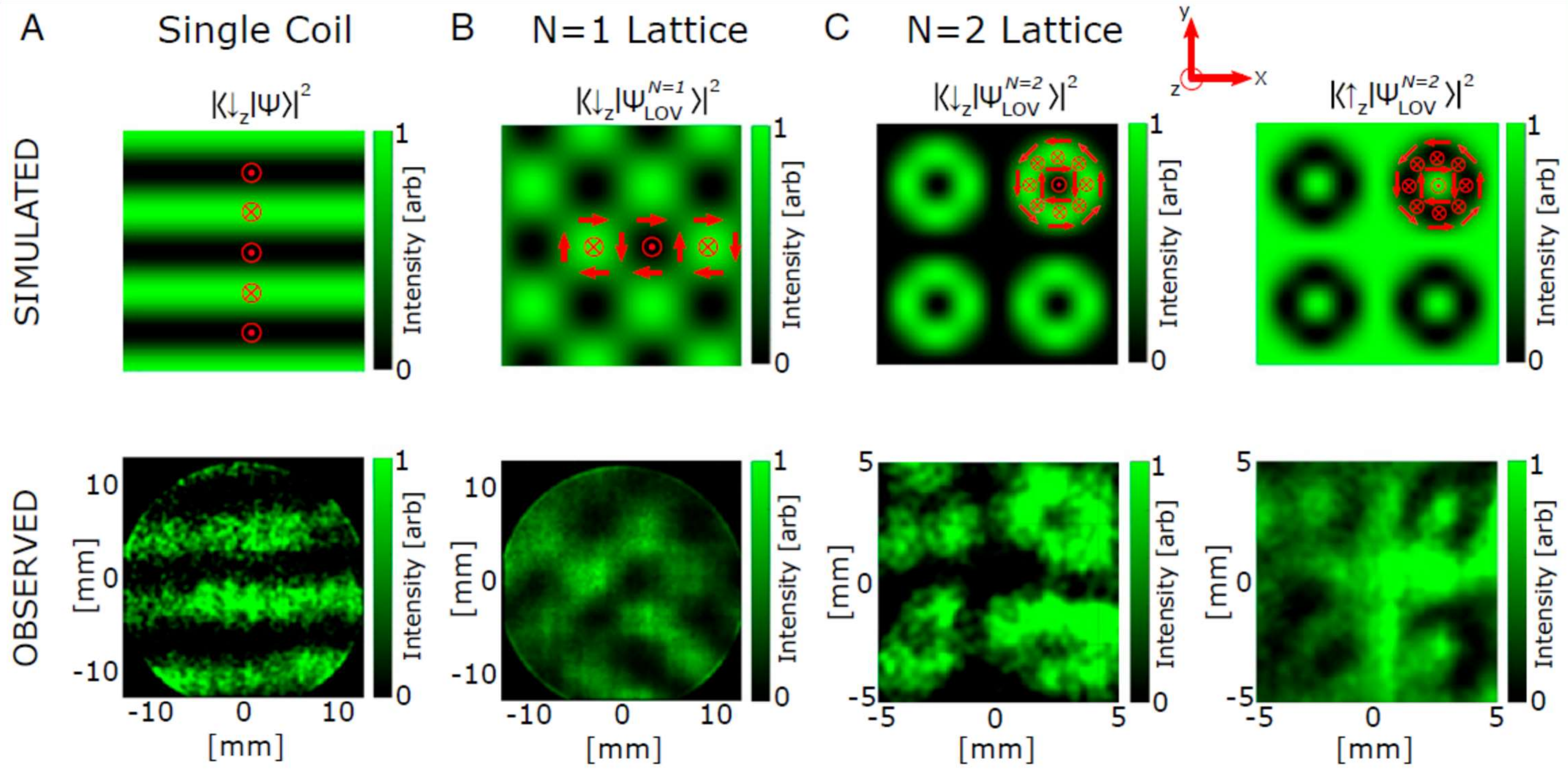

Fig. 2. The simulated and observed spin-dependent intensity profiles. A Gaussian filter as well as an intensity gradient was added to each observed image, to highlight the features of interest. The currents on the (first, second, third, and fourth) triangular coil were set to (*A*) (0, 0, 0, and 2.5 A), (*B*) (2.5, 2.5, 0, and 0 A), and (*C*) (5, 5, 5, and 4 A). The spatially varying spin direction (before the spin filtering) is overlaid on the simulated intensity profiles via the red arrows. The N = 1 lattice exhibits a vortex antivortex structure, and its spin-dependent intensity profile resembles a checkerboard pattern. The N = 2 lattice appears as a lattice of doughnut/ring shapes. Good qualitative agreement is shown between the simulated and observed intensity profiles.

20328–20332 | PNAS | October 8, 2019 | vol. 116 | no. 41

New J. Phys. 20 (2018) 103012 https://doi.org/10.1088/1367-2630/aae3ac

New Journal of Physics
The open access journal at the forefront of physics

Deutsche Physikalische Gesellschaft DPG
IOP Institute of Physics

Published in partnership with: Deutsche Physikalische Gesellschaft and the Institute of Physics

PAPER

Methods for preparation and detection of neutron spin-orbit states

D Sarenac[1,2], J Nsofini[1,2], I Hincks[2,3], M Arif[4], Charles W Clark[5], D G Cory[2,6,7,8], M G Huber[4] and D A Pushin[1,2]

$$|n,\ell,s\rangle = \mathcal{N}\xi^{|\ell|}e^{-\frac{\xi^2}{2}}\mathcal{L}_n^{|\ell|}(\xi^2)e^{i\ell\phi}|s\rangle$$

$$\psi_{\ell,n_r}(r,\phi)=\mathcal{N}\left(\frac{r}{\sigma_\perp}\right)^{|\ell|}e^{-\frac{r^2}{2\sigma_\perp^2}}\mathcal{L}_{n_r}^{|\ell|}\left(\frac{r^2}{\sigma_\perp^2}\right)e^{i\ell\phi}$$

$$E = \hbar\omega_\perp(2n_r + |\ell| + 1)$$

$$|\Psi_{SO}\rangle = \frac{1}{\sqrt{2}}(|n_\uparrow,\ell_\uparrow,\uparrow\rangle + e^{i\beta}|n_\downarrow,\ell_\downarrow,\downarrow\rangle$$

Various alloys can be engineered to have $b_c \sim b_m$, for instance a 50:50 Fe:Co alloy pos $(b_c + b_m) = -0.047$. Such materials are routinely used for neutron optics [32, 33]. For e

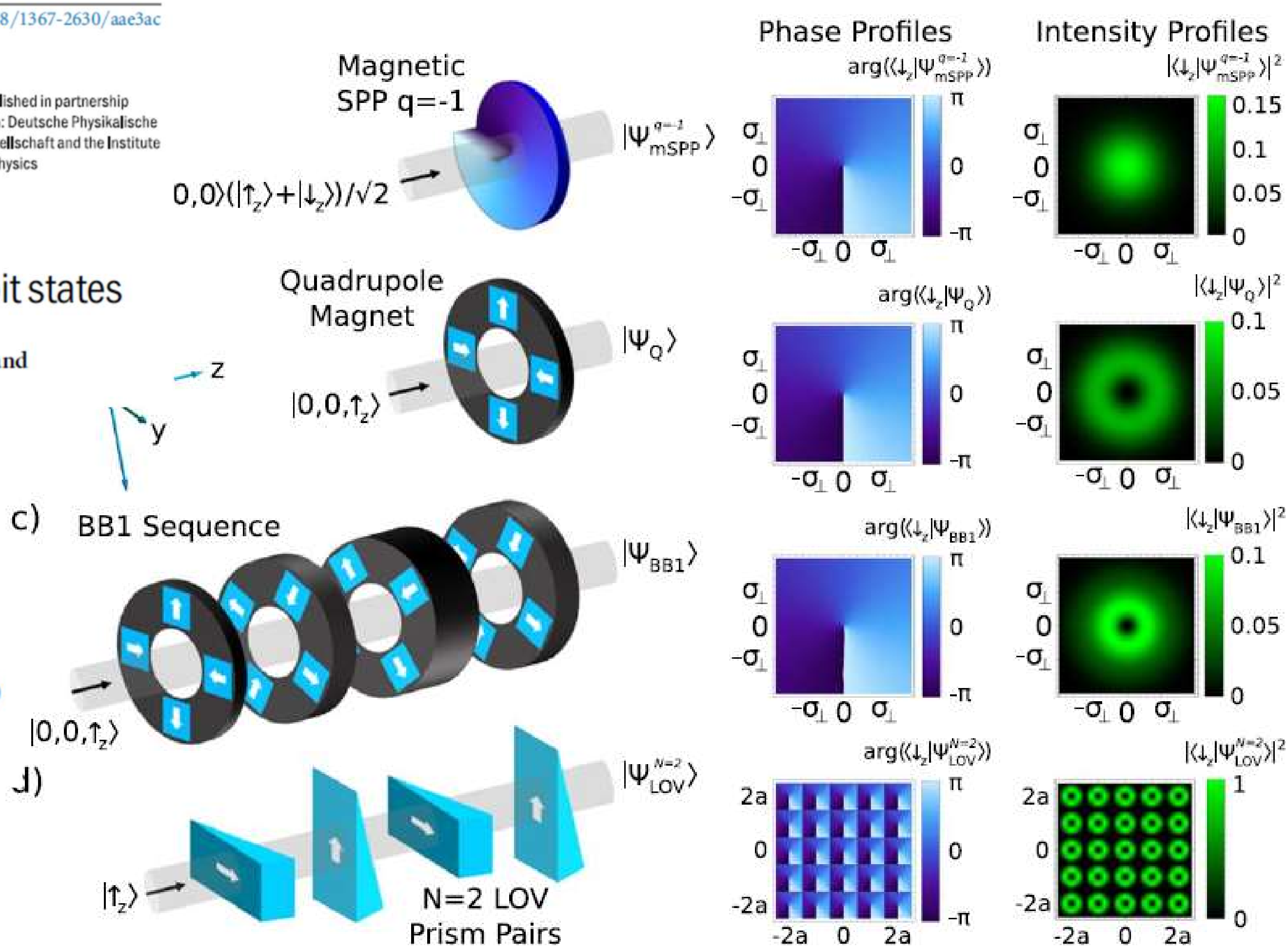

Figure 1. Four methods of producing neutron spin-orbit states. The phase and intensity profiles of the output states, post-selected on the spin state correlated to the OAM, are shown on the right. (a) An incoming neutron wavepacket in a coherent superposition of the two spin eigenstates passes through a magnetic SPP which is made out of a material with equal magnetic and nuclear scattering lengths, thereby inducing an azimuthally varying phase for only one spin state. (b) A spin-polarized neutron wavepacket passes through a quadrupole magnetic field which induces the spin-orbit state [18]. After transversing the quadrupole field, the intensity profile of the spin state correlated to the OAM has a ring shape. (c) A sequence of quadrupoles with appropriate length and orientation acts as a BB1 pulse which increases the radii at which the spin and OAM are maximally entangled. (d) In analogy to the LOV prism pairs capable of generating lattices of optical spin-orbit states [34], a sequence of magnetic prisms can be used to approximate the quadrupole operator and produce a lattice of neutron spin-orbit states.

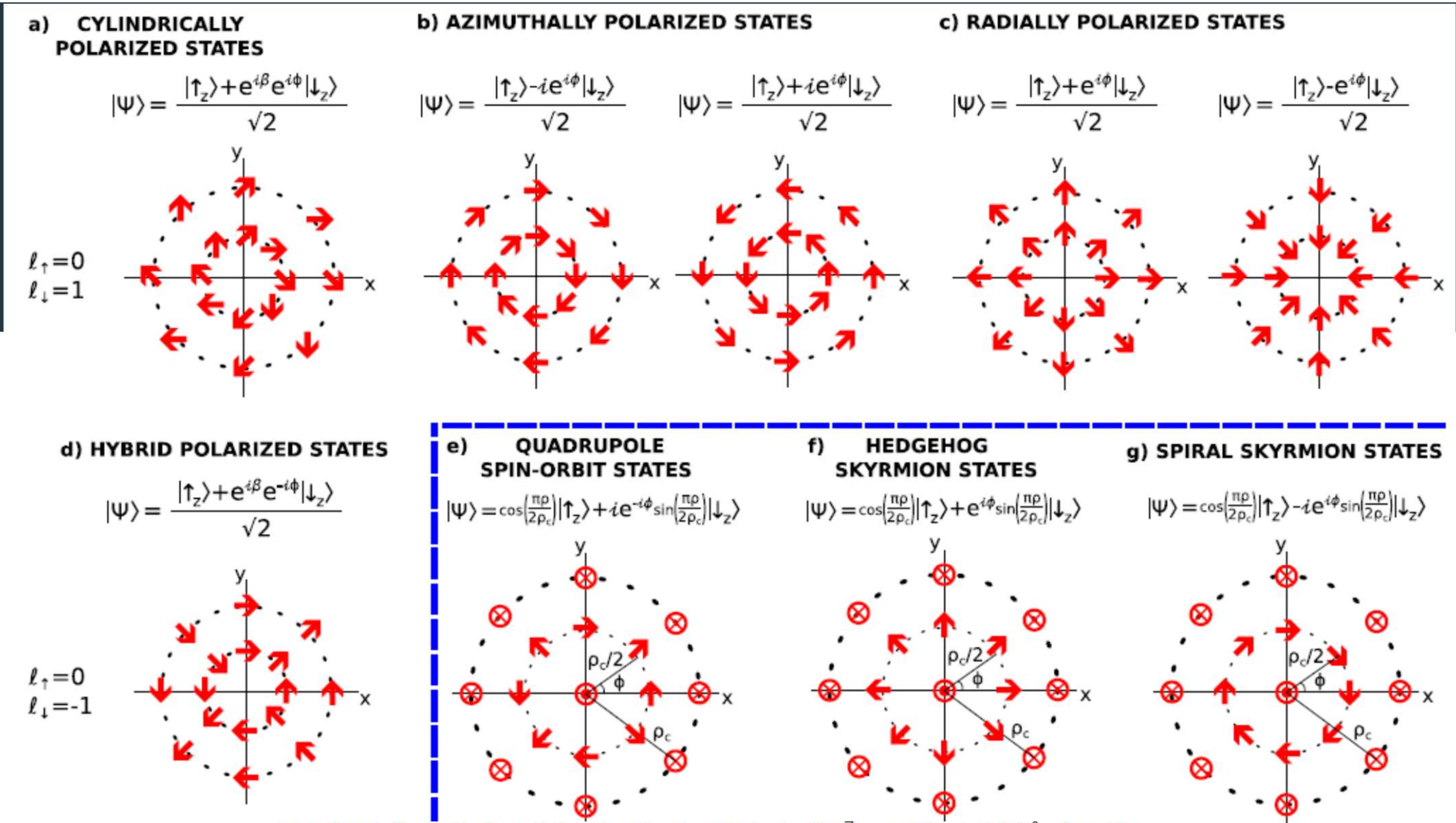

(a) 'cylindrically polarized states' where the spin orientation is given by $\vec{P} = \cos(\beta)\hat{\rho} + \sin(\beta)\hat{\phi}$, where β is an arbitrary phase;

(b) 'azimuthally polarized states' which are a subset of cylindrically polarized states where $\vec{P} = \pm\hat{\phi}$;

(c) 'radially polarized states' which are a subset of cylindrically polarized states where $\vec{P} = \pm\hat{r}$; and

(d) 'hybrid polarization states' where $\vec{P} = \sin(2\phi + \beta)\hat{r} + \cos(2\phi + \beta)\hat{\phi}$, where β is an arbitrary phase.

The more recent technique: arrays with $N = 2500*2500$ on silicon substrates

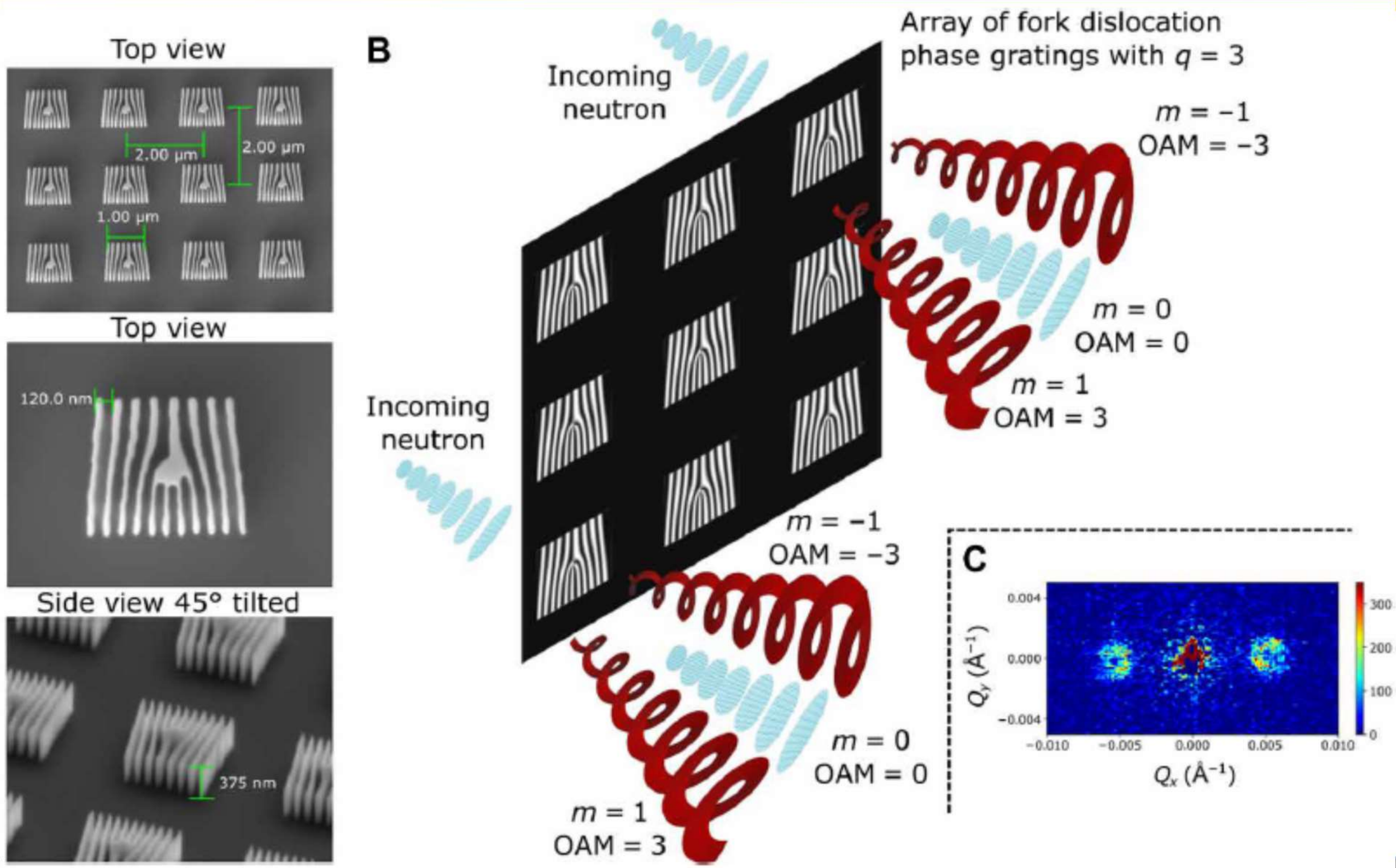

Sarenac *et al*., *Sci. Adv.* **8**, eadd2002 (2022)

Make a hologram of neutron diffraction gratings

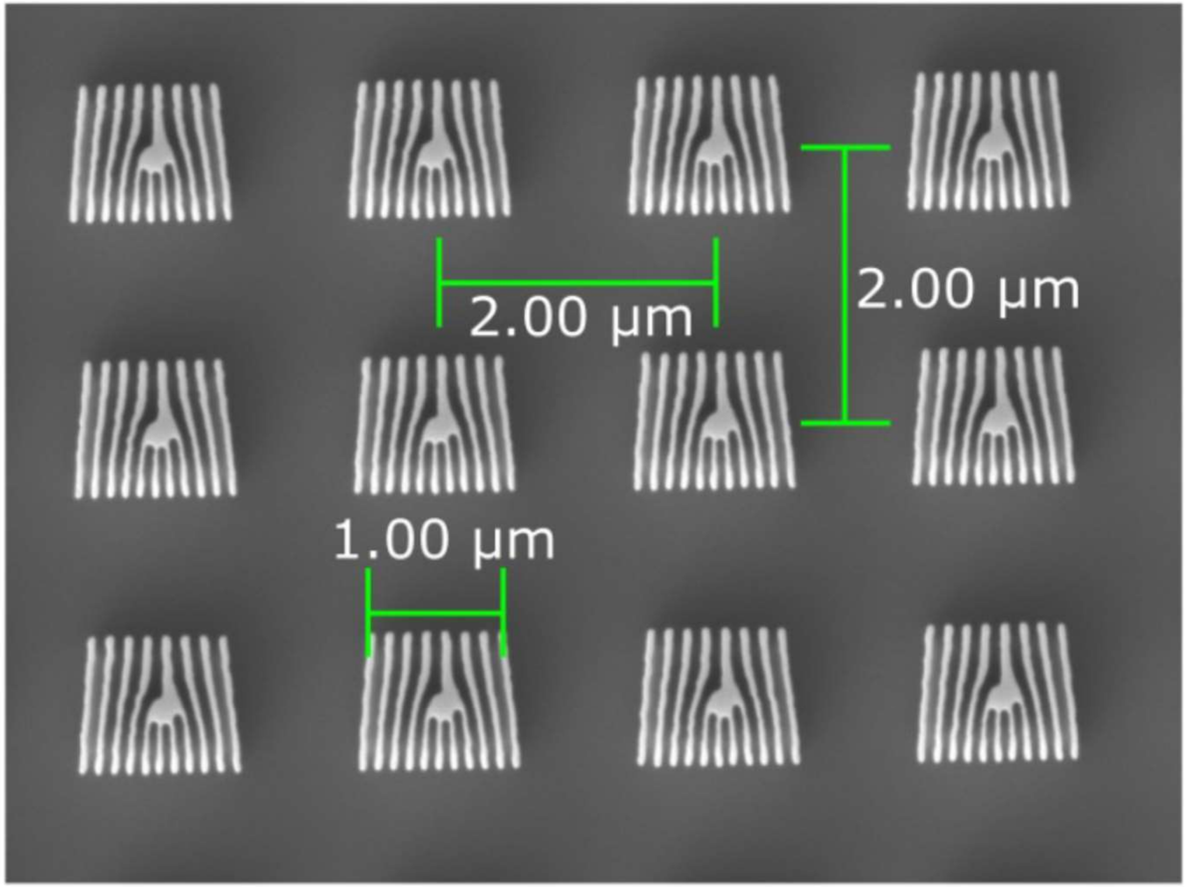

2500 x 2500 =
6,250,000
gratings in square array

Sarenac *et al*., *Sci. Adv.* **8**, eadd2002 (2022)

Side view of neutron diffraction gratings

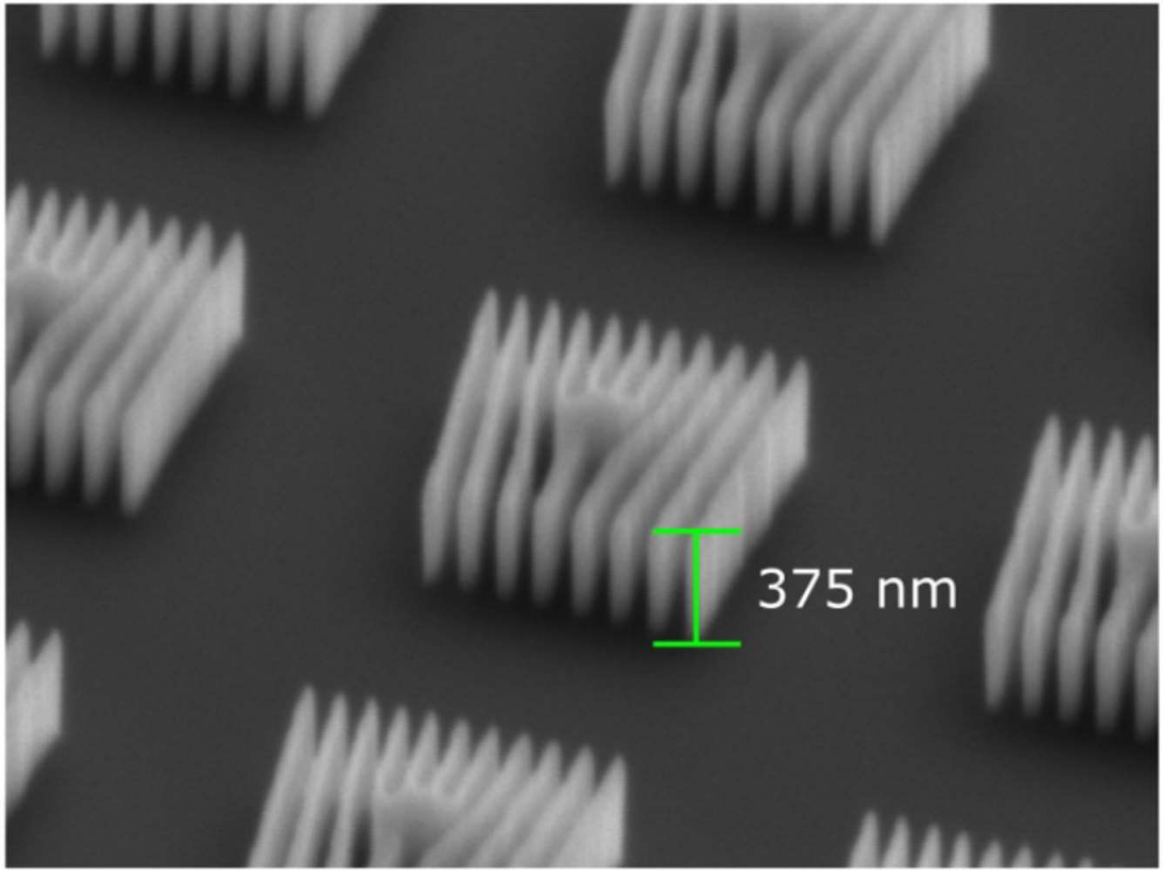

2500 x 2500 =
6,250,000
gratings in square array

Sarenac *et al*., *Sci. Adv.* **8**, eadd2002 (2022)

q=3

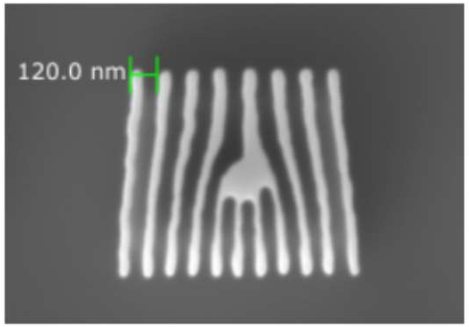

q=7

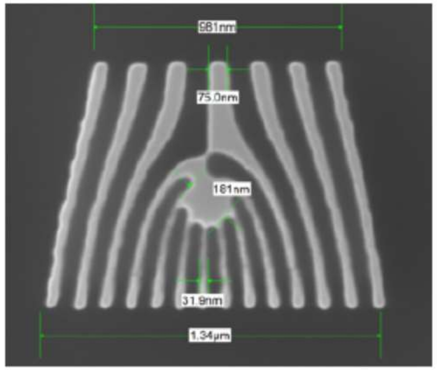

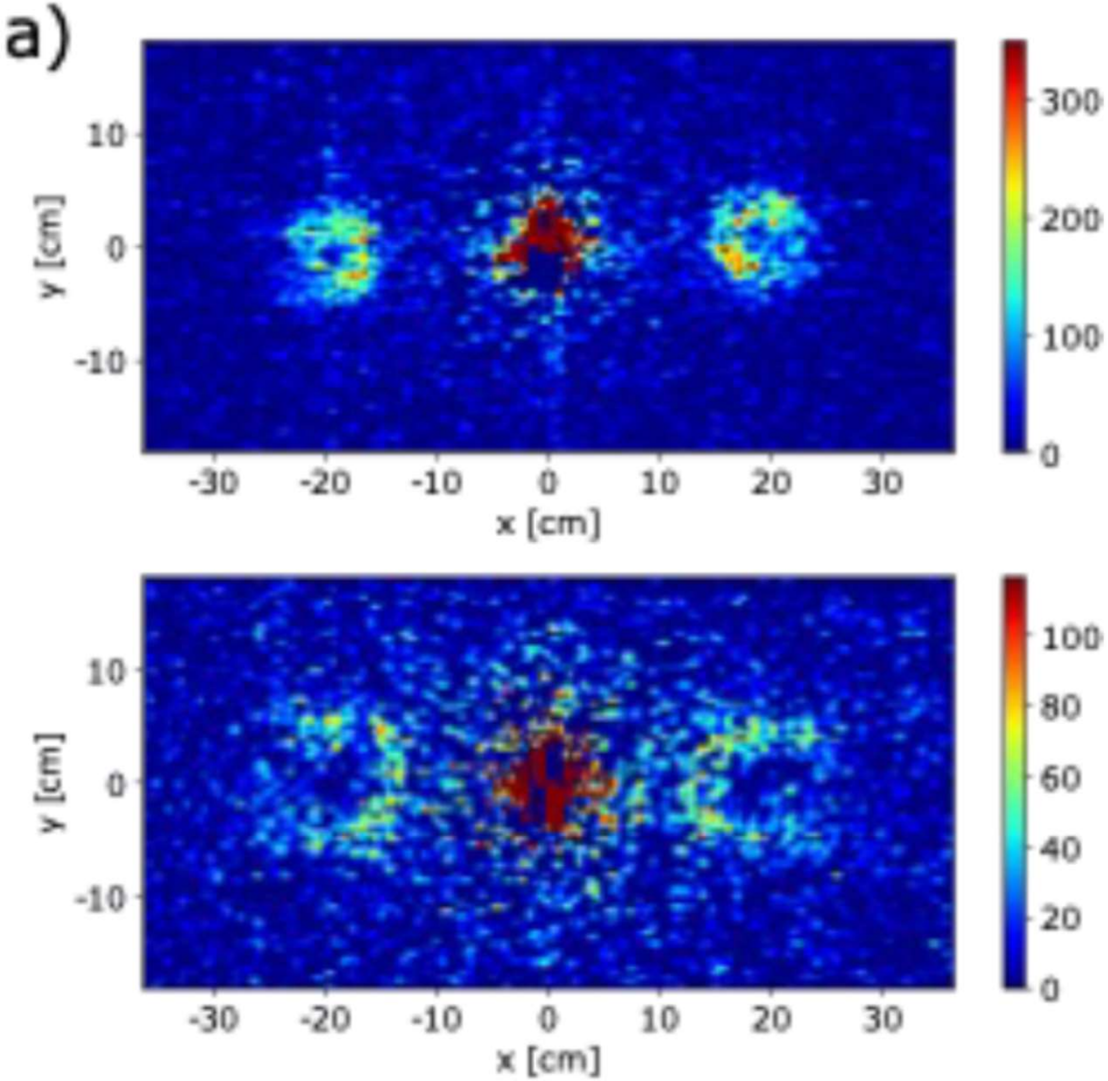

Sarenac *et al.*, *Sci. Adv.* **8**, eadd2002 (2022)

The more recent technique: arrays with $N = 2500*2500$ on silicon substrates

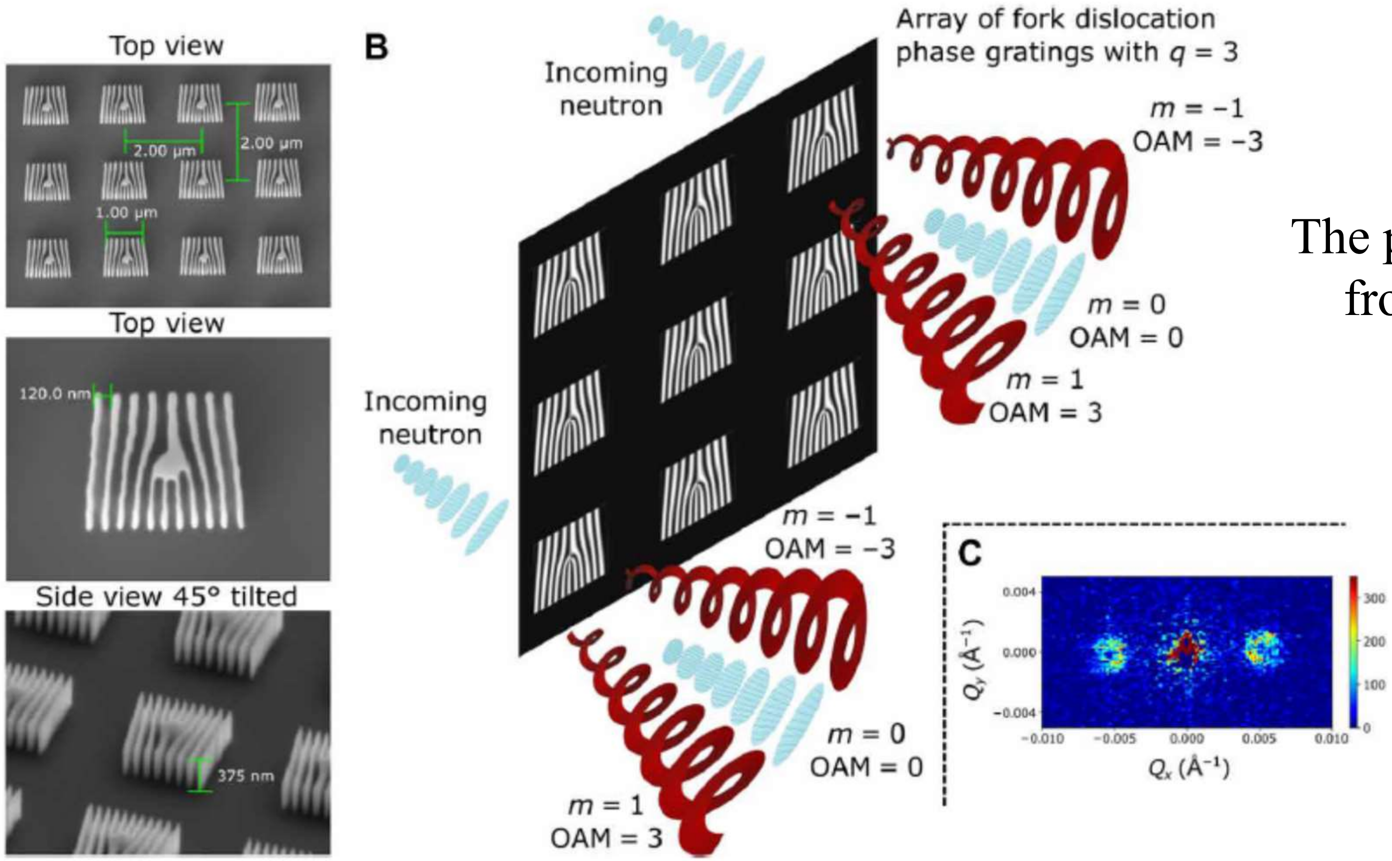

The phase gratings were placed 17.8 m away from a 20-mm diameter source aperture

The distance from the phase grating to the camera was 19 m, and the camera size spans an area of ≈1 m^2, with each pixel being ≈5.5 mm by 4.1 mm in size.

At the High Flux Isotope Reactor at Oak Ridge National Laboratory

Airy photons and electrons

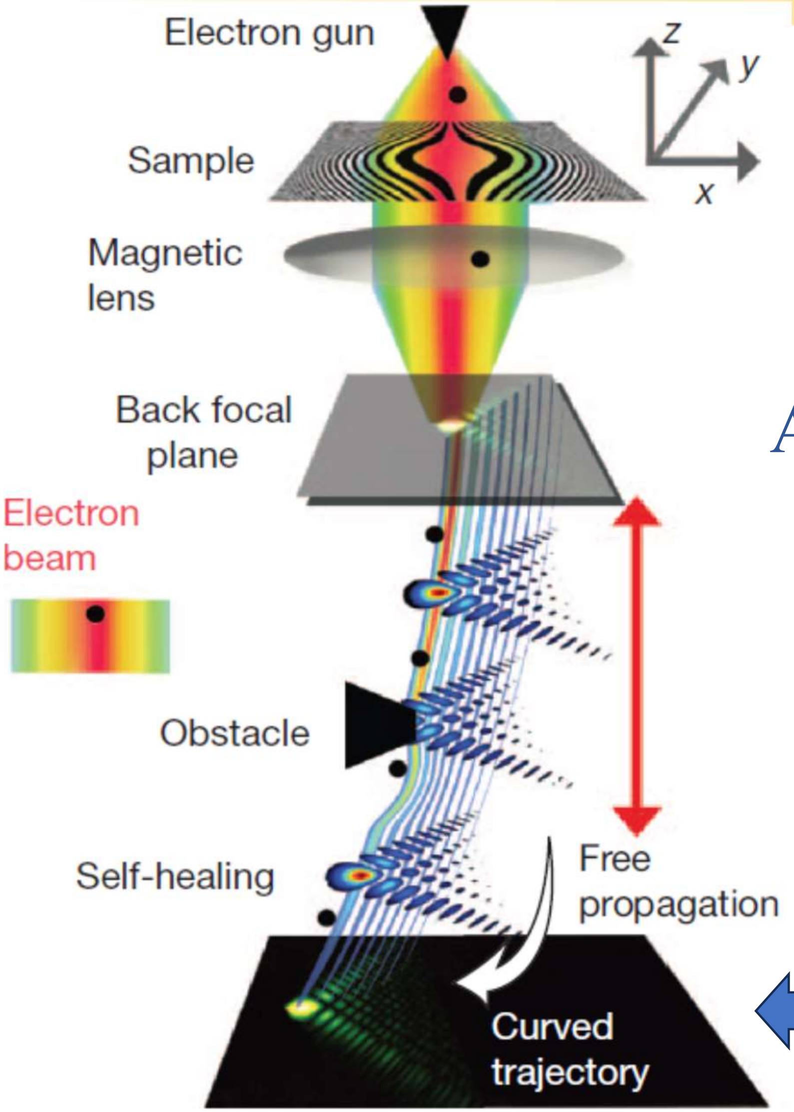

J. Baumgartl, et al.,
Nature Phot. 2, 675 (2008)

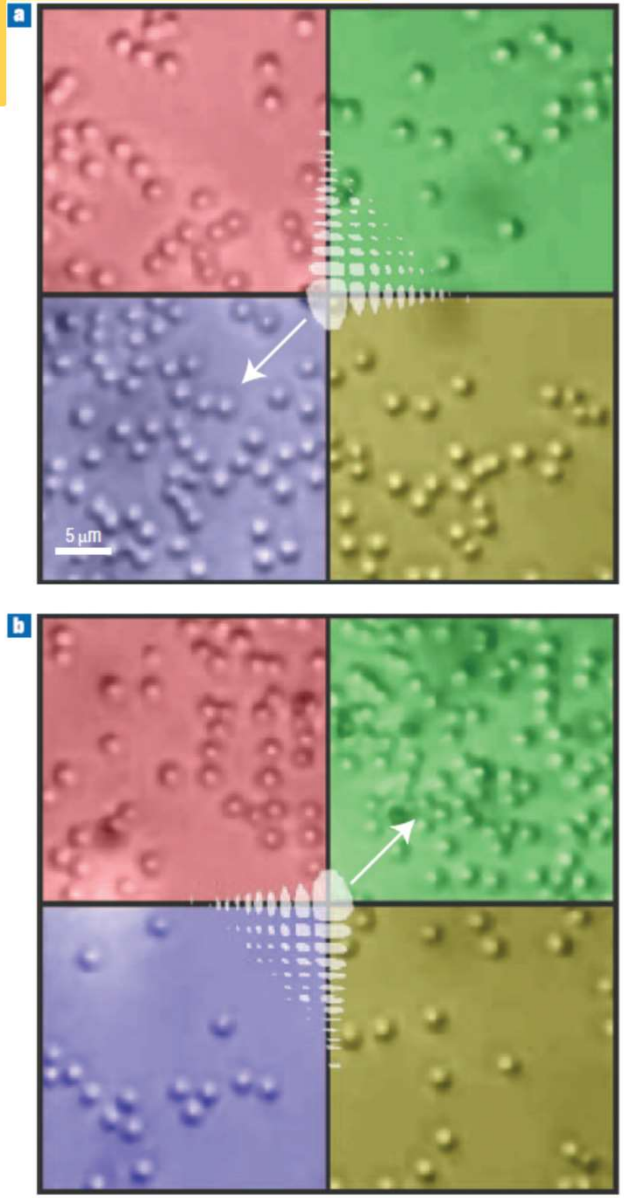

A snowblower for particles!

N. Voloch-Bloch, et al.,
Nature (London) 494, 331 (2013)

Non-stationary states in magnetic field

An electron in a constant and homogeneous magnetic field: the stationary Landau state

$$\Psi(\boldsymbol{r},t) = \mathrm{const}\left(\frac{\rho}{\rho_{\mathrm{H}}}\right)^{|\ell|} L_{n_{\mathrm{H}}}^{|\ell|}\left(\frac{2\rho^2}{\rho_{\mathrm{H}}^2}\right)\exp\left\{-\frac{\rho^2}{\rho_{\mathrm{H}}^2}+\mathrm{i}\ell\phi+\mathrm{i}p_z z-\mathrm{i}\varepsilon t\right\},$$

$$\varepsilon = \varepsilon_\perp + \frac{p_z^2}{2m},$$

$$\varepsilon_\perp = \frac{\langle(\hat{\boldsymbol{p}}_\perp^{\mathrm{kin}})^2\rangle}{2m} = |\omega_{\mathrm{L}}|\left(2n_{\mathrm{H}} + |\ell| - \mathrm{sgn}(e)\ell + 1\right)$$

An electron in a magnetic lens (solenoid) with sharp boundaries

A non-stationary Landau-like state?

$$\Psi_{n,l}(\rho,t) = N\frac{\rho^{|l|}}{\sigma^{|l|+1}(t)}L_n^{|l|}\left(\frac{\rho^2}{\sigma^2(t)}\right)\times$$

$$\exp\left[il\varphi - i\Phi_{\mathrm{G}}(t) - \frac{\rho^2}{2\sigma^2(t)}\left(1 - i\frac{\sigma^2(t)}{\lambda_{\mathrm{C}}R(t)}\right)\right]$$

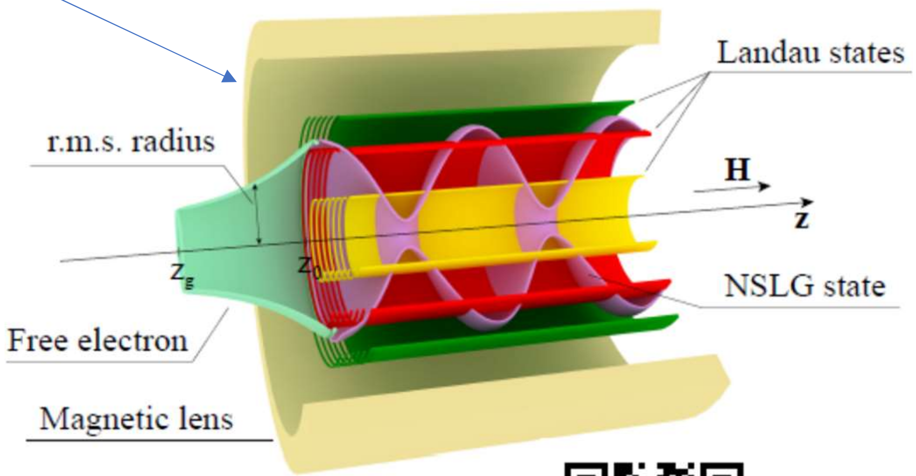

Sizykh, et al., arXiv: 2306.13161v1;
Zou, Zhang, Silenko, arXiv: 2207.14105v1

Non-stationary states in magnetic field

We substitute this to the Schrödinger equation and get:

$$\frac{1}{R(t)} = \frac{\sigma'(t)}{\sigma(t)},$$

$$\frac{1}{\lambda_C^2 R^2(t)} + \frac{1}{\lambda_C^2}\left[\frac{1}{R(t)}\right]' = \frac{1}{\sigma^4(t)} - \frac{1}{\sigma_L^4};$$

$$\frac{1}{\lambda_C}\Phi_G'(t) = \frac{l}{\sigma_L^2} + \frac{(2n+|l|+1)}{\sigma^2(t)}.$$

$$\sigma_L = \sqrt{2/|eH|}$$

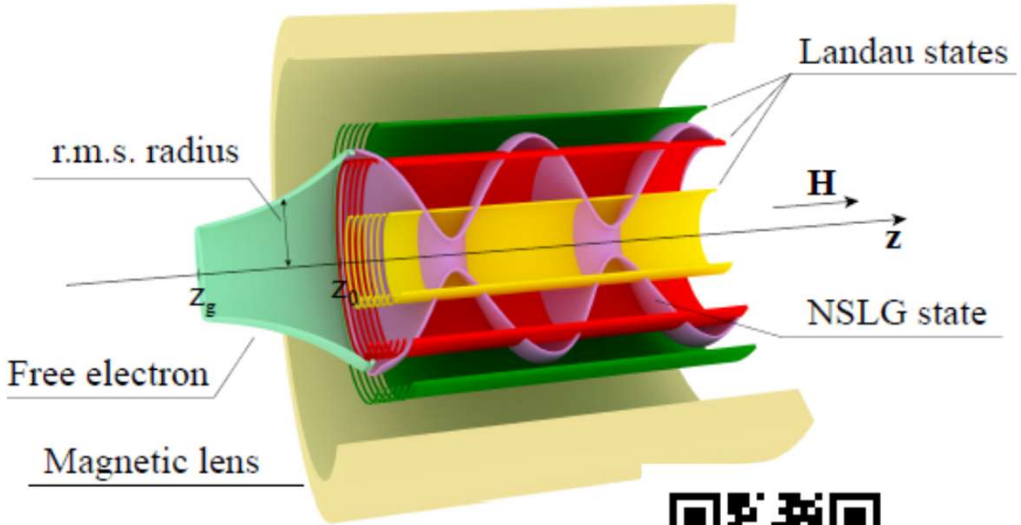

Only a very special choice of the initial conditions yields the customary Landau state!

$$\sigma(t) = \sigma_L,\ \sigma'(t) = 0,\ \Phi_G(t) = \varepsilon_\perp t,$$

Sizykh, et al., arXiv: 2306.13161v1;
Zou, Zhang, Silenko, arXiv: 2207.14105v1

Non-stationary states in magnetic field

Suppose that at t=0 a free LG state enters the solenoid:

$$\sigma(t_0) = \sigma_0 = \frac{\rho_0}{\sqrt{2n+|l|+1}}, \qquad \rho(t) = \sqrt{2n+|l|+1}\,\sigma(t),$$

$$\sigma'(t_0) = \sigma'_0 = \frac{\rho'_0}{\sqrt{2n+|l|+1}}. \qquad \sigma_{\mathrm{L}} = \sqrt{2/|eH|}$$

So now the mean energy becomes greater:

$$\langle E_\perp \rangle = \frac{\omega}{2}(2n+|l|+1)\frac{\sigma_0^2}{\sigma_{\mathrm{L}}^2}A^2 + \frac{\omega}{2}l \geq \varepsilon_\perp$$

And the rms radius also becomes greater:

$$\rho_{\mathrm{st}}^2\big|_{\mathrm{NSLG_H}} = \rho_{\mathrm{L}}^2\frac{\sigma_0^2}{\sigma_{\mathrm{L}}^2}A^2 \geq \rho_{\mathrm{L}}^2$$

$$A^2 = \frac{1}{2}\left(1 + \left(\frac{\sigma_{\mathrm{L}}}{\sigma_0}\right)^4 + \left(\frac{\sigma'_0\sigma_{\mathrm{L}}^2}{\lambda_C\sigma_0}\right)^2\right)$$

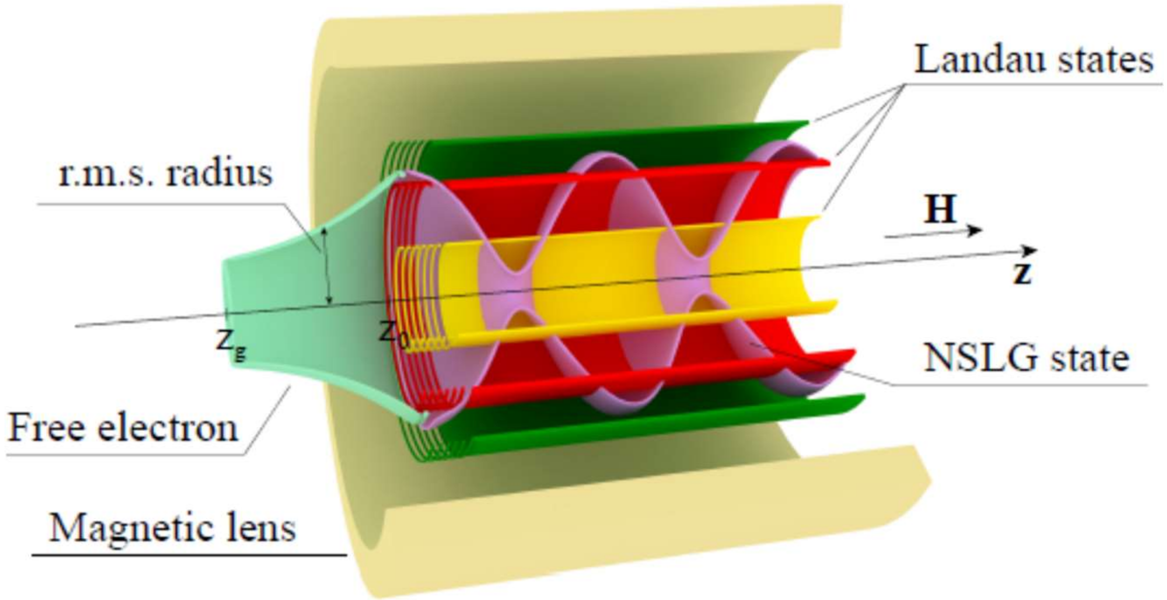

Quantum betatron oscillations

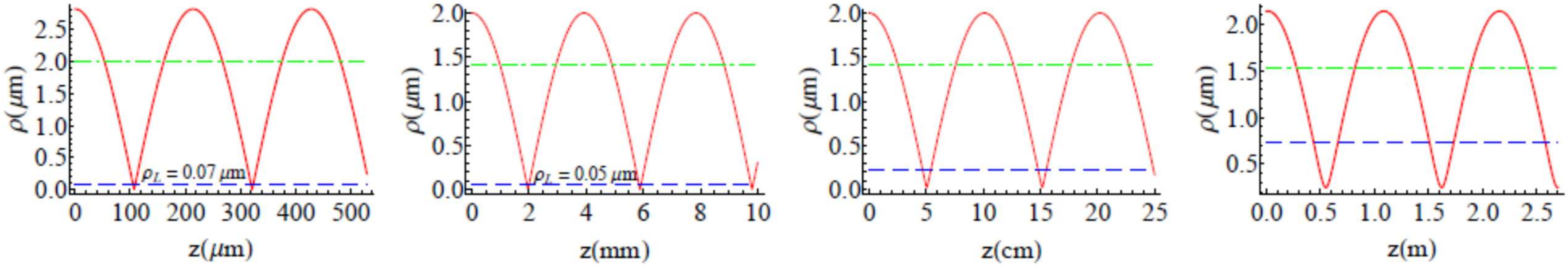

(a) (b) (c) (d)

Figure 2: Oscillations of the r.m.s. radius of the NSLG$_{\rm H}$ wave packet in a magnetic field (solid red line), the stationary radius $\rho_{\rm st}$ (dot-dashed green line) and the r.m.s. radius of the Landau state (dashed blue line). The parameters are listed in Table I. (a) SEM, (b) TEM, (c) medical linac, (d) conventional linac.

$$\xi_1 = \frac{\sigma_{\rm L}}{\sigma_0},$$

$$\xi_2 = \frac{|\sigma_0'|\sigma_{\rm L}^2}{\lambda_{\rm C}\sigma_0}.$$

Setup	$E_\parallel$	v	H	$\rho_{\rm L}$	d	$z_{\rm R}$	ρ_0	$d\rho/dz\|_{z=z_0}$	ξ_1	ξ_2
SEM	100 eV	$0.02c$	1 T	72.6 nm	5.16 cm	5.16 cm	2.82 μm	27 pm/μm	0.025	6.6×10^{-4}
TEM	200 KeV	$0.70c$	1.9 T	52.7 nm	10 cm	179 cm	2 μm	62 pm/mm	0.026	3.9×10^{-5}
Medical linac	1 MeV	$0.94c$	0.1 T	0.23 μm	10 cm	243 cm	2 μm	0.34 nm/cm	0.115	5.5×10^{-4}
Linac	1 GeV	c	0.01 T	0.72 μm	100 cm	258 cm	2.14 μm	0.28 μm/m	0.339	0.045

Table I: Experimental scenarios for observing the oscillations of the r.m.s. radius $\rho(z)$. We take $\sigma_{\rm w} = 1\mu$m, $n = 0$, $l = 3$. The parameters $\xi_1 = \sigma_{\rm L}/\sigma_0$ and $\xi_2 = \sigma_0'\sigma_{\rm L}^2/(\lambda_{\rm C}\sigma_0)$ reflect the discrepancy between the NSLG$_{\rm H}$ state and the Landau one, the latter being reproduced when $\xi_1 = 1$ and $\xi_2 = 0$.

Sizykh, et al., arXiv: 2306.13161v1

Quantum scattering theory beyond the plane-wave approximation

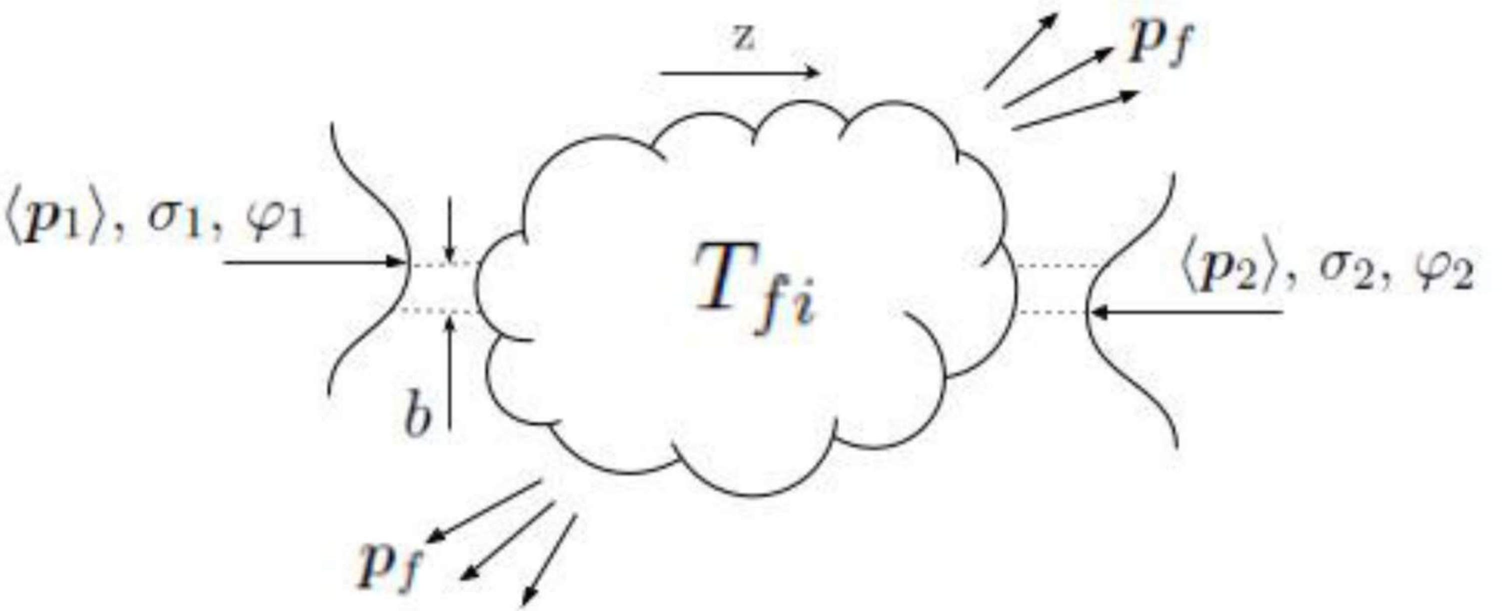

$$d\sigma_{\text{gen}} = \frac{dW}{L}.$$

The generalized cross section

Scattering of general wave packets

$$dW = |S_{fi}|^2 \prod_f V \frac{d^3 p_f}{(2\pi)^3} = \int \frac{d^3 p_1}{(2\pi)^3} \frac{d^3 p_2}{(2\pi)^3} \frac{d^3 k}{(2\pi)^3} \mathcal{L}(\boldsymbol{p}_i, \boldsymbol{k}) d\sigma(\boldsymbol{p}_i, \boldsymbol{k}),$$

The probability

$$\mathcal{L}(\boldsymbol{p}_i, \boldsymbol{k}) = \upsilon(\boldsymbol{p}_i) \int d^4x d^3R e^{i\boldsymbol{k}\boldsymbol{R}} n_1(\boldsymbol{r}, \boldsymbol{p}_1, t) n_2(\boldsymbol{r} + \boldsymbol{R}, \boldsymbol{p}_2, t)$$

The correlator

$$L = \int \frac{d^3 p_1}{(2\pi)^3} \frac{d^3 p_2}{(2\pi)^3} d^4x \upsilon(\boldsymbol{p}_i) n_1(\boldsymbol{r}, \boldsymbol{p}_1, t) n_2(\boldsymbol{r}, \boldsymbol{p}_2, t).$$

The luminosity
via the Wigner functions

$$\upsilon(\boldsymbol{p}_i) = \frac{\sqrt{(p_{1\mu} p_2^{\mu})^2 - m_1^2 m_2^2}}{\varepsilon_1(\boldsymbol{p}_1) \varepsilon_2(\boldsymbol{p}_2)} = \sqrt{(\boldsymbol{u}_1 - \boldsymbol{u}_2)^2 - [\boldsymbol{u}_1 \times \boldsymbol{u}_2]^2},$$

Scattering of general wave packets

When the wave packets are wide:

$$d\sigma_{\text{gen}} = d\sigma^{\text{incoh}} + d\sigma^{\text{int}} + \mathcal{O}((\delta p)^2),$$

$$d\sigma^{\text{incoh}} = \frac{dW^{\text{incoh}}}{L},$$

$$dW^{\text{incoh}} = \int \frac{d^3 p_1}{(2\pi)^3} \frac{d^3 p_2}{(2\pi)^3} d^4 x v(\boldsymbol{p}_i) n_1(\boldsymbol{r}, \boldsymbol{p}_1, t)\, n_2(\boldsymbol{r}, \boldsymbol{p}_2, t) d\sigma^{(\text{pw})}(\boldsymbol{p}_i).$$

Even the first term is NOT yet the plane-wave cross section!

Scattering of general wave packets

The correction due to quantum interference:

$$d\sigma^{\text{int}} = -\frac{1}{L}\int \frac{d^3 p_1}{(2\pi)^3}\frac{d^3 p_2}{(2\pi)^3} d^4x\, v(\boldsymbol{p}_i)\, n_1(\boldsymbol{r},\boldsymbol{p}_1,t)\frac{\partial n_2(\boldsymbol{r},\boldsymbol{p}_2,t)}{\partial \boldsymbol{r}}\, d\sigma^{(\text{pw})}(\boldsymbol{p}_i)\,\partial_{\Delta\boldsymbol{p}}\zeta_{fi}^{(\text{pw})}(\boldsymbol{p}_i)$$

$$M_{fi}^{(\text{pw})} = |M_{fi}^{(\text{pw})}|\exp\{i\zeta_{fi}^{(\text{pw})}\},$$

$$\partial_{\Delta\boldsymbol{p}} = \frac{\partial}{\partial \boldsymbol{p}_1} - \frac{\partial}{\partial \boldsymbol{p}_2},$$

$$\zeta_{fi}^{(\text{pw})} = \arctan\frac{\text{Im}M_{fi}^{(\text{pw})}}{\text{Re}M_{fi}^{(\text{pw})}} = \text{inv}$$

DK, Serbo, PRD 101, 076009 (2020)

Collision of a Gaussian packet with a vortex packet

S-channel at $\sqrt{s} \gg m_\mu$ $\quad e^+(p_1)e^-_{\text{tw}}(p_2(\phi_2)) \to \mu^+(p_3)\mu^-(p_4)$

$$\frac{d\sigma^{\text{incoh}}_{\text{CM}}}{d\Omega_3} = \frac{d\sigma^{(\text{pw})}_{\text{CM}}}{d\Omega_3}\left(1 + \frac{p_\perp^2}{s_0} g(\theta_3) + \mathcal{O}\left(\frac{p_\perp^4}{s_0^2}\right)\right),$$

$$g(\theta_3) = -\frac{\cos\theta_3}{1+\cos^2\theta_3}(2 + \cos\theta_3 - 4\cos^2\theta_3 + 5\cos^3\theta_3),$$

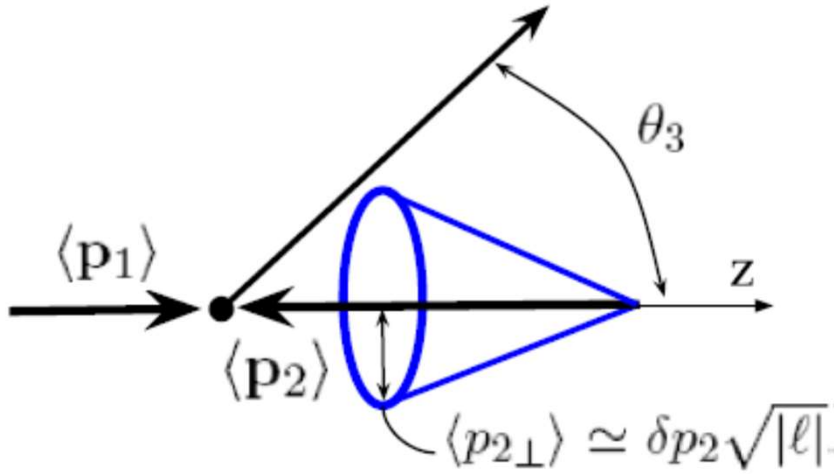

Leptons: $\delta p_2 \lesssim 1$ keV, $\quad \sqrt{s_0} > 1$ GeV $\quad \longrightarrow \quad \frac{p_\perp^2}{s_0} \sim \frac{(\delta p_2)^2}{s_0}|\ell| \lesssim \underline{10^{-12}|\ell|}$

Hadrons: $p_{(\text{tw})}p \to X, \quad p_{(\text{tw})}\bar{p} \to X, \quad e p_{(\text{tw})} \to ep, \quad$ etc.

$$\frac{p_\perp^2}{s_0} \sim \frac{(\delta p_p)^2}{s_0}|\ell| \lesssim \underline{10^{-8}|\ell|}$$

Probing the phase in plane-wave scattering

Eur. Phys. J. C (2016) 76:661
DOI 10.1140/epjc/s10052-016-4399-8

THE EUROPEAN PHYSICAL JOURNAL C

CrossMark

Regular Article - Experimental Physics

Measurement of elastic pp scattering at $\sqrt{s} = 8$ TeV in the Coulomb–nuclear interference region: determination of the ρ-parameter and the total cross-section

TOTEM Collaboration

$$\boxed{d\sigma^{\mathrm{PW}} \propto |M_{fi}^{\mathrm{em}} + M_{fi}^{\mathrm{strong}}|^2}$$

With the vortex particles, the cross section does depend on the amplitude's phase already at the tree level!

Quantum interference

$$d\sigma^{\text{int}} = -2\sigma_{12}^2 \frac{1}{L} \int \frac{d^3p_1}{(2\pi)^3}\frac{d^3p_2}{(2\pi)^3} v(p_i) I_\ell^{\text{corr}}(p_i;b)\, d\sigma^{(\text{pw})}(p_i)$$
$$\times \left(b_{\text{eff}} - \frac{\sigma_{12}^2}{\sigma_{12}^2(\Delta u_\perp)^2 + \sigma_{12,z}^2(\Delta u_z)^2}\Delta u(\Delta u b_{\text{eff}})\right)\cdot \partial_{\Delta p}\zeta_{fi}^{(\text{pw})}(p_i),$$

An effective impact-parameter
(akin to the Goos-Hänchen shift in optics):

$$b_{\text{eff}} = b + \ell \frac{p_2 \times \hat{z}}{p_{2\perp}^2}.$$

Scattering assymetry:

$$\mathcal{A} = \frac{d\sigma_{\text{gen}}(b_{\text{eff}}) - d\sigma_{\text{gen}}(-b_{\text{eff}})}{d\sigma_{\text{gen}}(b_{\text{eff}}) + d\sigma_{\text{gen}}(-b_{\text{eff}})} = \frac{d\sigma^{\text{int}}(b_{\text{eff}})}{d\sigma^{\text{incoh}}(b_{\text{eff}})}$$

In the perturbative regime
for ep, pp very roughly:

$$\frac{d\sigma^{\text{int}}}{d\sigma^{\text{incoh}}} = \mathcal{O}\left(\alpha \frac{p_\perp}{\sqrt{s}}\right) \lesssim \alpha(10^{-5}\text{–}10^{-4}),$$

DK, Serbo, PRD 101, 076009 (2020)